The Mechanics of a Hydrogel Contact Lens on the Human Eye with a Lubricating Tear Layer

by

Kevin Douglas Day

Submitted to the Department of Mechanical Engineering
in partial fulfillment of the requirements for the degree of

Science Master's of Mechanical Engineering

at the

MASSACHUSETTS INSTITUTE OF TECHNOLOGY

May 9, 1997

Author .....
Department of Mechanical Engineering
May 9, 1997

Certified by .....
Mary C. Boyce
Associate Professor of Mechanical Engineering
Thesis Supervisor

Accepted by .....
Ain A. Sonin
Chairman, Department Committee on Graduate Students

Eng.

The Mechanics of a Hydrogel Contact Lens on the Human Eye with a Lubricating Tear Layer

by

Kevin Douglas Day

Submitted to the Department of Mechanical Engineering on May 9, 1997, in partial fulfillment of the requirements for the degree of Science Master's in Mechanical Engineering

Abstract

The mechanics governing the fit of a soft contact lens on the eye are examined through the development of a finite element analysis model. A linearly elastic lens is placed on a rigid eye with a lubricating viscoelastic tear layer. The mechanics of fit are described in terms of the pressure distribution through the tear layer, the contact pressure at the lens/tear interface, the tear film thickness, and the bending and membrane stresses in the contact lens itself. A parametric study is performed to investigate the impact of model assumptions of initial tear film thickness, tear film material properties, and eye geometries on the results predicted by the numerical simulations. Further study is performed to investigate the impact of certain geometric lens parameters and how variations in lens thickness, sagittal height, bevel curve design, and back surface design affect the mechanics of the contact lens.

A three dimensional model is also developed to investigate mobility and stability issues. The strain energy is monitored as the lens is moved across the eye as it would move during a blink of the eye. Mobility is measured both through the total strain energy present in the lens and the strain energy gradient near the equilibrium position of the lens as a function of displacement on the eye. In addition to strain energy values, the force required to move the lens across the surface of the eye is monitored. The long term goal of this work is to develop a numerical tool to assist in the design and development of new lens geometries for better fit and mobility of soft contact lenses.

Thesis Supervisor: Dr. Mary C. Boyce
Title: Associate Professor, Mechanical Engineering

Acknowledgments

In the preparation of this document, I received a lot of support and guidance. I would particularly like to acknowledge my loving fiance Bonnie for her willingness to listen and for her strength, love, and support that was unfailing through the last two years. I would also like to thank my Mother and Father for their interest and encouragement. My friends back home were also great at supporting me and understanding the diminishing amount of correspondence as the due date for the thesis rapidly approached.

I would like to thank Dr. Mary Boyce for the assistance and guidance that was much required during certain periods of the project. I appreciated her willingness and dedication to listen and to discuss the work in progress. I enjoyed our working relationship as Dr. Boyce encouraged a collaborative relationship as opposed to simply dictating what needed to be done. Furthermore, whenever a problem occurred, I know that Dr. Boyce would support me and help me work through to a solution. I would also like to thank Dr. Doug Hart who was very helpful in working with the fluid aspects of the project. I would also like to thank Dr. Peter Hagmann for his support and assistance through the term of the project.

The Mechanics and Materials group was tremendous in their willingness to work together. I would like to thank Clarence for the near continual barrage of questions he helped me work through and answer. Even when he was most busy he was willing to help solve problems and work with me and other members of the group. Oscar and Nick were a wonderful resource to discuss and brain storm new ways approaching problems, not to mention a formidable force on the courts. I would like to thank Ulf who not only was willing to discuss work related problems but also to discuss a more broad spectrum of issues that made my time at MIT even more meaningful. Vivianne was also a good person to be able to discuss some of the issues relating to the project with. I would like to thank Jorgen who always greeted my requests for help with a smile and gave me had a great knack of fixing the problems. I would like to thank Ganti, Hong Dai, Manish, Shrihari, Gu, Ron Rezac, Brian Gearing, Mike, Patricia, Prakash, and Brian Gally for their support and friendship over the past two years.

Finally, I would like to thank those people whose friendship made the hard work easier to bear. It has been a great two years! Thank you all!

Table of Contents

1 Introduction and Background of Soft Contact Lens Mechanics. 11
1.1 Introduction 11
1.2 Motivation 13
1.3 Background 14
1.4 Thesis Outline 17
2 Development of the Model. 21
2.1 Modeling Considerations 21
2.2 Model Description 23
2.3 Boundary Conditions 31
2.4 Loading Procedure 34
3 Verification of the Model. 37
3.1 Introduction 37
3.2 Results from the General Model 38
3.3 Verification of the Results 45
3.4 Parametric Study of Modeling Assumptions 50
3.5 Summary 64
4 Parametric Study of Lens Parameters. 65
4.1 Outline of Parameters of Interest 65
4.2 Parametric Study of Lens Design 65
4.3 Summary of the Parametric Lens Study 80
4.4 Example of Implementing the Results into a Design Setting 80
5 Development of the Three Dimensional Model. 83
5.1 Motivation behind the Three Dimensional Model 83
5.2 Development of the Three Dimensional Model 85
5.3 Loading Procedure 88
5.4 General Results from the Model 88
5.5 Verification of the Model 90
5.6 A Measure of Mobility 91
5.7 Parametric Study of Lens Features on Mobility 93
5.8 Discussion of Results 99
5.9 Summary 101
6 Future Directions and General Summary of the Results Presented. 103
6.1 Future Directions 103
6.2 Implementation into a Design Setting 104
6.3 Summary 105
Appendix A User Subroutine to control Positioning of the End of the Lens 107
Appendix B Calculation of Poiseuille's Flow for an Axisymmetric Disk 111
References 113

List of Figures

Figure 1.1: General Anatomy of the Eye. 11
Figure 1.2: Attributes of the Soft Contact Lens. 12
Figure 2.1: Comparison between linear and non-linear analysis for small strain. 22
Figure 2.2: Comparison between linear and non-linear analysis for large strain. 23
Figure 2.3: Eye Geometry used for Parametric Study. 26
Figure 2.4: Axisymmetric model of the entire system. 28
Figure 2.5: Illustration of the end node of the contact lens lifting off the tear layer. 33
Figure 3.1: Undeformed and Deformed Axisymmetric Model. 37
Figure 3.2: Mises stresses in the Contact Lens. 38
Figure 3.3: Axial (longitudinal) Stresses in the end of the contact lens. 39
Figure 3.4: Graph of the Contact Pressure at the tear/lens Interface. 40
Figure 3.5: Comparison of tear film pressure and contact pressure. 41
Figure 3.6: Comparison of Mises Stresses and the Pressure in the Tear Film..... 41
Figure 3.7: Graph of the tear film thickness distribution. 43
Figure 3.8: Correlation between tear film pressure and the tear film thickness. 43
Figure 3.9: Graph of the Bending and Stretching Stresses in the Contact Lens. 44
Figure 3.10: Comparison between Simulation and the results of Jenkins and Shimbo. 46
Figure 3.11: Contact Pressure for Jenkins and Shimbo Simulation. 47
Figure 3.12: Pressure Distribution in a tear layer for Jenkins and Shimbo simulation. 48
Figure 3.13: Tear Film pressure distribution of the Martin and Holden experiment. 50
Figure 3.14: Effect of No Tear Film on Contact Pressure Distribution. 51
Figure 3.15: Effect of No Tear Layer on the Contact Lens Bending Stresses. 52
Figure 3.16: Effect of Tear Film Thickness on Tear Film Pressure Distribution. 53
Figure 3.17: Effect of Tear Film Thickness on Lens Bending Stresses. 53
Figure 3.18: Undeformed model of the Non-uniform Tear Film Thickness. 54
Figure 3.19: Deformed model of the Non-uniform Tear Film Thickness. 54
Figure 3.18: Effect of a Non-uniform Initial Tear Film thickness Distribution. 55
Figure 3.19: Effect of Non-uniform Initial Film thickness on Tear Film Pressure. 56
Figure 3.20: Effect of Non-uniform Initial Film thickness on Lens Bending Stresses... 56
Figure 3.21: Effect of Tear Fluid Shear Moduli on Tear Film Pressure Distribution. .. 58
Figure 3.22: Effect of Tear Fluid Shear Moduli on Tear Film thickness. 58
Figure 3.23: Effect of Relaxation Time on Tear Film Pressure Distribution. 59
Figure 3.24: Effect of Eye Geometry on the Tear Film Pressure Distribution. 61
Figure 3.25: Effect of Eye Geometry on Lens Bending Stresses. 61
Figure 3.26: Effect of Viscoelastic Lens Properties on Tear Film Pressure. 63
Figure 3.27: Effect of Viscoelastic Lens Properties on Lens Bending Stresses. 63
Figure 4.1: Base Geometry Contact Lens Thickness Profile. 66
Figure 4.2: Effect of Lens Thickness on Tear Film Pressure Distribution. 68
Figure 4.3: Effect of Lens Thickness on Tear Film Thickness. 68
Figure 4.4: Effect of Lenticular Thickness on Tear Film Pressure Distribution. 70
Figure 4.5: Effect of Lenticular Thickness on Lens Bending Stresses. 70
Figure 4.6: Effect of Optical Thickness on Tear Film Pressure Distribution. 72
Figure 4.7: Effect of Optical Thickness on Tear Film Thickness. 72

Figure 4.8: Illustration of modifications to the bevel radius. 73
Figure 4.9: Effect of Bevel Radius on the Tear Film Pressure Distribution. 74
Figure 4.10: Effect of Bevel Radius on the Tear Film Thickness. 74
Figure 4.11: Effect of Lens Sagittal Height on Tear Film Pressure Distribution. 76
Figure 4.12: Effect of Lens Sagittal Height on Lens Bending Stresses. 76
Figure 4.13: Effect of Back Optical Zone Radius on Tear Film Pressure Distribution. 78
Figure 4.14: Effect of Back Optical Zone Radius on Tear Film Thickness. 78
Figure 4.15: Effect of Back Optical Zone Radius on Lens Bending Stresses. 79
Figure 4.16: Tear Film Pressure for First Iteration of the New Lens Design. 81
Figure 4.17: Comparison of First and Second iteration of the New Lens Designs. 82
Figure 5.1: Plane Strain Model of the Contact Lens on the Eye with No Tear Layer. ..84
Figure 5.2: Total Strain Energy in the Contact Lens as a function of Displacement. ...84
Figure 5.3: Illustration of Frequently used Mesh refinement. 86
Figure 5.4: Contact Pressures for 3 Dimensional Model with MPC constraints. 86
Figure 5.5: Three Dimensional Mesh of the Contact Lens. 89
Figure 5.6: Strain Energy Density for the 3-D Model of the Contact Lens. 89
Figure 5.7: Strain Energy Density for the 2-D Model of the Contact Lens. 90
Figure 5.8: Strain Energy Density for the Displaced Contact Lens. 91
Figure 5.9: Strain Energy as a function of Lens position on the Eye. 92
Figure 5.10: Force Required to Move the Lens as a function of Lens Position. 92
Figure 5.11: Effect of Lens Thickness on Strain Energy as a function of position. 94
Figure 5.12: Effect of Lens Thickness on Force required to move the Lens. 94
Figure 5.13: Effect of BOZR on the Strain Energy as a function position. 96
Figure 5.14: Effect of BOZR on the Force required to move the Lens. 96
Figure 5.15: Effect of New Lens Design on the Strain Energy. 98
Figure 5.16: Effect of New Lens Design on the Force Required to move the Lens. 98
Figure 5.17: Strain Energy Density for Lens with Tear Layer & 4 mm Limbus..... 100
Figure 5.17: Strain Energy Density for Lens with no Tear Layer & 8 mm Limbus.... 100
Figure 5.17: Illustration of Mid-plane not Reflecting the True Lens Geometry 101

Chapter 1

Introduction and Background of Soft Contact Lens Mechanics.

1.1 Introduction

In recent years, contact lenses have become an increasingly popular alternative to standard eye glasses, especially in the western world. Even though the increase in usage is quite recent, contact lenses are actually quite an old technology. The first lens was made by Adolf Fick in 1887[28]. These lenses were made of glass and were unfortunately, very uncomfortable to wear. Contact lenses have come a long way since those earlier years, and yet, there is still much that is not understood about their fundamental behavior.

There are several types of contact lenses that are currently commercially available. Bearing similarities to the first contact lenses made by Adolf Fick, one variety of contact lenses is gas permeable hard lenses. These lenses are quite stiff and only cover the cornea over the iris and pupil (see figure 1.1). The other type of lens which was developed in the 1970's is the soft contact lens. This lens is much more flexible than it's predecessor and it is larger in diameter. These lenses are typically made out of high water content hydrogels.

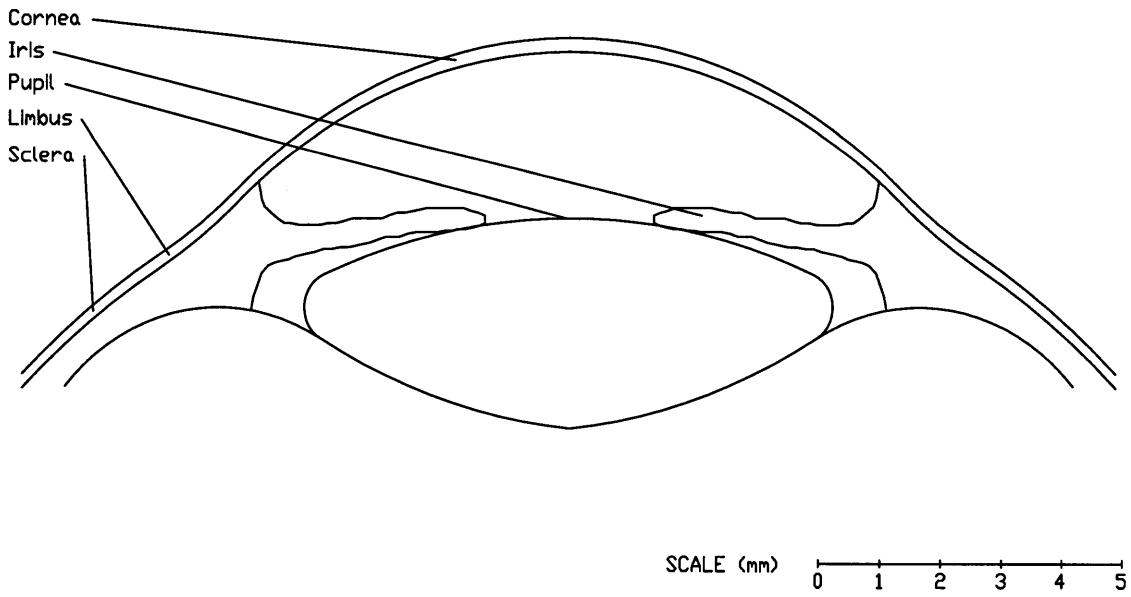

Figure 1.1: General Anatomy of the Eye.

The water content can vary from 35% up to 80%. Soft lenses are very thin disks in shape, and generally range from 70 - 200 microns thick. The lens covers the entire cornea and limbus, and covers part of the sclera (see figure 1.1). This lens is generally more comfortable than the hard lenses and does not fall off the eye as easily due in part to the increased size. Within the group of soft contact lenses, there are two main varieties: daily wear contact lenses and extended wear contact lenses which were introduced in the 1980's. Although quite similar, extended wear lenses are worn for several weeks at a time and tend to be thinner than standard daily wear contact lenses.

For discussion purposes, some standard features of the soft contact lens are shown in figure 2. The lens here is broken down into three different sections. The optical zone covers the cornea and it is through this region that the contact lens achieves the required optical characteristics to correct vision. The lenticular zone covers the limbus of the eye where there is a reverse curvature in the cross section of the eye (see figure 1.1). Finally, the bevel zone is located at the edge of the lens where there is a dramatic decrease in lens thickness. The portion of the lens that is against the eye is referred to as the back surface, whereas the front surface of the lens is exposed to the air. The sagittal height of a lens is defined as the vertical distance from the apex of the lens to the edge of the lens (see figure 1.2). As the sagittal height is increased, the lens is said to have a steeper fit.

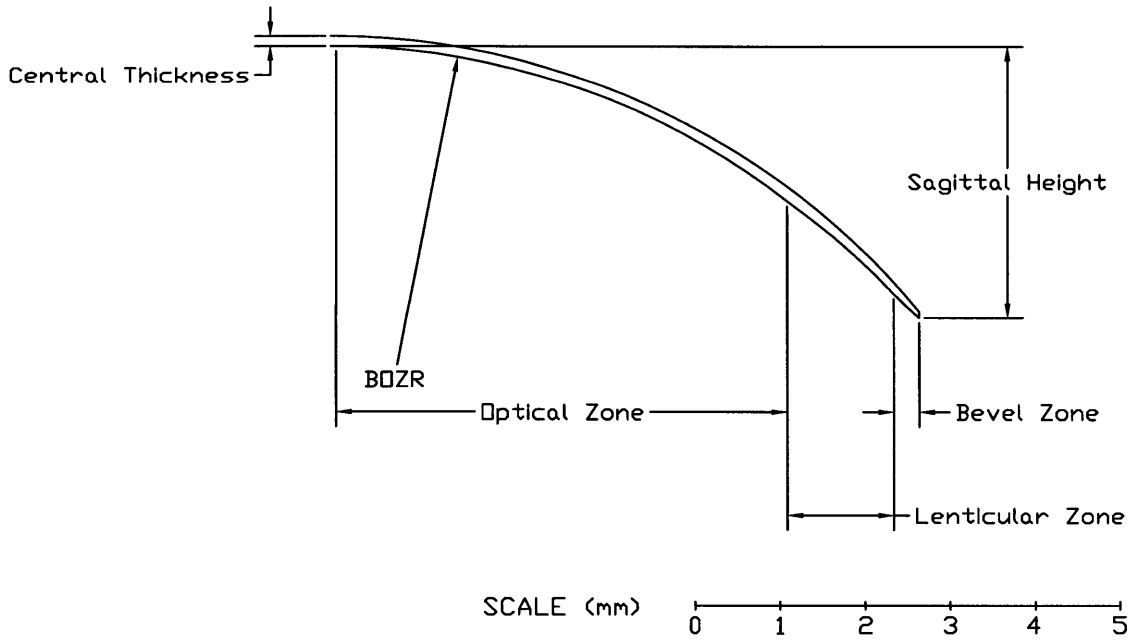

Figure 1.2: Attributes of the Soft Contact Lens.

1.2 Motivation

The vision care industry is a large and very profitable field. In 1993 in the United States alone, over $12 billion was spent on vision care products and other medical durables [29]. In recent years, contact lenses have accounted for a large portion of this field. Soft hydrogel lenses, disposable soft lenses, and extended wear lenses have all been introduced with large market potential. With this sizable consumer base, there is a strong push for companies to make better products to try and obtain a larger share of the market.

Contact lenses have had problems, however, achieving acceptance among some people. Issues such as lens comfort and ease of handling have been identified as features that can limit the appeal of contact lenses. Problems have also been encountered with lenses causing permanent damage directly to the cornea. Corneal ulcers have increased in recent years especially with the introduction of extended wear contact lenses[1]. There are numerous mechanisms that are believed to be responsible for causing corneal damage and irritation. Mechanical abrasion of the lens on the eye lid can cause discomfort and abrasion on the corneal surface has been suggested as a significant mechanism for corneal irritation and damage[1]. Oxygen transport to the corneal surface is also critical in maintaining a healthy epithelial layer. The epithelial layer is the outermost portion of the eye that is exposed directly to the tear layer and any other external elements that contact the eye surface. If the lens does not permit enough oxygen transport through the lens, the cornea can sustain damage. Oxygen transport is reduced as the contact lens becomes thicker and so there has been much work into developing thinner lenses. Unfortunately, additional problems have developed with the thin lenses. Lens dehydration has been identified as a cause of corneal desiccation, especially with these thin lenses that dehydrate at a faster rate than thicker ones[19]. If debris gets trapped under the lens and there is inadequate tear fluid exchange to remove it, corneal lesions can occur leading to eye irritation[20]. Motion of the lens can serve to remove the debris trapped between the lens and the eye. Contact lenses also tend to be a site for increased bacterial growth and this can lead to further corneal irritation and possible infection.

To solve the problems facing contact lens development, manufacturers have looked at modifying numerous design parameters in an attempt to develop a better contact lens. As mentioned previously, to improve the permeability of the lenses, making thinner lenses

was identified as one way to improve oxygen transport through the lens. There is a limit to how thin a lens can be made both from excessive dehydration and from problems with handlability. To improve tear film flow and reduce possible mechanical abrasion with the corneal surface, soft contact lens geometries have been modified in an attempt to develop a more comfortable fit on the eye. These modifications have involved changing the thickness of the lens, the sagittal height or steepness of fit, the back radius of curvature of the lens, and numerous other more subtle changes. Most of these modifications were, however, based on empirical data and a trial and error development process. As making new lens geometries can be very expensive for the contact lens manufacturers, this has slowed the evolution of the contact lens. Furthermore, with the empirical development, there is no opportunity for optimization as there is no fundamental understanding of the contact lens mechanics.

The goal behind developing a model of the soft contact lens as it rests on the human eye is to gain a more complete understanding of the mechanics involved. With such a model, it is hoped that a more analytical approach can be taken towards lens design and development. If the stress state of the lens and the tear layer is known, geometric modifications can be made to reduce maximum stress concentrations and maximum contact pressures while maintaining adequate suction pressures to ensure a stable fit of the lens. With a shift away from empirical reliance and a move towards a solid understanding of the parameters that affect the contact lens mechanics, better lens designs can be developed in a shorter period of time. This will save the industry costly research and development time and money, and could speed up the evolution of the contact lens.

1.3 Background

In recent years, there has been a lot of work published on investigating various aspects of contact lenses. Most results addressing the mechanics of contact lenses can be classified into three main areas: analytical modeling, empirical modeling, and clinical trials. Although limited, there has been some work in numerical modeling as well.

1.3.1 Analytical Modeling

Although much work has been done in analyzing the mechanics of contact lenses, the focus has been on simplified geometries of the eye and the contact lens itself. Hayashi and

Fatt[3] developed a model to predict the forces involved in retaining a contact lens on the eye. This, however, was done with a spherical eye and a spherical constant thickness cap for a lens. Although this work applied well to the case of a rigid contact lens on the eye, it was not applicable to soft contact lenses. Soft lenses take on a rather complex geometry where the lens continues past the limbus. Here, the limbus is defined to indicate the transition region between the cornea and the sclera. Conway and Richman[4] investigated a flexible lens but the analysis was limited to a one dimensional model that was insensitive to any geometric effects of the eye.

Jenkins and Shimbo[2] developed an analytical solution that did consider the effects of eye geometries with a lens that continued past the limbus but it did not account for a tear layer. Pressure distributions were estimated based on complete conformity of the lens to the eye surface. The analysis was also limited to membrane stresses, thus neglecting bending stresses in the lens. Bending stresses are negligible over regions where the curvature of the hydrogel lens and the eye are similar and through these regions, the values predicted can be used. Near the limbus, however, where there are dramatic differences in initial curvature between the eye and the soft contact lens, bending stresses cannot be neglected and are indeed dominant. Therefore, the results that Jenkins and Shimbo obtained past the corneal region are quite suspect. This section of the lens should have a significant impact on lens motion and comfort as well.

Taylor and Wilson[5] took an opposite approach to Jenkins and Shimbo and neglected all strain energy from non-bending deformation. Here, the focus was centration mechanisms and the differential strain energy of the lens in off-centered positions. Bending stresses seem to be the dominant factor in centration but hoop stresses may play a significant role with lens stability and over all fit of the lens as suggested by Kikkawa[18]. Although the results of Taylor and Wilson give a good indication towards the centration mechanisms, other issues of lens mechanics need to be addressed.

1.3.2 Empirical Modeling

Martin[6,7] has been a prime contributor in experimental work. He has developed a 1:1 physical model of the eye. The entire model was submerged in artificial tear solution thereby negating any surface tension effects of the tear layer. Martin drilled 0.75 mm

diameter holes in a perspex (PMMA) model eye for pressure taps and measured the pressure distribution in the tear layer. Due to the small scale of the model, however, results have been limited to four data points from the apex to the edge of the contact lens. This low resolution makes the work insensitive to any geometric subtleties, especially around the limbus and at the edge of the lens. The results obtained by Martin showed that the pressure under the high water content lens (70% water content) ranged from 0.1 kPa vacuum gauge pressure at the center of thin lenses (center thickness 0.08 mm) to 0.2 kPa vacuum gauge pressure at the center of thicker lenses with a steeper fit (center thickness 0.15 mm). These average readings are informative but a more precise measurement would be preferred when attempting to identify details of the lens design responsible for optimal fit, comfort, and motion.

1.3.3 Clinical Trials

Clinical results have provided contact lens practitioners the most useful data to date. Although qualitative in nature, lens fit subject to numerous design considerations have been investigated. Young, Holden and Cooke[8] investigated the effect of varying the back optic zone radius, the back surface design, the edge thickness and back vertex power on lens fit and comfort. In this paper, the back surface design and steepness of fit were identified as major factors affecting comfort and fit with edge thickness having a negligible effect on comfort of fit within the range studied (0.12 to 0.24 mm). Studies like the one by Pesudovs and Phillips[9] have compared the fit of some commercially available lenses to determine which lenses have the best clinical results. They also identified that lens preference is primarily based on comfort and handling while quality of vision was a secondary factor. Although these types of results are useful for designing more comfortable and stable lenses, they do not indicate exact mechanisms nor do they allow for design optimization. All design modifications must be done on a trial and error basis, costing manufacturers time and money.

1.3.4 Numerical Modeling

Research in the area of numerical modeling of contact lens mechanics has been limited. Funkenbusch and Benson[16] have recently developed a finite difference model of a geometrically accurate eye and contact lens. Unfortunately, there were numerous model-

ing assumptions that limit the application of the results. In the model presented, it is assumed that there is a uniform pressure acting normal to the lens' anterior surface and it is assumed that this value is known. It is also assumed that the only reaction force is due to physical contact of the lens on the eye. From general lubrication theory, it seems unlikely that the tear layer would be displaced completely and it is generally accepted that the contact lens moves on a thin tear film. In effect, Funkenbusch and Benson have assumed a liquid with zero viscosity. Although the tear layer has low viscosity at high shear rates (close to water), the viscosity is quite high under low shear rates[13]. Thus, it would be preferred if some fluid effects could be included in the model. An additional assumption that seems questionable is that the Poisson's ratio for the lens was taken as 0.25. As the material is a hydrogel which is a polymer in the rubbery region, these materials typically have a Poisson's ratio close to 0.5 [17]. One major obstacle for current numerical modeling is the absence of accurate empirical results to validate the models. For this reason, numerical results are still somewhat in question with no means for complete validation of the results. Although not as rigorous, validation against some of the analytical results can be used over certain regions of the solutions provided. Thus, the numerical results can be shown to have an acceptable level of validation.

As illustrated by the discussion of previous work done on analyzing the mechanics of soft hydrogel contact lenses, there is still no satisfactory model that describes the mechanics. Models lack lubrication or fluid considerations, accurate geometries of the lens and eye, and/or realistic boundary conditions. There is a real need for a comprehensive and accurate model to describe the mechanics of the contact lens on the eye so that a fundamental understanding can be achieved.

1.4 Thesis Outline

This thesis addresses the mechanics of the fit of a soft hydrogel contact lens on the human eye with a lubricating tear layer through the development of a finite element method (FEM) model. Through this model, the lens mechanics are investigated in a state of quasi-equilibrium. The goal of this work is to develop a geometrically and physically accurate representation of the soft contact lens on the eye. The primary values that will be used to describe the lens mechanics are the pressure distribution in the tear layer; the interference

pressure distribution between the lens and the tear layer (i.e. the tractions required to maintain contact between the lens and the tear); the tear layer thickness profile; and the stress distributions produced in the soft contact lens itself. Detailed examination of the tractions and stress distributions resulting from fitting a lens to an eye should lead to quantitative understanding of the parameters which govern lens comfort.

The development of the model begins in the second chapter with the development of a two dimensional, axisymmetric model. To develop this model, the system is broken down into its three main components. These components are the eye, the contact lens and the tear layer. Each component is discussed with respect to modeling assumptions and geometric and material properties. These components are brought together to form one single model through a discussion of the boundary conditions. The boundary conditions are applied in an attempt to achieve the most realistic results possible.

Verification of the model is pursued in the third chapter. First, the results from a standard simulation are discussed. Validation is achieved through a comparison of numerical results against a range of analytical results predicted by Jenkins and Shimbo. Results are further supported by a comparison of the simulation results against experimental results obtained by Martin. Results of the simulation are then further validated with a sensitivity analysis. Here modeling assumptions are tested to determine the robustness of the model. Three modeling assumptions are investigated. Material properties of the tear layer are investigated as are variations in the tear film thickness and the limbus radius of the eye.

With the working two dimensional axisymmetric model, a parametric study of modifications in lens parameters is performed in chapter four. Here, six different lens parameters are identified as possible significant elements in determining the mechanics of the contact lens. Variation of the parameters are taken from the initial simulation run that was discussed previously in chapter three. These parameters are: overall lens thickness, lens thickness through the lenticular region, the lens thickness through the optical region, the bevel radius of the lens, the sagittal height of the lens, and the back optical zone radius.

With this fundamental understanding of the lens mechanics from the two dimensional analysis, a three dimensional model is developed in chapter five. This model is developed so that non-axisymmetric deformations of the lens can be investigated. The analysis is

done to investigate the motion of the soft contact lens on the eye. Modeling assumptions that differ from the axisymmetric model are discussed and justified. There is also a discussion of some of the problems encountered with the slightly more complex model. Then, results from the simulation are discussed with particular reference to the strain energy density in the lens in both the centered and off-centered positions and how these results might affect the lens mobility and stability.

Finally, results are summarized and implications of the work are discussed in chapter six. Possible implementation of the work is discussed and some design hypotheses are proposed that could be used in a design setting. Limitations of the work performed are also discussed with suggestions of possible future work that could lend further insights into the long term mechanics of soft contact lenses.

Chapter 2

Development of the Model

2.1 Modeling Considerations

The first important decision in modeling the system consisting of the eye, the tear layer, and the contact lens, in order to investigate the contact lens mechanics was to determine the best means of analysis. Closed form analytical solutions are very appealing as they allow for simple parametric analysis. Once the closed form solution is found, various lens profiles can be investigated and optimization can be achieved even if numerical methods are necessary. Unfortunately, for the case presented, it does not appear that an accurate model can be developed in a closed form. The subtle complexities of the lens geometry control comfort and therefore must be modeled accurately for complete understanding. Therefore, with non-trivial geometries and fluid interaction with deformable solids, accurate closed form solutions become very difficult to develop.

Finite element analysis (FEA) has been an increasingly popular means of analyzing complex systems. There are drawbacks, however, with FEA. Parametric analysis can become more time consuming as an iterative approach must be taken if the solution is non-linear. As with any numerical code, problems can arise with computation time and divergence of the solution. The benefits in using a finite element method (FEM) on complex problems though are that geometry can be accurately described. As developments in new contact lens geometries can involve very subtle changes in the thickness profile, the analysis must be very sensitive to slight geometric changes. With these considerations in mind, FEA was chosen as the most feasible means of analysis.

The FEM modeling for this work was done using a commercial non-linear finite element code, ABAQUS[10]. Computation was done on both a Hewlett Packard Series 735 and a Dec Alpha 500 workstation. This package was chosen based on its excellent reputation as a non-linear numerical solver. Non-linear analysis is required due to effects from large deformations of the lens when placed on the eye and due to the inherent high degree of contact between the different elements. If linear analysis is used, the stiffness matrix for the finite elements is not updated based on deforming geometries. As the lens undergoes

severe deformation, the stiffness matrix must be updated to reflect the modified geometry. The effect of including non-linear analysis can be shown through a simple example of a beam in bending.

Here we compare the results of a linear and a non-linear analysis. The example being considered involves a beam in plane strain with a Young's modulus of 0.8 MPa and a Poisson's ratio of 0.49. The beam is modeled with quadratic elements. The load applied to the beam that is 5 mm in length and 1 mm in thickness is 0.003 N. Given relatively small strains, the two methods yield similar results. Below, the axial stress state is shown for small displacements (figure 2.1). Comparing the two results for the given example, the maximum stress predicted differs by about 15%. The maximum displacement predicted by the non-linear analysis which was -1.51 mm is only 0.01 mm more than the displacement predicted with the linear analysis, a difference of less than 1%.

In contrast to this lower level of deformation, the case presented in figure 2.2 is subject to a load of 0.01 N. Here, the maximum axial tension is over estimated by 65%. This dramatic over estimation is due to the constant stiffness matrix that does not reflect the deformed geometry. The deflection of the beam based on the non-linear analysis is reported to be -3.63 mm, much less than the -5.0 mm predicted by the linear analysis.

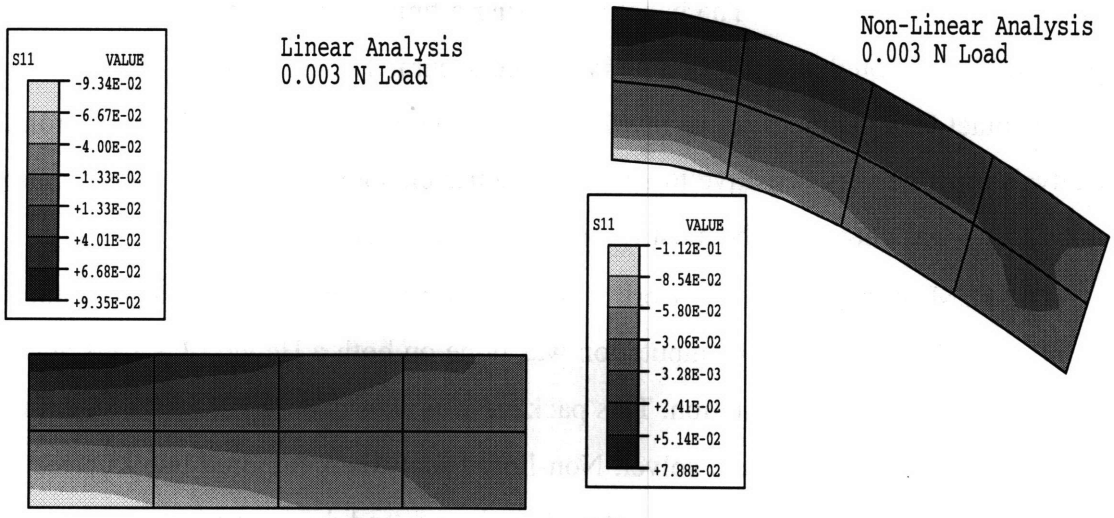

Figure 2.1: Comparison of axial stress state between linear and non-linear analysis for small strain conditions.

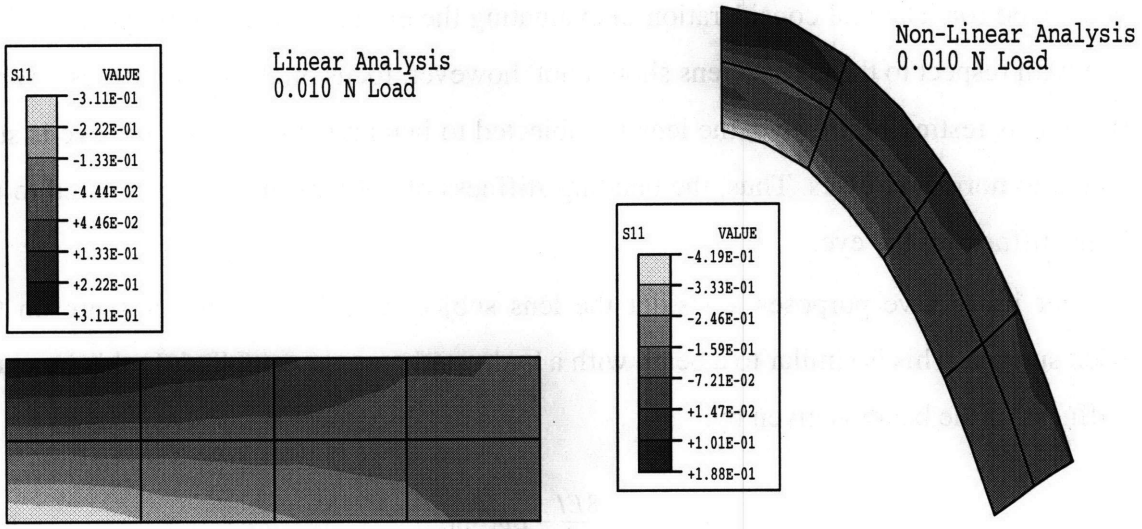

Figure 2.2: Comparison of axial stress state between linear and non-linear analysis for large strain conditions.

As the contact lens undergoes severe elastic deformation when placed on the eye, a non-linear analysis is required.

2.2 Model Description

To describe the model in detail, the three elements involved will be dealt with individually. Both geometric and material properties of the elements will be discussed. These sections will address similarities between previous modeling work and our proposed model. Finally, the eye, the tear layer, and the contact lens will be assimilated into a coherent model through a discussion of the boundary conditions applied.

2.2.1 The Eye

There have been numerous studies to look into the material properties of the eye tissue or scleral tissue. The tensile strength of the scleral tissue has been reported on the order of 1 to 100 MPa. More recently, Battaglioli and Kamm measured the compressive properties of scleral tissue and found these to be much lower. Young's Modulus was measured to be on the order of 25 to 40 kPa[21]. These measurements make the bulk stiffness of the eye

of similar order of magnitude as the contact lens material (generally taken as about 800 kPa). Thus, it would seem initially that the elastic material properties of the eye must be accounted for. The real consideration in evaluating the effective material properties of the eye with respect to the contact lens should not, however, focus on the bulk stiffness. When the lens is resting on the eye, the lens is subjected to bending stresses and the eye is subjected to normal stresses. Thus, the bending stiffness of the lens must be compared to the bulk stiffness of the eye.

For illustrative purposes, consider the lens subject to a hydrostatic pressure on the back surface. This is similar to a beam with a hydrostatic pressure applied. In this case, the stiffness of the beam is given by:

$$k_{Lens} = \frac{8EI}{L^3} \sim Eb\left(\frac{h}{d}\right)^3 \tag{2.1}$$

where h is the thickness of the beam, d is the beam length, b is the beam width, and I=1/12 bh^3. Here h << d so k_{Lens} << E.

In contrast, consider the eye as a sphere subject to a hydrostatic pressure. Here, the stiffness in the radial direction is given by:

$$k_{Eye} = \left(\frac{\pi}{4}\right)\frac{Ed}{(1-2\upsilon)} \sim \frac{Ed}{(1-2\upsilon)} \tag{2.2}$$

where ν, the Poisson's ratio, for the scleral tissue has been measured at 0.48 [21]. Thus, as the denominator is very small, k_{Eye} becomes very large. Thus k_{Eye} >> E. By these calculations, k_{Eye} >>> k_{Lens}. So even though the scleral tissue has a Young's Modulus that is of the same order of the contact lens Young's Modulus, the eye is much more stiff. Although interfacial pressure can cause significant stresses and strains in the contact lens, any normal stresses applied to the eye surface will result in negligible corneal strain.

As a second basis for the rigidity assumption, the intraocular pressure (IOP) of the eye was considered. The eye is internally pressurized. The mean IOP reported by Kragha was 16.6 mm Hg or 2.2 kPa[22]. Provided that tear film pressures are maintained well below this level, the assumption of eye rigidity should be valid.

This means that the eye surface can be modeled as rigid relative to the contact lens. As the tear layer is much more compliant than the contact lens, the eye is rigid relative to all

other elements in the model. The assumption of a rigid eye is also supported by previous work in the field as most studies do make this assumption [2-5,11].

Although the dimensions of the human eye do not vary a lot from person to person[28], taking one specific eye geometry as representative for all people is unrealistic. Research has shown that there are at least five distinctive eye shapes [12]. Thus, the eye geometries used must be carefully chosen to match the lenses being investigated. As briefly outlined in the first chapter, the eye has three main sections: the cornea, the limbus, and the sclera. It will be assumed for this research that the eye is radially symmetric. Generally the vertical diameter of the eye is slightly less than the horizontal diameter, but the differences are quite small. Some visual impairments are derived from a non-radially symmetric cornea, often termed an astigmatism. Although of interest to contact lens manufacturers, these eye types will not be investigated in the current research.

In recent research into contact lenses, numerous eye geometries have been used. The sclera is generally considered as spherical, and with a radius of 11-13 mm [2,3,5,16]. Although many papers did consider the cornea as a sphere [3,4] it is generally accepted that an elliptical cross section is more representative. Values used range from a central radius of curvature of 7-9 mm [2,5,16]. In a recent paper by Funkenbusch and Benson, the radius for the limbus was quoted as being 3 mm [16].

For the parametric study, the cornea was modeled as axially symmetric with an elliptical cross section and a chord diameter of 12 mm (see figure 2.3). The eccentricity was taken as 0.39 and the central radius as 7.75 mm. These values reflect clinical measurements provided by CIBA/Vision. The radius of the limbus was assumed to be 8 mm in the parametric study and it was taken to be tangential to the cornea and the sclera. The motivation for filleting the limbus was twofold. First, a sharp angle between the cornea and the sclera would make for problematic numerical solutions. The first order discontinuity could pose convergence problems. Second, photographic studies have been performed on the eye that show a smooth transition between the cornea and the sclera [12]. The sclera was assumed to be spherical with a radius of 12 mm. The corneal sagittal height, which is defined as the height from the center of the cornea to the point of intersection between the cornea and the sclera, is 1.73 mm. The values correspond quite closely to other eye geometries that have been used in similar previous studies [2].

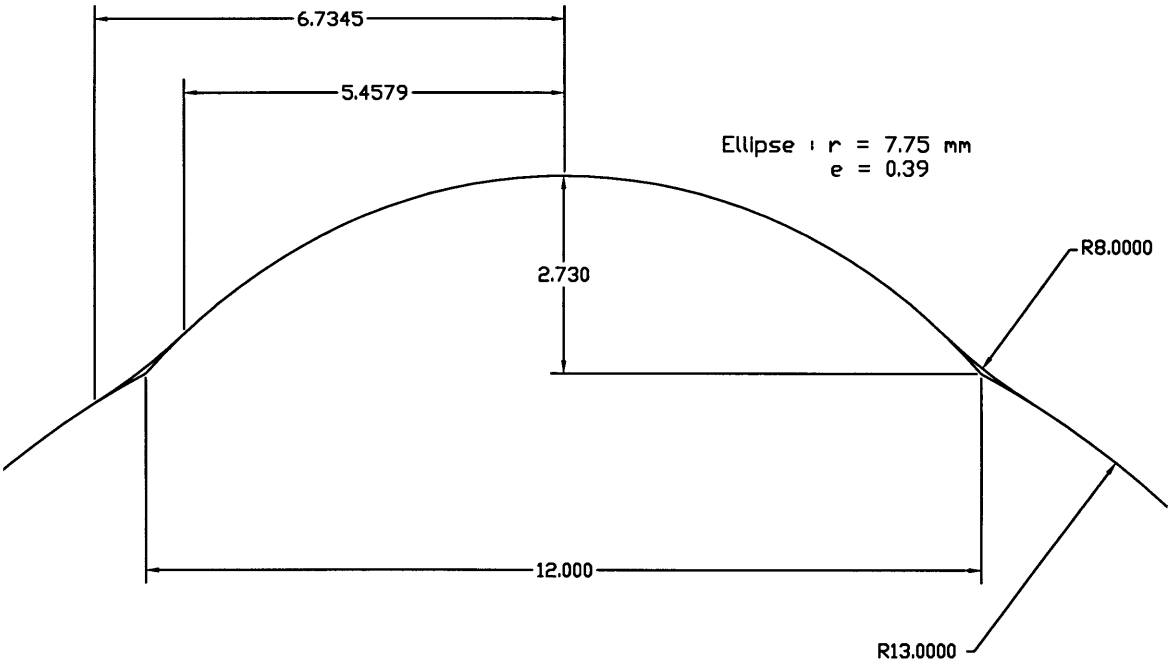

Figure 2.3: Eye Geometry used for Parametric Study.

2.2.2 The Contact Lens:

As stated earlier, soft contact lenses are made out of high water content hydrogels. The hydrogels tend to be lightly cross-linked polymers such as poly(2-hydroxyethyl methacrylate) (polyHEMA) [23]. Water content can vary from 35% up to 80%. This high water content tends to yield a viscoelastic behavior as observed in work by Kikkawa[24]. The time constant observed for relaxation in the hydrogels is on the order of 5 seconds. This rate of relaxation would be much less than the rate of relaxation through the tear layer flow. It was thus assumed that the relaxation mechanism of the lens would be negligible compared to the relaxation mechanism of the tear layer.

Based on this reasoning, the soft contact lens was assumed to behave as an isotropic linear elastic solid. The material properties of the lens were determined based on experimental results provided by CIBA/Vision. The Young's modulus was found to be 0.8 MPa. To determine the Poisson's ratio, the general make-up of the contact lens was considered. As stated earlier, the lens is a highly hydrated, rubbery polymer lattice. Polymers in the rubbery region tend to be incompressible as does the water in the lattice. Thus, a Poisson's ratio of 0.49 was assumed as the lens is nearly incompressible.

In previous research, many different lens geometries have been investigated. Unfortunately, as much of the current research is being sponsored by contact lens companies, complete details of the contact lens geometries are not made available. There is some limited information, however, given about most of the lenses. Generally, the center thickness of a lens is on the order of 100 - 200 microns[2-5,8,14,16]. Often, a lens gets a little thicker towards the lenticular section of the lens and then tapers off to the edge. The base curve radius which is the radius of curvature of the back of the lens, is generally slightly steeper than that of the eye. Values are quoted in the range of 7-9 mm [2-5,8] but these values correspond to the specific eye geometry under investigation.

For this investigation into contact lens mechanics, a test lens geometry was used. This lens was chosen as a typical lens that might be fitted to the eye geometry that has been described above. Based on the eye geometry, the effective base curve of the lens was taken to be 8.6 mm. The center thickness is 125 μm and this increases to a maximum thickness of about 150 μm through the lenticular region. The cross section profile of the optical zone is fixed based on the required lens diopter, which for this lens, is -0.5 dp. A low diopter lens was chosen so that the thickness profile would be more uniform than for higher diopter lenses. As the diopter increases in magnitude, the difference in curvatures between the back and front surfaces of the lens through the optical region increase. This yields a thinner lens at the apex and a thicker lens at the edge of the optical region for large negative diopter lenses. The more uniform lens profile provides a more appropriate test lens for the following parametric study.

To model the contact lens, eight-node and six-node quadratic axisymmetric reduced integration elements were used (ABAQUS type CAX8R and CAX6R). Quadratic elements were used instead of linear elements to better incorporate the initial curvature as well as the resulting deformation of the lens itself. The use of axisymmetric elements allows for three dimensional analysis with two dimensional computation where the additional stiffness from the hoop resistance is inherently contained in the element stiffness formulation. The stress state obtained using the reduced integration elements was compared against results obtained using full integration elements and there was no significant difference. Thus, for reduced computation time, the reduced integration elements were used. The six node triangular elements were only used at the edge of the lens for mesh

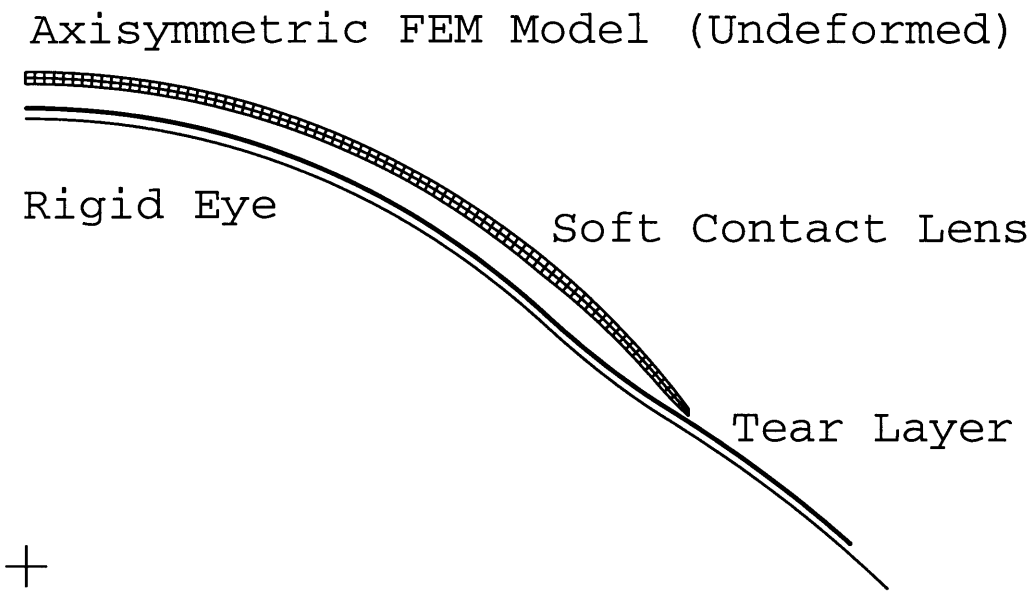

Figure 2.4: Axisymmetric model of the entire system comprising the soft contact lens, the tear layer and the eye.

refinement. The mesh used was a simple band with two elements across the thickness (figure 2.4).

2.2.3 The Tear Layer

The tear layer is a very complicated fluid structure. Within the thin tear layer, there is a mucous layer, an aqueous layer, and a lipid layer.[13] The tear film performs two main functions. During blinking, the tear film provides lubrication so that the epithelial surface of the eye is not damaged by the eye lid motion. The ideal fluid to perform this function would have a very low viscosity. When the eye is open, however, the tear film must resist drainage and film break-up so that the epithelial surface does not dehydrate. For this purpose, the ideal fluid would be highly viscous, demonstrating limited flow and a high resistance to evaporation. Thus, from the required functioning of the tear layer, it seems unlikely that it would be a standard Newtonian fluid.

Recent investigations into the viscosity of tears has identified that human tear fluid is a non-Newtonian fluid exhibiting shear-thinning. Tiffany investigated the viscosity of human tears at various shear rates ranging from 2 to 160 sec^{-1} [25]. During blinking, the

tear film is put under severe rates of shear. At this level of shear, the viscosity of the film is close to that of water. Reported values of viscosity by Tiffany are around 1.5 mPa•sec. At shear rates below 5 sec^{-1}, the viscosity of the tear fluid dramatically increases. Tiffany reported values as high as 9 mPa•sec for dry eyes, and around 5 mPa•sec for normal eyes. These results were limited to shear rates of 2 sec^{-1} because for lower shear rates, torsional force readings were very small with large errors. It is expected that the viscosity of the tear fluid would increase beyond the reported 5-10 mPa•sec range for very low shear rates.

Modeling of the tear film must reflect this non-Newtonian behavior. As the equilibrium resting position of the lens on the eye will involve low rates of shear, the fluid must demonstrate highly viscous behavior at the final equilibrium solution. As a good first approximation to this behavior, the tear film will be modeled as a viscoelastic material with a rapidly decreasing shear modulus but constant bulk modulus. The reduction in shear modulus will cause the tear film to flow when subjected to shear stresses. This will give the tear film weak shear resistance and yet maintain bulk properties.

The shear properties of the tear film material are defined using a Prony series. The defining equation is given as follows:

$$K(t) = K_{inf} + \sum_{i=1}^{nk} K_i \exp\left(-\frac{t}{t_{ik}}\right) \tag{2.3}$$

where K(t) is the shear relaxation function, K_{inf} is the long term shear modulus, $(K_{inf}+\Sigma K_i)$ is the instantaneous shear modulus, t_{ik} is the characteristic relaxation time, and nk is the number of terms used in the Prony series to define the shear relaxation function. The initial shear modulus of the tear fluid is taken as 6.7 kPa and the bulk modulus is kept constant at 333 kPa (corresponds to E=0.02 MPa, v=0.49). Tiffany measured the relaxation time for tears to stabilize after a blink on a normal eye to be on the order of 0.3 seconds [25]. Thus, with a time constant of 50 ms, the system should be close to a quasi-equilibrium state within 5 to 6 time constants or 0.3 seconds. The shear modulus is reduced by 95% over the given relaxation time with only one Prony term (nk=1). This means the ratio of bulk modulus to shear modulus is 1000:1.

With the material properties set, the focus shifts to the initial thickness of the tear layer on the eye. In earlier studies, the thickness of the tear layer was thought to be on the order

of a few microns [2-4]. These estimates were based on very rough measurements and there was some question towards their validity. More recently, Prydal and Dilly[15] performed a study using laser interferometry and later using confocal microscopy. These results predicted a much thicker tear layer of about 40 microns. Prydal and Dilly proposed that previous measurements of 4 to 7 microns for the tear film thickness did not include the mucus layer at the base of the tear film. Additionally, Holt, Boyce, and Hart have measured the tear film thickness to be in the range of 30 - 60 μm on a model eye [30].

Unfortunately, results from confocal microscopy are still somewhat preliminary. The results appear promising but there have been difficulties making in vivo measurements due to involuntary eye movements and insufficiently sensitive video cameras. As there is still some question towards the actual thickness of the tear layer, a thickness of 20 microns was assumed. The literature will be closely watched in the coming months and years to see if more reliable and reproducible results are published in terms of tear film thickness.

Another assumption made was that the tear film thickness was uniform over the entire eye. Currently, there is very little information that indicates how the tear film thickness varies over the eye. It seems likely that there might be some gathering of the tear fluid at the base of the eye, especially at the limbus where there is a slight cusp in the cross section of the eye. Unfortunately, there do not appear to be any measurements that support this supposition. Thus, with no reliable information, uniform thickness seemed to be the best assumption.

The tear layer was modeled using eight node quadratic axisymmetric reduced integration elements (ABAQUS type CAX8R). As for the contact lens, the quadratic elements were used to best represent the initial curvature and resulting deformation of the tear layer. Results generated using the reduced integration elements were compared against results from both full integration elements and hybrid elements (often used when materials are nearly incompressible). Results were identical with all element types so reduced integration elements were used for reduced computation time. The mesh used for the tear layer only involved a single thickness row of elements. The elements were refined in areas where the contact pressures were expected to be high and at the section where the lens edge contacted the tear layer.

2.3 Boundary Conditions

With the individual members of the model defined in terms of material properties and general geometry, the model must now tie these members together through the boundary conditions. There are two main interfaces that must be considered. At the first interface, the viscoelastic tear layer contacts with the rigid eye surface. At the second interface, the viscoelastic tear layer contacts with the deformable elastic contact lens.

2.3.1 Contact

The first concern in modeling surface interactions is to incorporate contact between the two materials in question. Modeling contact requires that the two surfaces don't overlap, and that there is an equilibrium balance achieved across the interface. Naturally, each individual body must also be in a state of equilibrium.

There are numerous techniques that can be used to model contact. One of the earlier methods used was that of the penalty method. In the penalty method formulation, the contact pressure is taken as a linear function of the penetration depth of the slave surface into the master surface. The slave surface is defined as the softer surface that is constrained against penetrating into the more rigid master surface. The master surface, however, can penetrate into the slave surface. Generally, the constant coefficient of the linear term is assumed to be known. This means that there are no additional degrees of freedom introduced, and the stiffness matrix is not increased in size. Although the method tends to predict a more stiff system as it is overly constrained, results are reasonable and computation time is not significantly increased.

Another means of looking at contact is by using a method of Lagrange multipliers. This method allows for large relative tangential motion between two surfaces and it is applicable to the most general case of contact. The central concept is to link the degrees of freedom of the two surfaces if there is contact occurring. By introducing Lagrange multipliers as the contact forces, additional degrees of freedom are introduced into the formulation. By introducing the new degrees of freedom, the size of the stiffness matrix is increased. With sliding contact, only one degree of freedom is added per node but if there are friction effects leading to sticking contact, two degrees of freedom are added per node to account for the tangential tractions in addition to the normal contact pressure. As the

number of operations required to solve a system of linear equations is proportional to n^3 [31], where n is the size of the stiffness matrix, an increase in the size of the stiffness matrix dramatically increases computation time. This method does, however, give a more accurate numerical representation with the increase in computation time.

There are additional numerical methods to solve for contact, but the different methods tend to lie in-between the simplicity of the penalty method and the exhaustive nature of the Lagrange multipliers method. These alternative methods balance the need for accuracy with the need for reduced computation time. Although the model of the contact lens resting on the eye involves a large degree of contact, computation facilities were adequate to compute solutions based on the Lagrange multipliers formulation within a reasonable time. Additionally, contact formulations based on the Lagrange multiplier method was available with the commercial package being used. Thus, contact interaction was modeled using the standard library of contact elements provided through the commercial package ABAQUS.

Interaction between the tear layer and the rigid eye surface used 3-node axisymmetric interface elements (ABAQUS type IRS22). This defines the rigid surface as the master surface and the bottom surface of the tear layer as the slave surface. In a similar manner, interaction between the tear layer and the hydrogel lens was governed by surface definitions[10] with the lens being the master surface and the tear layer being the slave surface.

2.3.2 Surface Interaction

The tear layer, although being modeled as a viscoelastic solid, should behave as a liquid. As there is only small flow of the tear layer and as the quasi-steady state condition is being investigated, interface shear effects were considered to be negligible. Thus, the friction at both interfaces was assumed to be zero. This assumption also decreases the computation time as a purely frictionless surface requires only one additional degree of freedom to model contact as discussed above.

One of the main mechanisms that holds the contact lens to the eye is the capillary action of the tear layer, or its surface tension. This was identified as an important element to include in the model. To simulate surface tension effects, all surfaces that come into contact with the tear layer are imposed with a no separation boundary condition. This

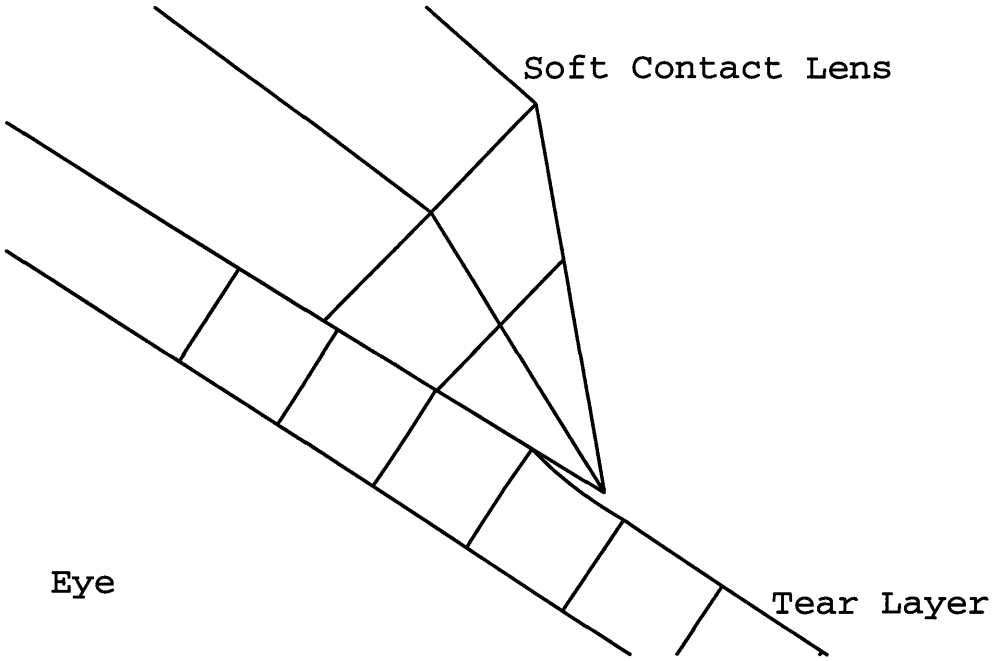

Figure 2.5: Illustration of the end node of the contact lens lifting off the tear layer.

forces the tear layer to maintain contact with the lens and the eye once initial contact is made even under a negative gauge pressure condition. As a check towards the validity of this assumption, the magnitude of the contact pressures much be checked to ensure that cavitation is not predicted.

The difficulty with the no separation boundary condition is that although it keeps the nodes of the tear layer in contact with the lens and eye, it does not keep the nodes of the lens in contact with the tear layer. Therefore, the end node of the lens can lift off the tear layer surface. This is illustrated in figure 2.5.

In order to maintain contact between the lens and tear layer at the lens edge, a multi-point constraint (MPC) subroutine was written that constrained the lens' edge node to lie on the piece-wise continuous quadratic surface defined by the front surface of the deforming tear layer. The coordinate of the lens' end node is monitored continually in the x-direction and the y position is calculated such that the node lies on the tear surface. The coordinates of the tear layer surface were obtained through a passive user element with zero stiffness that was defined over the contact region of the tear layer. The coding of the user subroutine is provided in Appendix A.

There were some convergence problems when the edge of the lens passed directly over a node in the tear layer. In this case, not only was there a transition between the constraining MPC equation, there was also a conflict between the MPC subroutine and the no separation boundary condition. To ease this problem, the convergence criteria were temporarily relaxed for one increment to allow for the transition. This meant that the maximum allowable ratio of the largest residual to the corresponding average flux norm was set to $5 \cdot 10^{-2}$ from the standard value of $5 \cdot 10^{-3}$. Once the transition region was cleared, convergence criteria were reset to the normal default values.

2.3.3 Global Boundary Conditions

As a final boundary condition, a constraint was imposed in the radial direction at the center of rotation of the model against any displacements. This condition applied to all components of the model. The boundary condition was applied to model the axisymmetric symmetry of the geometry and loading. To ensure a unique solution, a reference point and frame had to be taken. The rigid eye was chosen as the reference frame, and it was constrained against all motion and rotation.

2.4 Loading Procedure

With the model of the contact lens on the eye with a lubricating tear layer developed, the final quasi-equilibrium solution must be found. To achieve this final stress state, a sequence of steps is taken. All steps in the analysis are based on non-linear analysis with linearly elastic material behavior with the exception being the final step, where the time dependent viscoelastic behavior of the tear layer occurs. Once an equilibrium position is found based on the linearly elastic material properties, then the viscoelastic analysis commences which allows for relaxation or flow of the tear layer. This ensures that a unique, elastic equilibrium starting point is found for the time dependent step of the analysis.

The loading procedure can be broken up into three main stages. The first stage involves positioning the tear layer on the eye. During the second stage, the contact lens is brought into contact with the tear layer. Finally, the third stage allows for the viscoelastic flow of the tear layer. Each stage will be considered in sequence.

To achieve full contact of the tear layer with the rigid eye, the tear layer was first given a rigid body displacement so that initial contact was just achieved. This had to be done slowly as the tear layer in its undeformed shape had the same geometry as the eye. This means that the nodes on the back surface of the tear layer will come into contact with the eye at the same time. Convergence of a solution with hundreds of nodal changes in contact state is not robust and must be achieved through very slight incremental displacements. Once the tear layer has come into contact with the eye, a negative suction pressure is applied between the eye and the back surface of the tear layer to ensure complete contact along the entire length of the interface. Once full contact is achieved, the constrained displacements and distributed loads applied to the model are removed and the system is allowed to achieve an unconstrained equilibrium state.

To position the soft contact lens on the tear layer, the first few steps taken are very similar for positioning the tear layer on the eye. First, the end of the lens is brought down past where the point of equilibrium is expected to lie. This brings the central section of the lens into contact with the tear layer although the end of the lens remains positioned away from the tear layer. Then a suction pressure is applied in between the lens and the tear film to achieve complete contact along the central back surface of the lens.

Normally, the end of the contact lens lifts off of the tear layer slightly with no constraints holding it down as shown previously in figure 2.5. To fix this, the end of the lens is displaced such that it just comes into contact with the tear film. Additionally, suction pressures are applied so that the lens is in full contact with the tear. As mentioned previously, the no separation boundary condition that is applied to the interface only constrains the nodes of the tear layer. This means that the end of the tear layer can still lift off the tear film. Thus, the MPC discussed earlier is applied so that the end of the lens lies on the piece-wise continuous upper surface of the tear layer. With full contact achieved along the back surface of the soft contact lens, constraints are released and the system can reach a unique final elastic equilibrium condition.

Once the system has reached an equilibrium position, the time dependent section of the analysis can take place. Here, the tear layer exhibits the stress relaxation mechanism of viscoelasticity. The model 'relaxes' for 6 time constants or 0.3 seconds. At the end of this

step, the lens is at a unique quasi-equilibrium state and the stress state of the system can be investigated.

As a final state has been reached, the investigation can focus on the results of the simulation. In particular, quantities like tear film thickness distribution, pressure distribution through the tear layer, plus bending and stretching stresses in the contact lens are observed. The results and their implications to the contact lens mechanics are discussed in the following chapter.

Chapter 3

Verification of the Model

3.1 Introduction

Any numerical model must be shown to have physical significance before the results are of any real value. This is a critical issue when considering the current model. This is also a challenging issue to address given the limited scope of reliable physical results pertaining to the mechanics of soft contact lenses. With few reliable physical results and no detailed results, numerical modeling is indeed challenging to validate. Thus, numerous approaches have been taken to give solid physical support to the results this research has yielded.

Before the model is validated, the standard results of the simulations must be presented and understood. As outlined previously, the primary values being investigated are the interference pressure at the tear/lens interface, the pressure distribution in the tear layer itself, the tear film thickness, and the stress state in the contact lens. Each of these results will be presented and the implications of the results will be discussed.

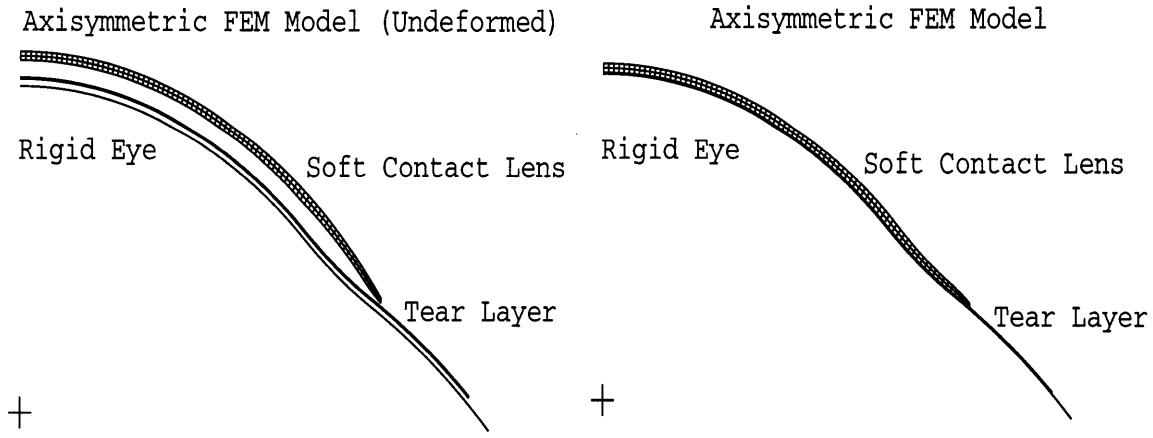

Figure 3.1: Undeformed and Deformed Axisymmetric Model.

3.2 Results from the General Model

Before the stress state of the system is outlined in graphical form, a more general overview of the mechanics of the system will be presented. As in chapter two, the system comprising of the contact lens, tear layer, and the eye is shown in its final deformed shape in figure 3.1. In addition to the final geometric configuration, an appreciation must be given for the general stress state of the system. The Mises stresses of the system are shown in figure 3.2 which reflect the scalar equivalent deviatoric stress in the lens and tear. The deviatoric stresses in the tear film are significantly lower than any of the stresses in the lens so the tear layer, which would be plotted as all one contour color, is omitted. The bending effects can be seen as the dominant deviatoric element in the model through the lenticular region and again at the edge of the lens. This implies that the lenticular and bevel zones will be the most sensitive to changes in the modeling parameters.

Throughout this thesis, bending stresses will often be discussed. The bending stresses are defined as the in plane, or longitudinal stresses at the back surface of the lens minus the longitudinal stresses at the central axis which represent the axial or membrane stresses through the lens. The longitudinal stresses are shown for the contact lens in figure 3.3. Only the end of the lens is shown as the axial stresses through the optical region are approximately constant. This plot is quite similar to the Mises stress plot and thus further

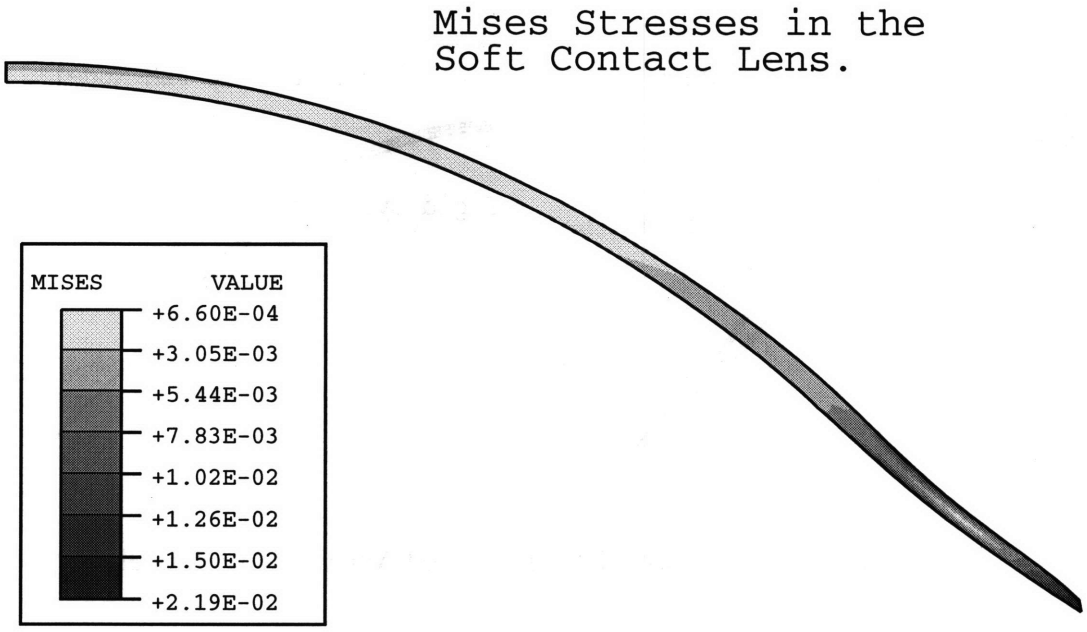

Figure 3.2: Mises stresses in the Contact Lens.

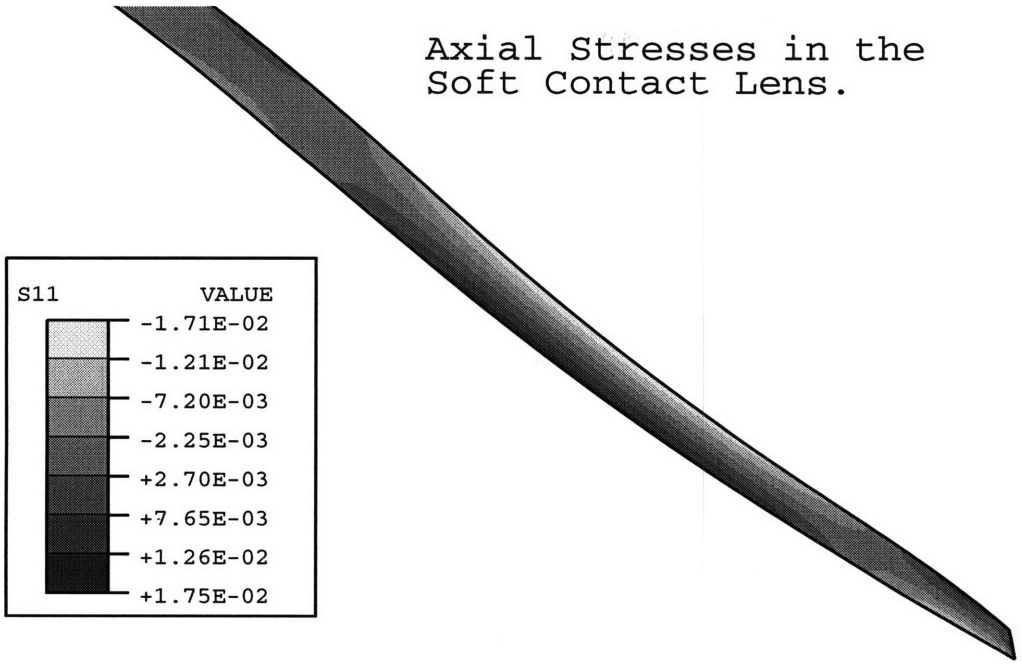

Figure 3.3: Axial (longitudinal) Stresses in the end of the contact lens.

supports that the bending stresses are the dominant factor in the contact lens mechanics. With this general overview of the system done, a more specific graphical analysis will be discussed.

The interface pressure between the soft contact lens and the tear layer is shown in figure 3.4. For this graph, the x-axis is the arc length distance from the apex of the lens measured in millimeters along the mid-plane of the lens. The y-axis shows the interface contact pressure and this is in units of kPa. The contact pressure is defined as the traction normal to the interface. A positive contact pressure refers to a force directed towards the tear layer. Thus a positive contact pressure results in a reduction in the tear film thickness which would reflect a compressive pressure on the tear layer. With the no separation boundary condition simulating the tear film surface tension effects, negative contact pressure acts as a suction on the tear layer, increasing the tear film thickness.

There are a few items to note that are significant to the results provided. A primary point of interest is the magnitude of the maximum pressure applied to the tear layer. As observed from figure 3.4, the interference pressure reaches a maximum value of 0.7 kPa near the end of the lens. The pressure near the lens apex is about 0.1 kPa. Also of interest is the largest contact pressure gradient which is approximately 3 MPa/m.

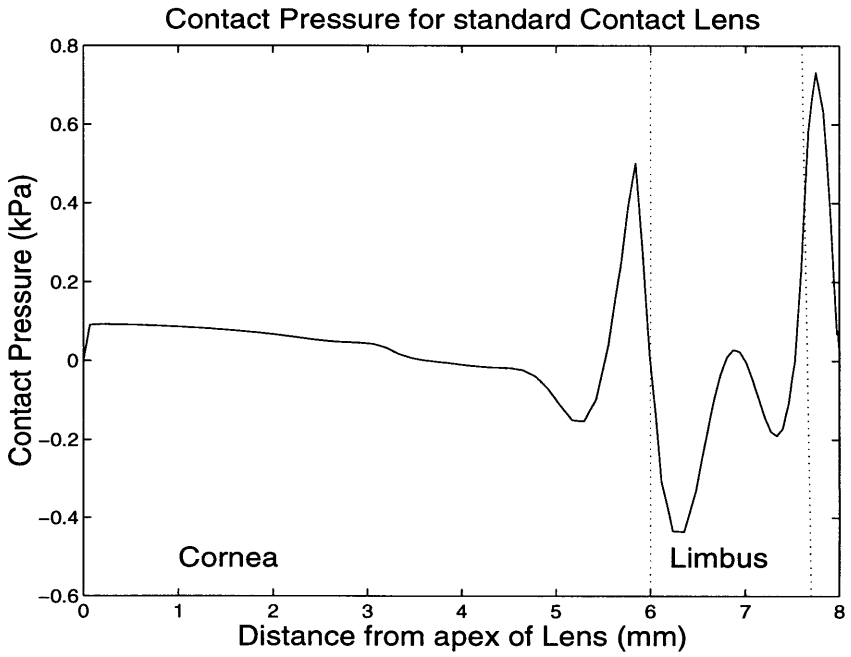

Figure 3.4: Graph of the Contact Pressure at the tear/lens Interface.

It should be emphasized that the fact that there is a pressure gradient through the tear layer is not a surprise. To achieve near conformity of the lens to the eye surface, a pressure gradient must exist through the tear layer. As the initial geometry of the lens is quite a different shape compared to the eye geometry, no one uniform pressure could be applied across the back surface of the lens to achieve this new shape. The only way this could be achieved is if the contact lens rested directly on the eye surface [16] or if the lens lifted off the eye enough so that it could return to its undeformed geometry.

As an interesting comparison to the interface contact pressures, the mid-plane pressure of the tear film is provided in figure 3.5. The axes of the graph are identical to the previous graph. Although the general trends are similar, the magnitudes of the mid-plane pressure are lower. The maximum pressure predicted is approximately 0.3 kPa and the largest pressure gradient is only 0.4 MPa/m. The pressure term is defined as one third the trace of the stress tensor. Ideally, for a fluid system in equilibrium (a state not reached here as there is only quasi-equilibrium due to the pressure gradient), the two reported values of interface contact pressure and mid-plane pressure should be the same as the fluid is in a state of hydrostatic pressure. Although in the simulations the shear modulus is reduced to 1000 times less than the bulk modulus, the tear film seems to still be supporting a significant

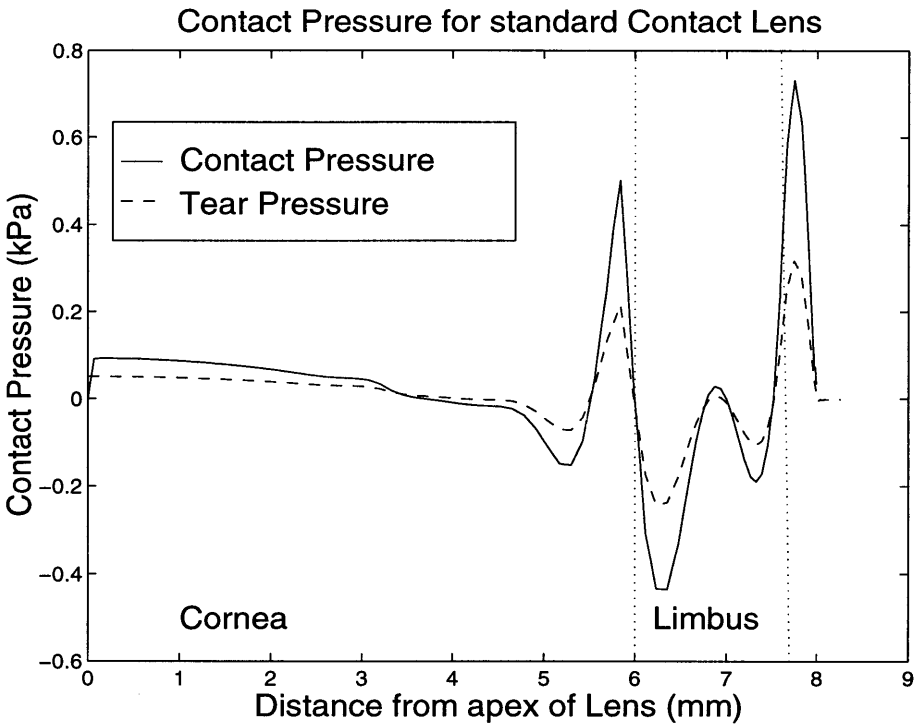

Figure 3.5: Comparison of the tear film pressure and the contact pressure at the tear/lens interface.

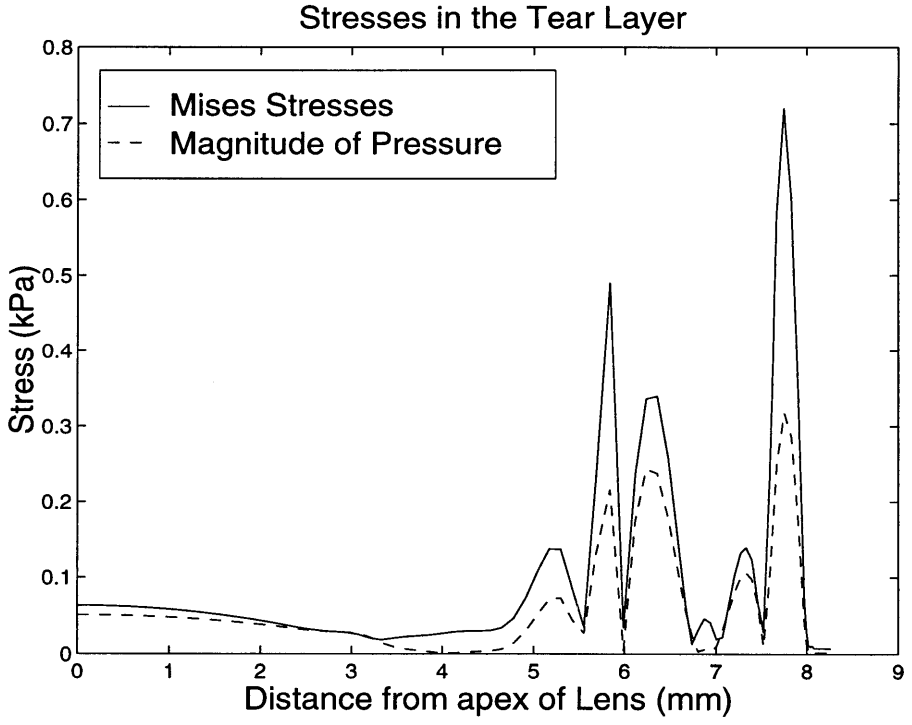

Figure 3.6: Comparison of the Mises Stresses and the Magnitude of the Pressure in the Tear Film.

amount of shear. In fact, through the tear film, the Mises stresses are on the same order and generally, even larger than the pressure readings (figure 3.6).

Unfortunately, reducing the shear modulus even further than the given amount did not appear possible. Attempts to further reduce the shear modulus resulted in convergence problems. As developed in chapter two, the shear modulus is reduced through the Prony series representation of the modulus in the viscoelastic analysis of the simulation. As the resistance to shear is reduced, the material becomes more compliant compared to the contact lens as the shear modulus is proportional to Young's modulus. This means that the stiffness of the two elements become dramatically different. This large difference in the stiffnesses is likely the leading reason for the convergence problems as it makes the problem ill-conditioned.

With the recognition of this discrepancy, it thus becomes important to identify which of these two quantities would be most representative of the pressures measured in an experiment similar to the one conducted by Martin and Holden where pressure taps are used to get a pressure reading. It seems reasonable that the mid-plane tear film pressure would best reflect the actual pressure in the system. This will compensate somewhat for the slight increase in the shear stress supported by the tear layer and give a more average pressure result.

The tear film thickness is the next value of interest and the results are plotted in figure 3.7. The vertical axis gives the tear film thickness in microns and the horizontal axis gives the arc length distance from the apex of the lens in millimeters. It should be noted that although the tear film thickness variations look severe, this is largely due to the increased magnification of the vertical axis with respect to the horizontal axis.

In comparing the tear film thickness to the tear film pressure distribution, there is a very useful correlation that appears to apply. From a visual inspection, it appears that the tear film thickness is a direct function of the pressure distribution. To investigate this further, a least squares approximation was done to match the pressure distribution to the displacement of the tear layer. The results of this investigation are found in figure 3.8. From this graph it does appear that the tear film thickness can be represented as a linear function of the pressure distribution. In this case, the correlation coefficient is -9.84. This presents

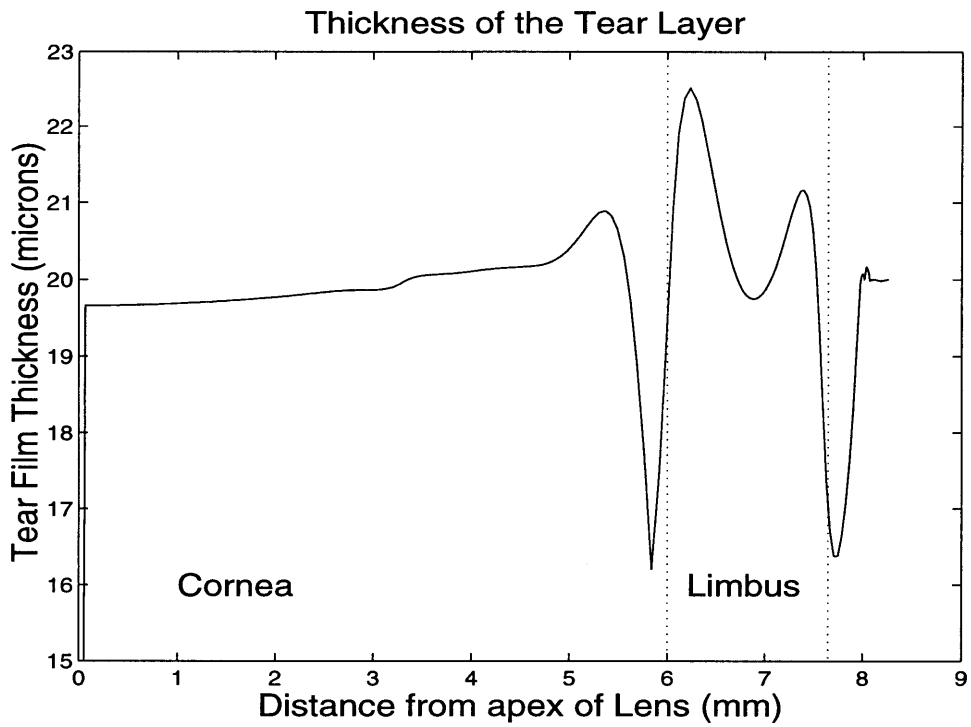

Figure 3.7: Graph of the tear film thickness distribution.

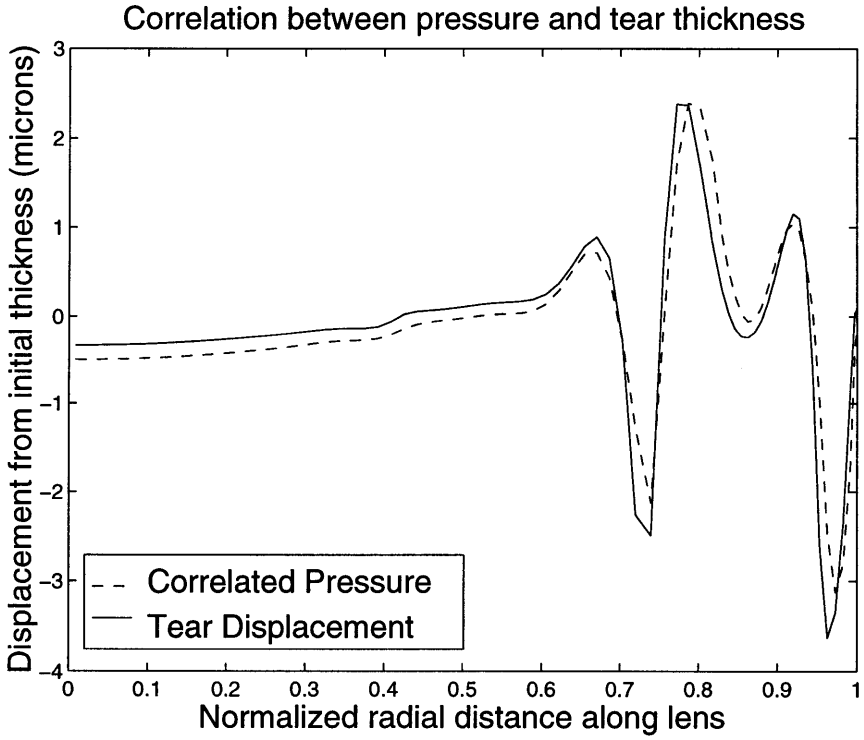

Figure 3.8: Correlation between the tear film pressure reading and the tear film thickness.

some significant potential as if it were possible to measure the tear film thickness under the lens, this might give an indication towards the stress state of the system. It should be emphasized that the correlation appears to be between the pressure in the tear film and the change in tear film thickness. If the initial tear film thickness is not constant or not known, then the correlation becomes much more difficult to determine.

The final parameter to be discussed here is shown in figure 3.9 and this graph illustrates the bending and stretching (or membrane) stresses experienced through the contact lens. There are two main features to highlight from this graph. First, near the apex of the lens, the membrane stresses are the dominant stresses. This demonstrates the need to include the membrane stresses in determining the lens mechanics. Throughout the optical zone, the difference in initial curvature between the contact lens and the eye is very small. This means that the bending stresses are going to be small and thus, the membrane stresses will dominate. The membrane stresses are not, however, the dominant stresses near the limbus. Here, the bending stresses are much larger in magnitude due to the dramatic difference in initial curvature between the eye and the lens. This means there is a transition between the predominant stress in the lens and both are significant to the model.

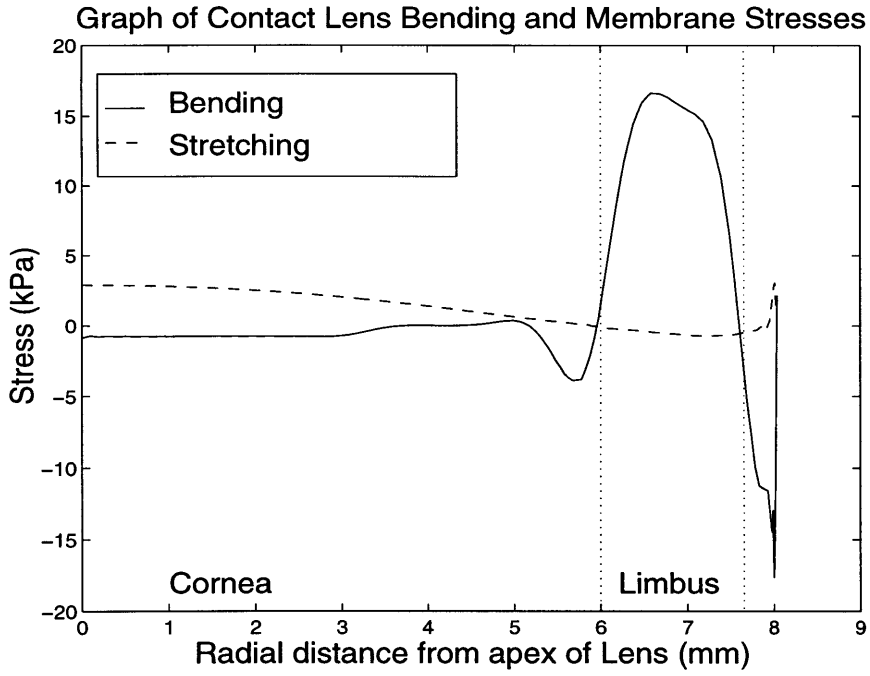

Figure 3.9: Graph of the Bending and Stretching Stresses in the Contact Lens.

3.3 Verification of the Results

There are four methods that will be discussed in this chapter to verify the results of the simulations. First, a simplified closed form solution is discussed to justify the magnitude of the pressure distributions and the pressure gradients predicted in the tear layer. Then, a comparison will be done against previously developed models found in the literature to show similar predicted results over a certain range of the solution. Third, a comparison will be done between the simulation and physical results observed by Martin in previous work done. Finally, a sensitivity analysis will be done to investigate how the model responds to changes in the given material and physical parameters. These methods give a solid level of confidence that the results are physically significant and that they accurately represent the proposed physical system of a contact lens resting on the human eye.

To get an initial indication that the model is producing realistic results, an estimation of the quasi-equilibrium flow rates was performed. Due to this, the lens was considered as a thin disk and the tear layer was treated as a thin film with a radial pressure gradient. By this definition, the problem becomes the classical Poiseuille's flow problem. The derivation is provided in appendix B. From this solution in cylindrical coordinates, the radial flow is given by the expression:

$$Q = \frac{\pi h^3 (P - P_o)}{6\mu \ln (R_o / r)} \tag{3.1}$$

where h is the tear film thickness, $(P - P_o)$ is the pressure difference, μ is the fluid viscosity, R_o is the reference radial distance and r is the position under investigation. Considering the most extreme case between the arc distance of 7 mm and 8 mm, the tear film thickness was taken as 18 μm and the pressure difference as 0.3 kPa. The tear viscosity is $8 \cdot 10^{-3}$ Pa•s as reported in the work of Tiffany[25]. Based on these calculations, the radial flow was estimated to be $8.6 \cdot 10^{-10}$ m^3/s or approximately 0.05 mL/min. This yields a flow velocity of 0.9 mm/s. This seems large and suggests magnitudes of the pressure spikes may be higher than would be clinically measured but it is derived from a very simplified analysis. The model assumes negligible changes in tear film thickness and it assumes a newtonian fluid which is not present in the real situation. Both of these assumptions render the model less accurate so results should only be taken as an order of magnitude estimate.

This analysis supports the no friction boundary condition applied. Based on the calculation, the shear stress on the wall is given by:

$$\tau_w = -\frac{h(P - P_o)}{2r\ln(R_o/r)} \tag{3.2}$$

Based on the given values, the estimated shear stress is 5 Pa. This value is not significant and therefore, the zero friction boundary condition should be applied to give the proper boundary conditions for the stress state of the soft contact lens.

As a second means of verifying the simulation results, a comparison was done against results published by Jenkins and Shimbo[2]. In this paper, Jenkins and Shimbo estimated a theoretical post lens pressure distribution based on membrane stresses over the entire length of the lens and complete conformity of the lens to the shape of the eye. Although the FEM simulations allow for bending stresses and generally do involve a lubricating tear layer, a comparison was done to observe how well the simulations matched the theoretical results.

The results from this verification test near the apex of the lens were encouraging and are shown beside the results of Jenkins and Shimbo in figure 3.10. The simulation used the

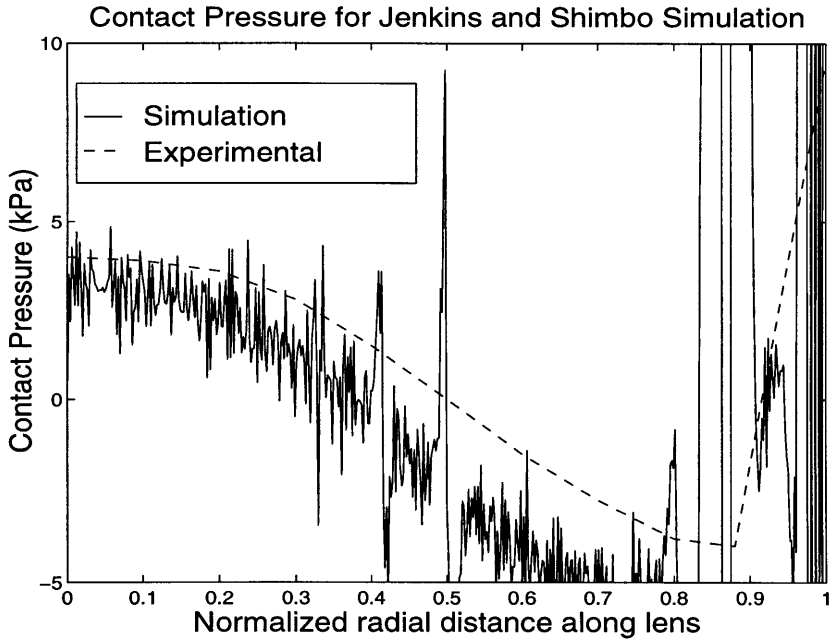

Figure 3.10: Comparison between Simulation's predicted contact pressure and the Theoretically determined results of Jenkins and Shimbo.

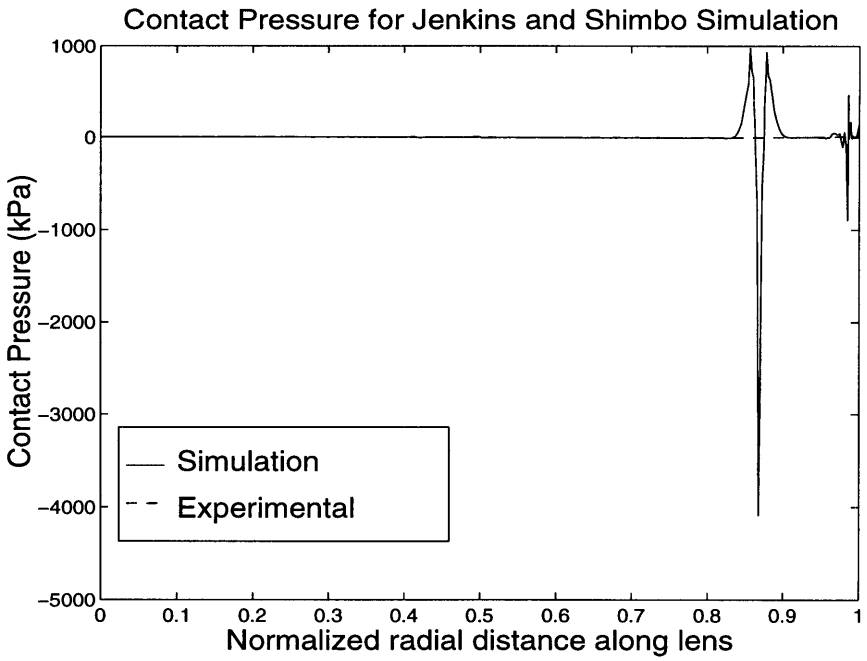

Figure 3.11: Contact Pressure for Jenkins and Shimbo Simulation.

same geometry as reported in the paper and no tear layer was included in an attempt to accurately replicate the results. Although there is significant noise in the numerical results based on hard contact of two solid bodies, the graphs are very similar. The maximum pressure at the apex is predicted to be about 3.5 kPa from the simulations and Jenkins and Shimbo calculated the value to be about 4.0 kPa.

In addition to lending credibility to the results of the simulations performed in this investigation, insight was gained into the significance of the bending stresses in the contact lens. Although the results compare well through the optical region, the results are very dissimilar through the lenticular region where bending stresses were expected to be a dominant factor. Here, Jenkins and Shimbo estimated the maximum negative pressure of 4 kPa where the numerical simulation predicted 4 MPa (see figure 3.11). The reason for this significantly higher value is based on the conformity of the lens to a sharp bend in the eye. This value predicted by the numerical simulation holds no physical meaning as it simply reflects the first order numerical discontinuity in the eye geometry. The simulation still illustrates, however, the dramatic need for the model to consider bending stresses in the lens as a significant factor in the model.

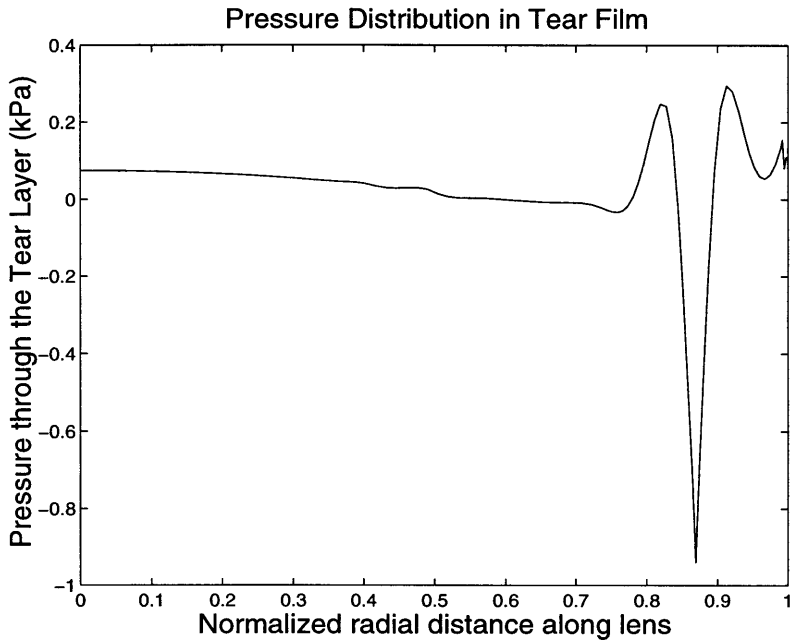

Figure 3.12: Pressure Distribution in the tear layer for the Jenkins and Shimbo simulation with the addition of a 20 μm tear layer.

The FEA model was also able to illustrate the need for including a tear layer in the simulations. An additional simulation was run with the Jenkins and Shimbo geometries with a 20 μm tear layer. With the tear layer, the pressure distribution through the tear layer decreased dramatically (figure 3.12). The maximum pressure was reduced from 4 MPa to less than 1 kPa. This demonstrates the significance the lubricating tear layer plays in the soft contact lens mechanics.

As a third verification check, results were compared against the physical results obtained by Martin and Holden. In this experiment, as described previously in chapter one, an eye was made out of PMMA with pressure taps drilled into it and the pressure distribution behind the lens was measured.

Unfortunately, these results do not provide an ideal comparison. As the resolution is very low for the physical results, verification can only be done on an average basis. The slight increases in pressure detected by the numerical model would not likely be seen in a model where the pressure tap is 0.75 mm in diameter. Sensitivity would have to be on the order of 0.1 mm to get an accurate picture of the characteristics the numerical model predicts.

The results of Martin and Holden are also difficult to match due to the method used to obtain the values. A pressure of 3.9 kPa was applied to the lens for a period of over a minute. Although the pressure used reflected the force applied to the lens by the eye lid, the eye would rarely apply those pressures over such a prolonged period of time. With the continually applied force, the tear film thickness under the lens would presumably be reduced further until the tear film thickness was very small. As will be shown later in the parametric study of modeling assumptions, the model is very sensitive to tear film thickness. If Martin and Holden have set up conditions where the tear layer is much thinner than the normal physiological case, the pressure readings would be expected to be much higher than normal.

There is also some concern towards the reported material properties of the contact lenses used. The elastic modulus for the high water content lenses used from CIBA/Vision were reported as 0.8 MPa. The elastic modulus for the 38% water content lenses used by Martin and Holden were reported to be 0.16 MPa and the elastic modulus for the 70% water content lenses were reported to be 25 kPa. These values seem very low. Although these values were used in these simulations, if they are significantly lower than the actual physical properties of the lenses, then the simulations will predict much lower pressure readings than the results obtained through the experiments.

In the experiment, Martin and Holden measured a pressure of approximately 90 kPa for the selected lens. Although this pressure decreased slightly towards the edge of the lens, this drop was not very significant. The tear film pressure distribution obtained by the simulation of the Martin and Holden experiment is shown in figure 3.13. The results obtained were significantly lower than the reading obtained in the physical experiment. A negative pressure of 5 Pa was recorded at the apex of the lens with the simulation where Martin and Holden reported values of 90 Pa. Although these results do not compare well in magnitude, the trends observed with the simulations compare well with the experimental results. The negative pressure reading is a maximum at the apex of the lens and decreases towards the limbus. Based on the 0.75 mm resolution of the pressure readings, the increased pressure readings near the limbus would not show up and the average reading would stay roughly constant through this region. If a larger elastic modulus was used

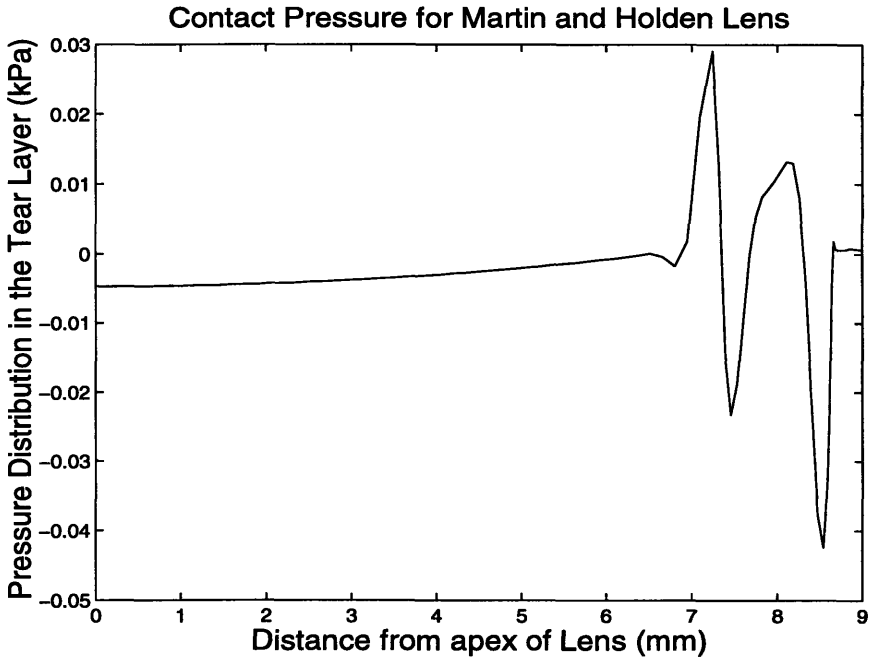

Figure 3.13: Tear Film pressure distribution from the simulation of the Martin and Holden experiment.

and the tear film thickness was reduced as might better reflect the initial conditions obtained in the experiments, it is expected that the results would match more closely.

3.4 Parametric Study of Modeling Assumptions

As a final step towards the validation of the numerical model, a sensitivity analysis was performed to investigate how the model responded to variations in the given parameters. The motivation for this was to see how slight errors in the given parameters might affect the results provided by the simulations. This is of particular interest as the model is somewhat ill conditioned due to the difference in stiffness between the contact lens and the tear layer. The parameters that have been investigated were 1) the effect of no tear film, 2) the effect of variations in tear film thickness, 3) the effect of the uniform tear film assumption, 4) the impact of the initial shear modulus of the tear layer, 5) the impact of the time of relaxation allowed for the viscoelastic tear layer, 6) the effect of the eye geometry, and 7) the effect of adding viscoelastic material properties to the hydrogel lens. For each simulation, all material and geometric properties were kept constant from the general model with only the specific parameter being changed.

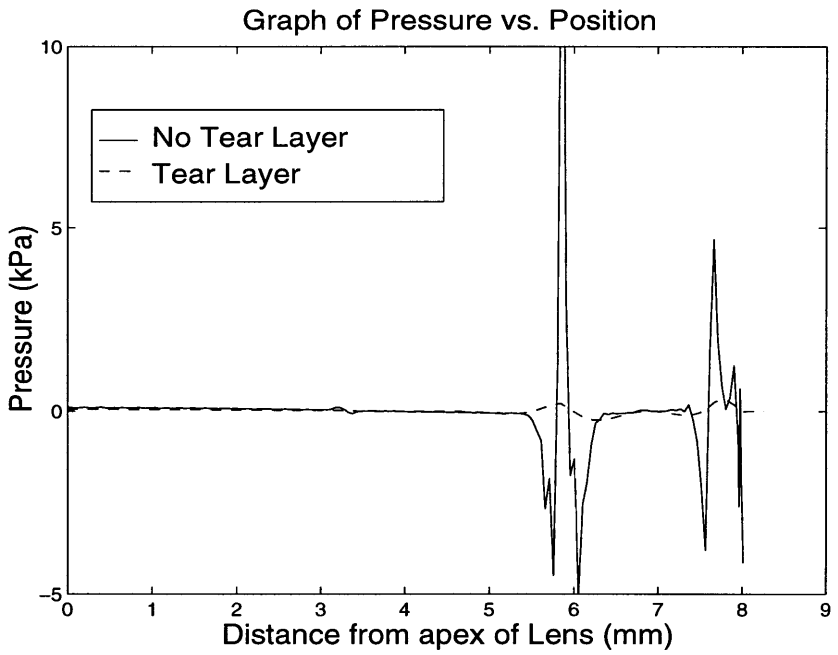

Figure 3.14: Effect of No Tear Film on Contact Pressure Distribution.

3.4.1 Effect of no Tear Layer

Removing the lubricating tear layer had the most dramatic effect on the results of the simulation. The interfacial pressure distribution between the lens and the eye with no tear layer is compared with the original pressure distribution in figure 3.14. In comparison with the pressure distribution predicted for the lens with a lubricating tear layer, the pressures exerted near the limbus are dramatically higher. One assumption that has been given for the previous mechanical models of a soft contact lens on the eye is that since the tear layer is thin, it should have negligible effects on the forces acting on the contact lens. Even the bending stresses in the contact lens itself are higher for the case of no tear layer as shown in figure 3.15. As the tear layer does have a dramatic effect on the overall mechanics on the lens, both at the interface and over the general stress state of the lens, incorporation of the tear layer must be an important aspect of any realistic model.

3.4.2 Effect of Initial Tear Film Thickness

To further investigate the impact of variations in the tear layer geometry, simulations were performed with initial tear film thicknesses of 10, 20 and 40 microns. For these simulations, the tear films were of uniform thickness over the entire cross section of the eye. The range of 10-40 microns reflected the various tear film thicknesses that have been

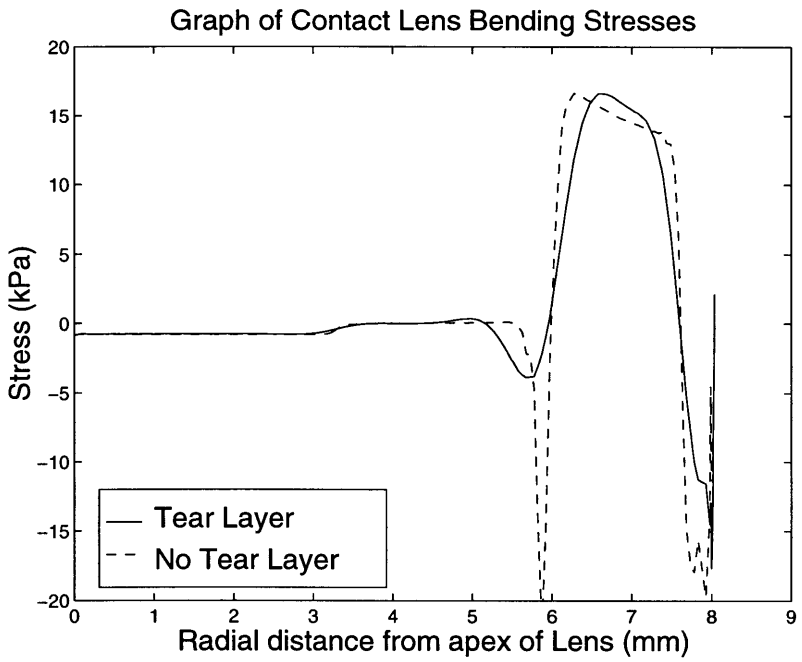

Figure 3.15: Effect of No Tear Layer on the Contact Lens Bending Stresses.

quoted in the literature as noted previously. The results with respect to the pressure distribution in the tear film are shown in figure 3.16. This graph illustrates that as the tear film thickness decreases, the magnitudes of the pressure distribution are amplified. The general characteristics of the pressure distribution are not altered significantly but the absolute magnitude is increased. The bending stresses in the lens are also increased around the limbus and at the edge of the lens for the thinner tear layer as shown in figure 3.17. Thus, not only is the stress distribution through the tear layer affected by the change in thickness but the stress distribution in the soft contact lens is affected too.

This once again emphasizes the sensitivity of the lens to slight changes in the final deformed configuration due to the tear layer. For results to be clinically viable, care must be taken to achieve an accurate representation of the tear layer. This addresses a need for better measurements of tear film thickness. Currently, Holt, Boyce and Hart [30] are investigating tear film thickness and there is a continuing effort to gain a better appreciation for the magnitude of the film depth and distribution.

3.4.3 Effect of Uniform Tear Film Thickness assumption

In the simulations, it was assumed that the tear film was initially at a uniform thickness. It is recolonized that this may not be a correct assumption as the assumption was

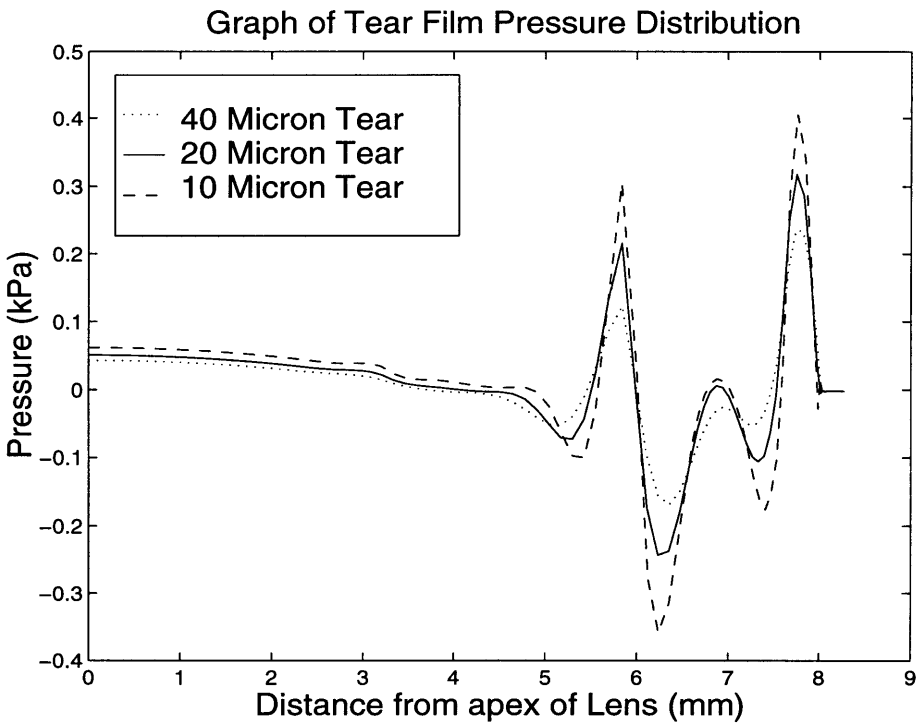

Figure 3.16: Effect of Tear Film Thickness on Tear Film Pressure Distribution.

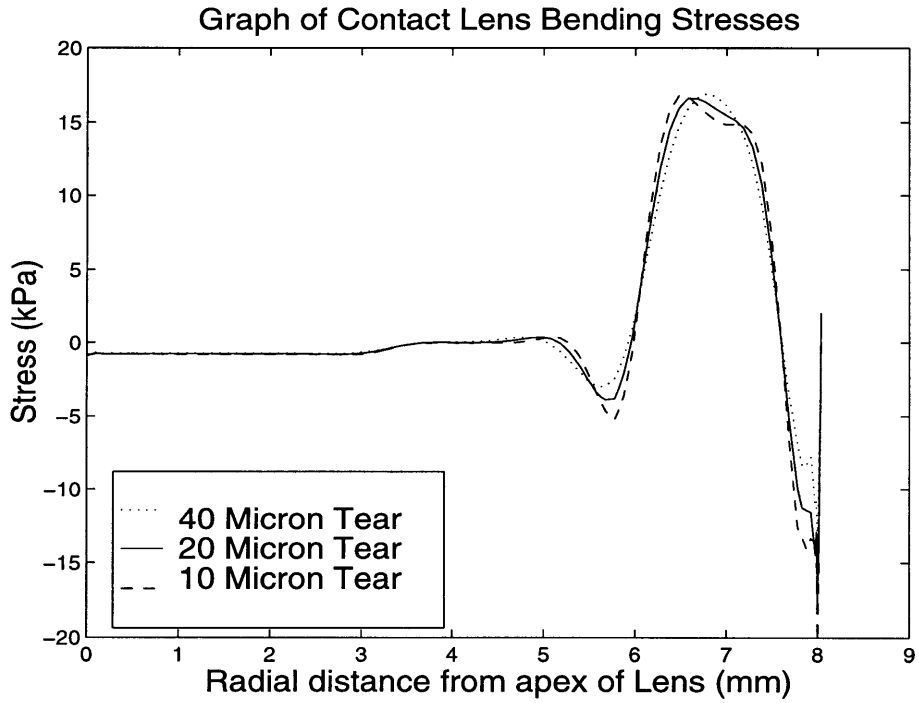

Figure 3.17: Effect of Tear Film Thickness on Lens Bending Stresses.

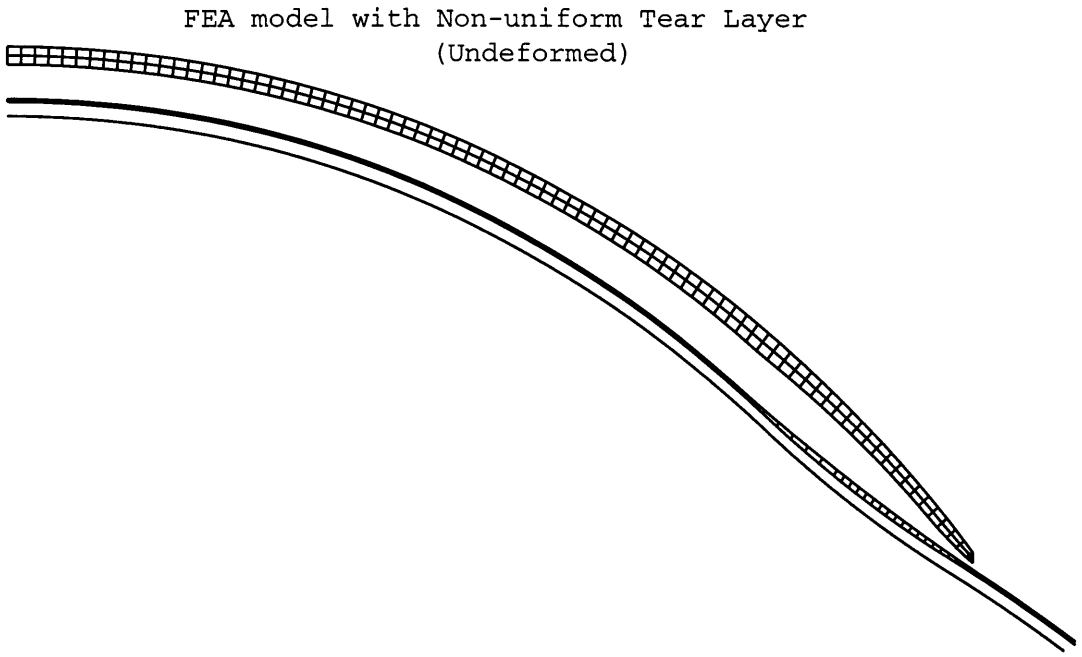

Figure 3.18: Undeformed model of the Non-uniform Tear Film Thickness.

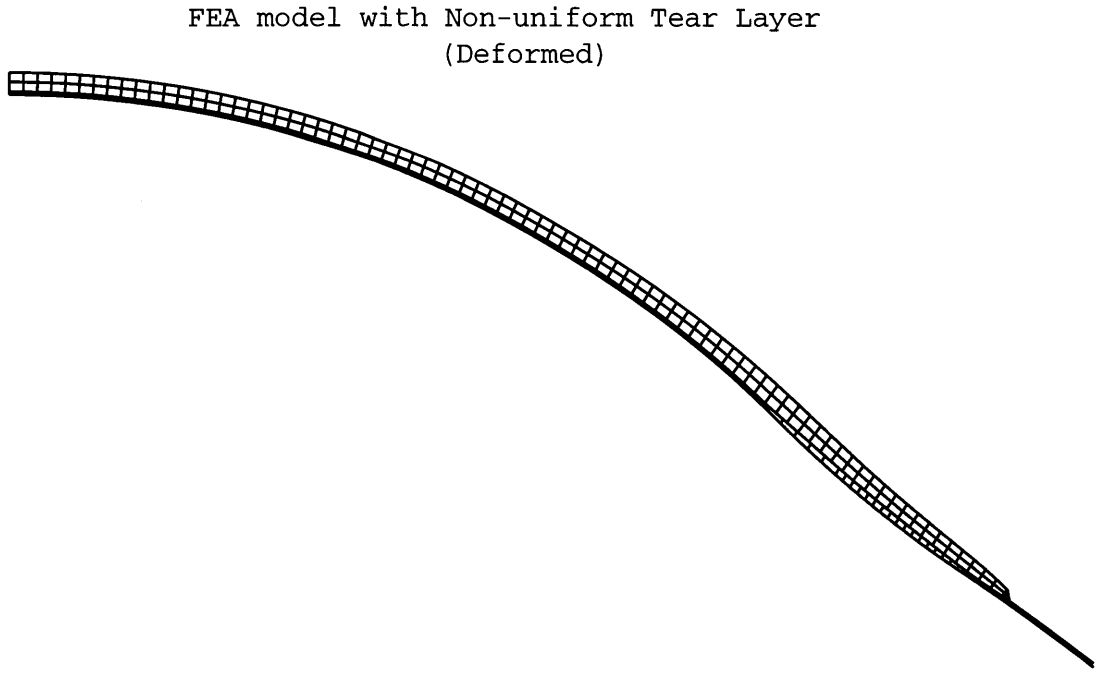

Figure 3.19: Deformed model of the Non-uniform Tear Film Thickness.

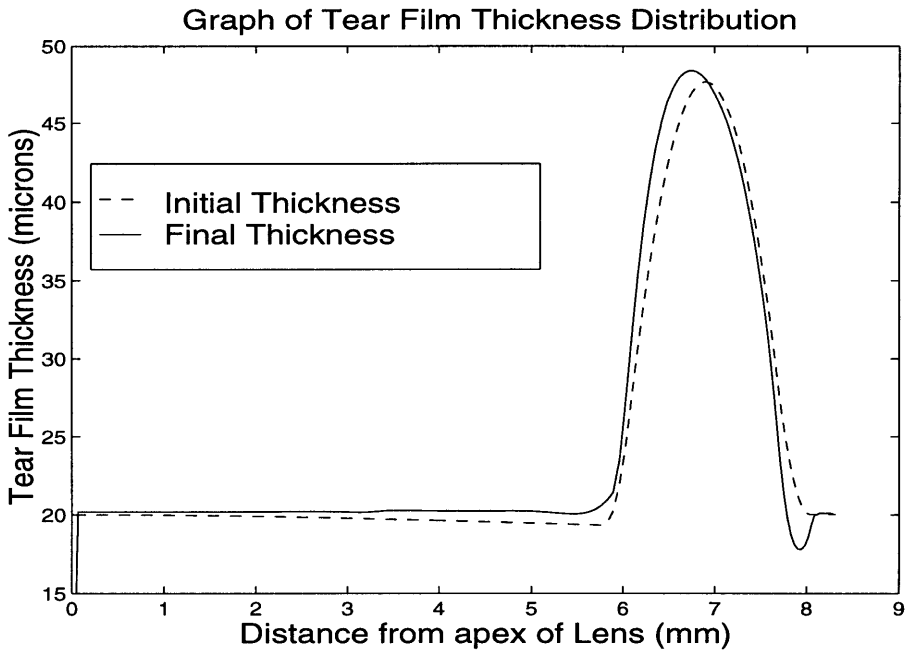

Figure 3.20: Effect of a Non-uniform Initial Tear Film thickness Distribution.

made based on a lack of experimental evidence. It could be hypothesized, that the initial tear film thickness distribution would include a thicker tear layer through the limbus. If this were the case, the pressure distributions predicted would be dramatically different. To investigate this difference, a simulation with a non-uniform initial tear film thickness was run. The undeformed and the deformed geometry of the model are shown in figures 3.18 and 3.19. From this illustration, it becomes apparent that the bending stresses should be less than in the standard initial tear film thickness model. Bending through the limbal region should be less as the len does not have to conform as tightly to the reverse curvature section of the eye. To illustrate the difference between the standard model and the new, non-uniform tear thickness model, the initial tear film thickness and the final tear film thickness are shown in figure 3.20. This graph demonstrates that with the initial increase in tear thickness, the amount of film deformation is reduced.

The pressure distribution for the simulation is shown in figure 3.21. Based on the reduced tear film deformation, it is not surprising that the pressures observed through the lenticular zone are less than the previous simulations. This is primarily due to the decrease in bending stresses in the contact lens (figure 3.22). As the limbus is filled with fluid, the contact lens does not have to conform as tightly to the eye geometry. This decrease in

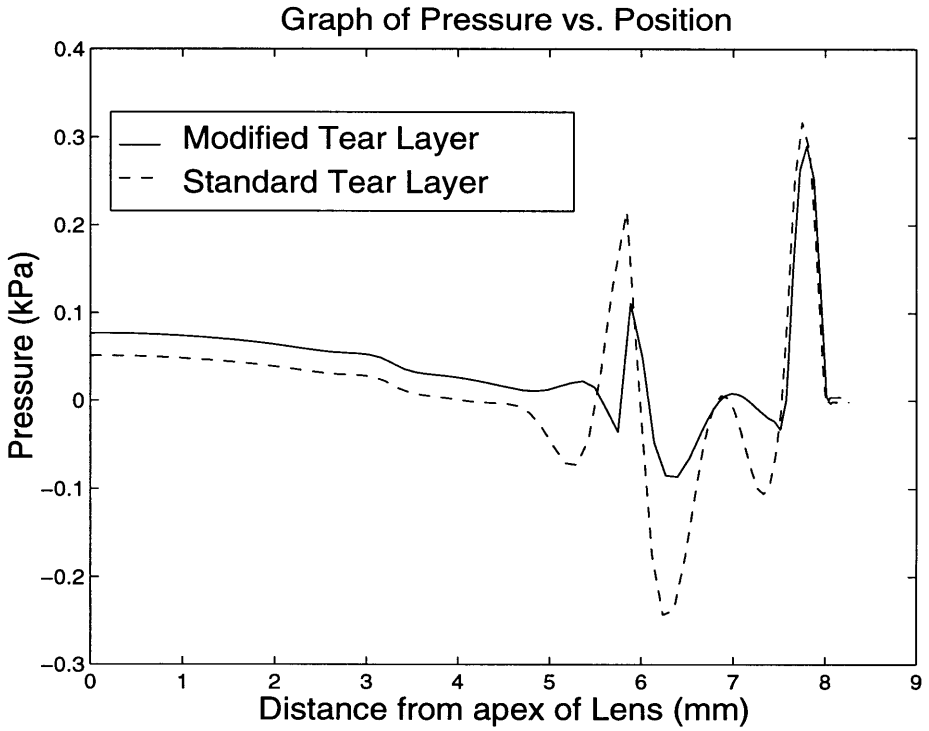

Figure 3.21: Effect of Non-uniform Initial Tear Film thickness on Tear Film Pressure Distribution.

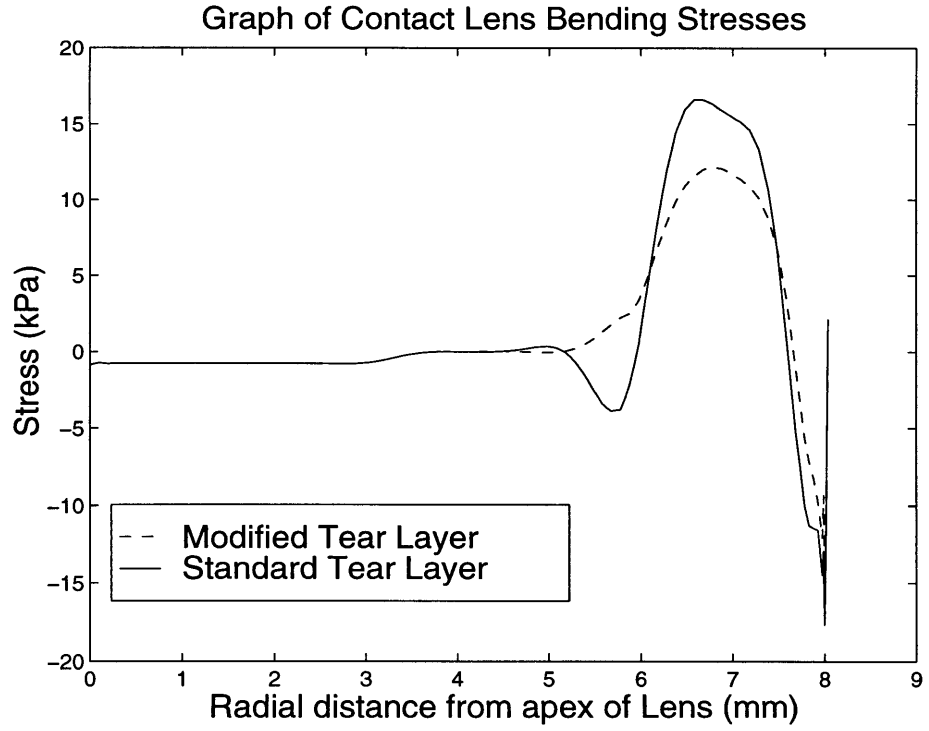

Figure 3.22: Effect of Non-uniform Initial Tear Film thickness on Lens Bending Stresses.

bending stresses through the lenticular region reinforces the above discussion on why the pressure distribution is reduced. This observation emphasizes the need for more accurate *in vivo* measurements of the tear film thickness as this leads to a significant alteration in the results of the simulation. To get the most effective numerical results, more experimental measurements are needed.

3.4.4 Effect of Tear Film Shear Modulus

To investigate the effect of the tear film material properties, a comparison of tear film pressure distributions was done between tear layers of different shear moduli. The shear moduli were taken in the range of 3.34 kPa to 13.5 kPa which corresponds to 100 to 25 times less than the shear modulus for the contact lens material. It should be reiterated that through the viscoelastic section of the analysis, the shear modulus is further reduced by 95%. This means that the shear moduli for the tear fluid range from 2000 to 500 times less than the shear modulus for the contact lens.

As reasonably expected, the simulation with the lower shear modulus demonstrated a greater propensity for stress relaxation and mass flow. Extreme tear film pressures were reduced by up to 75% with a reduction in shear modulus of 75% as seen in figure 3.23. This reduction was only observed where there was a significant pressure gradient. Near the apex of the lens where the pressure gradient is low, there was no significant decrease in the magnitude of the tear film pressure.

This reduction in pressure due to more flow within the tear film can be seen as a greater displacement in the tear film as shown in figure 3.24. An interesting result from the simulations is that the tear film thickness does not appear to scale proportionately with the pressure distribution changes. It was noted earlier that there appears to be a strong correlation between the changes in pressure and the changes in tear film thickness. It should be noted that the stresses will vary differently in the lenticular region compared to the optical region. The reason for this discrepancy is due to the different type of stresses that occur. Through the optical region, membrane stresses dominate so the stresses will vary as a function of the lens thickness. Through the lenticular region, the bending stresses vary as the cube of the lens thickness. This means that the pressures will not necessarily correlate linearly to the deformations in the tear film thickness. In fact, the addition of a cubed term

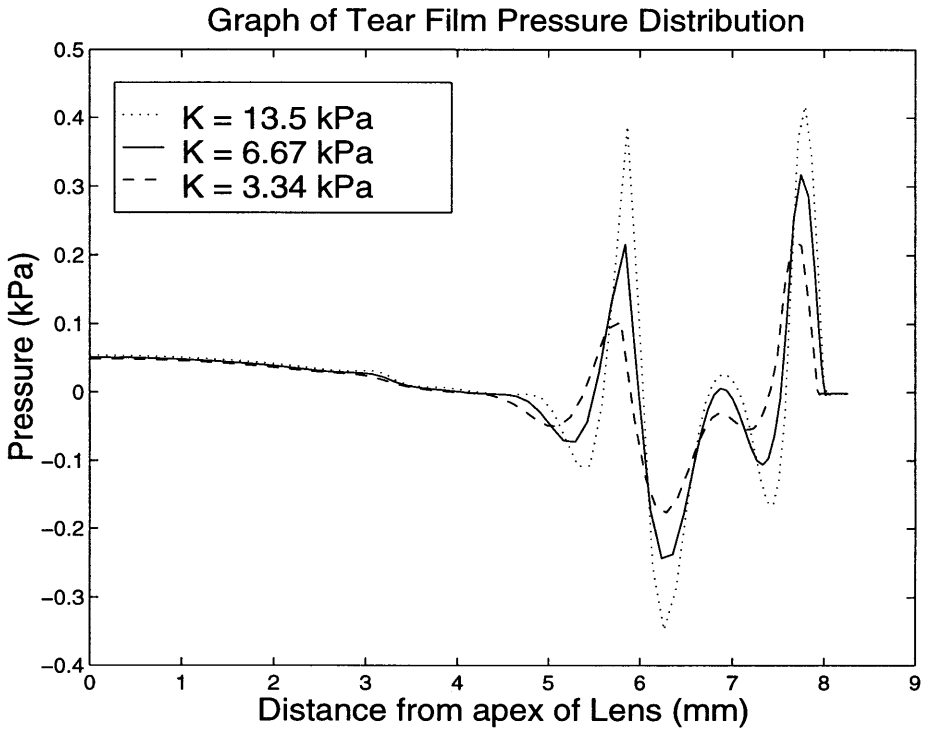

Figure 3.23: Effect of Tear Fluid Shear Moduli on Tear Film Pressure Distribution.

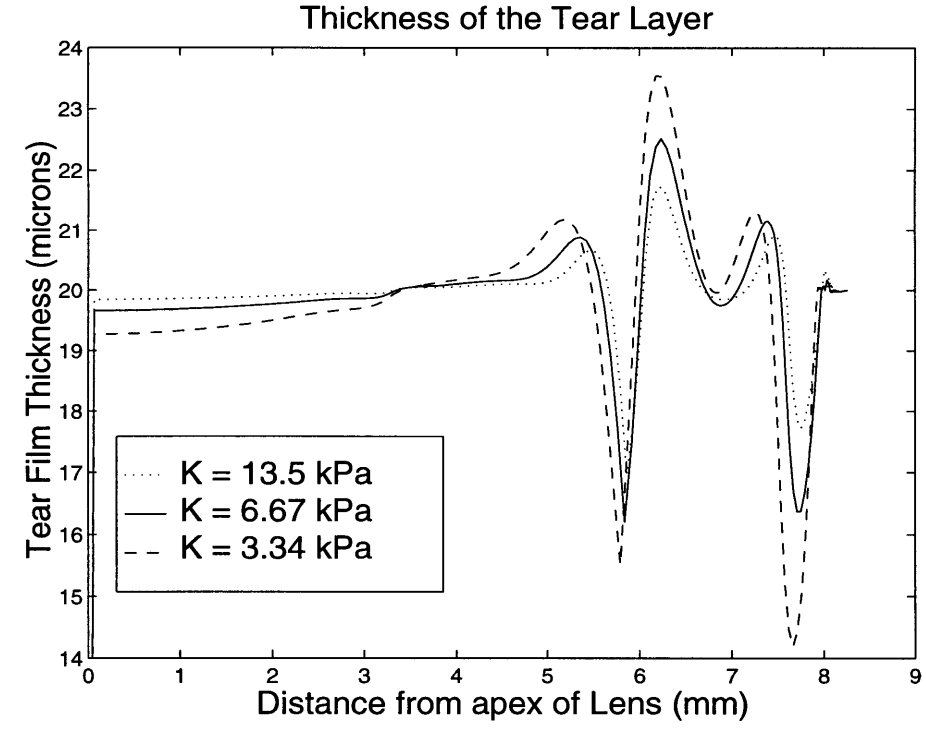

Figure 3.24: Effect of Tear Fluid Shear Moduli on Tear Film thickness.

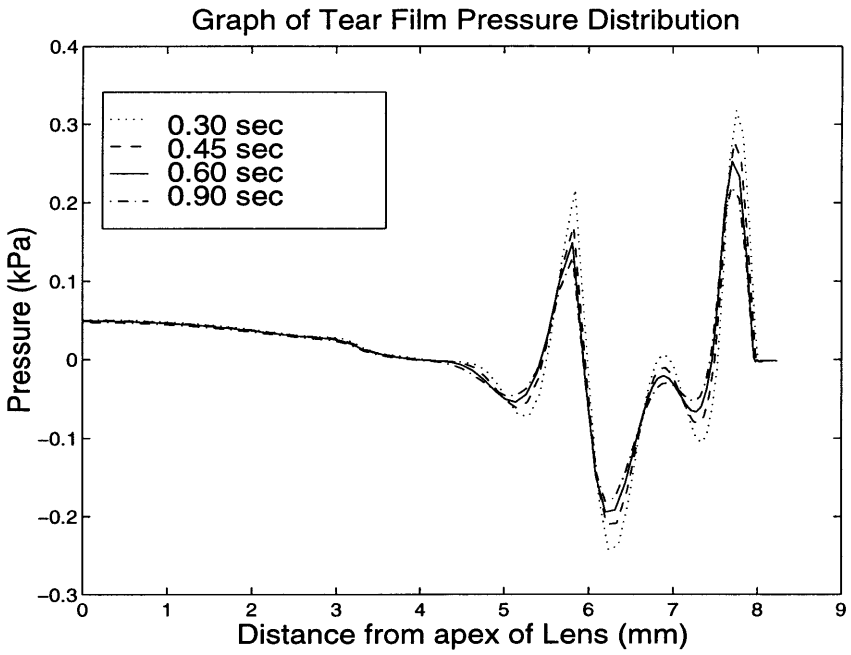

Figure 3.25: Effect of Relaxation Time on Tear Film Pressure Distribution.

may be required to determine an accurate relationship between the tear film thickness and the pressure state in the tear fluid. This result may put into question the validity of the assumed linear correlation and would make experimental correlation more difficult.

Although a further reduction in shear modulus would yield results more representative of a liquid tear layer, the convergence characteristics of the solution become less stable. Convergence was achieved for the shear modulus of 3.34 kPa, but the problem is ill conditioned from the stiffness differential between the tear layer and the contact lens. Thus, as the general trends seem independent of the shear modulus, the mid range value of 6.67 kPa will be used based on superior convergence characteristics. It is acknowledged that the actual tear film pressures might be slightly less than predicted by this model.

3.4.5 Effect of total allowed Relaxation Time

The next investigation that was performed looked at the effect of increased relaxation time to achieve a near equilibrium condition. The relaxation time was initially taken as 0.3 seconds which is six time constants. The relaxation time was further increased to 0.9 seconds or eighteen time constants. The pressure distribution curve is shown for various time constants from 0.3 to 0.9 seconds in figure 3.25. Although most stress relaxation within the tear layer is achieved after 0.3 s, it can be seen from the graph that there was still some

relaxation after the 0.3 s originally allowed. Beyond the 0.6 s mark, however, very little difference is observed in further increases in relaxation time. This suggests that a relaxation time longer than 0.6 s would yield no significant additional information. It would appear that allowing for some additional relaxation time beyond the given 0.3 s would result in more flow in the tear layer. This does, however, become quite computationally expensive. Thus, as most of the stress relaxation has occurred by the 0.3 s relaxation time, this will be used for most simulations. Should more accurate results become necessary, the relaxation time could be increased to 0.6 s.

3.4.6 Effect of Limbal Radius

To get a feel for how eye geometries might alter the mechanics of the soft contact lens resting on the eye, simulations were performed with a limbal radius of 4 mm and 2 mm in addition to the standard 8 mm radius. These values were used to include the range of values used by Funkenbusch and Benson who used a limbal radius of 3 mm[16]. These changes in eye geometry did account for a significant change in the overall shape of the tear film pressure distribution curve as can be seen in figure 3.26. As the radius of the limbus was decreased from 8 mm to 2 mm, the pressure in the tear film at the center of the limbus increased in magnitude to a larger suction pressure. As an interesting contrast to this increase in suction pressure, the compressive stress actually decreased slightly as the radius decreased. It should be noted though that the pressure at the apex of the cornea remains relatively unchanged as the radius of the limbus decreases.

The bending stresses experienced by the lens are shown in figure 3.27. These results illustrate the dramatic increase in bending stresses in the lens as the radius of the limbus decreases. The decrease in radius requires the lens to conform a much tighter curvature and thus the increase in bending stresses through the lens is expected. This does illustrate a concern for contact lens manufacturers; since eye geometry does vary for individuals, this may significantly affect the fit of a contact lens.

3.4.7 Effect of modeling the Contact Lens as a Viscoelastic material

For a final investigation into the modeling assumptions, the contact lens itself was modeled as a viscoelastic material. As stated earlier, the time constant for relaxation is on the order of 5 seconds. As a conservative estimate, the lens was given identical initial

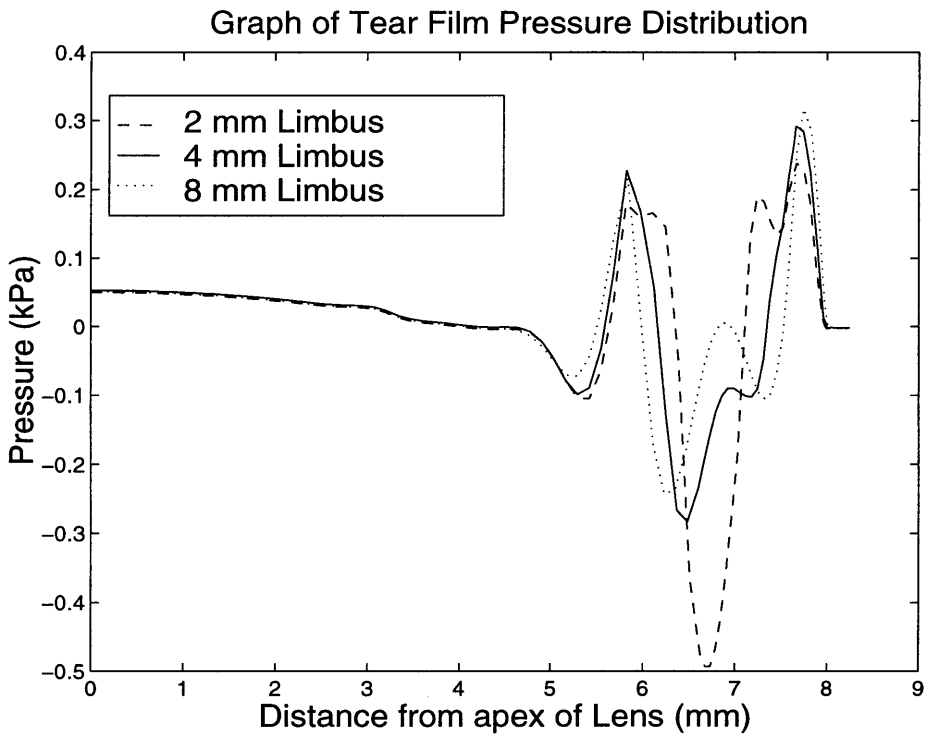

Figure 3.26: Effect of Eye Geometry on the Tear Film Pressure Distribution.

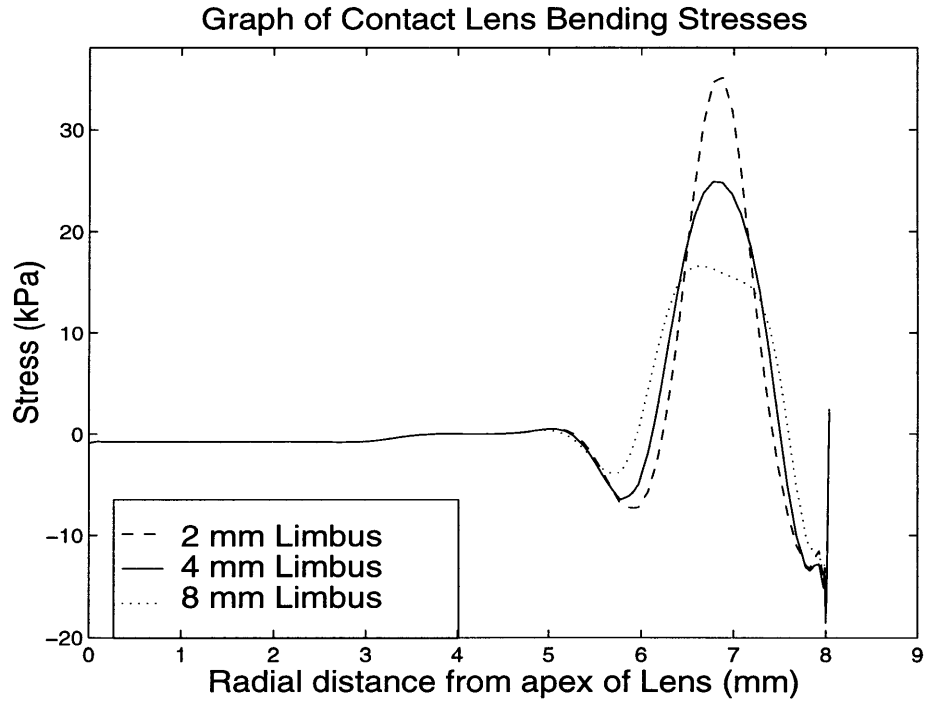

Figure 3.27: Effect of Eye Geometry on Lens Bending Stresses.

material properties with a time constant of 1 second and a relaxation in the shear modulus of 25% from 0.27 MPa to 0.20 MPa. As in previous work, the bulk modulus of the contact lens material was maintained at the initial value of 13.3 MPa.

As expected based on the different time constants for stress relaxation between the contact lens and the tear layer, adding the viscoelastic properties to the contact lens had very little effect on the stress state of the model. As shown in figure 3.28, the pressure distribution in the tear layer remains unchanged between the two simulations. Similarly, the bending stresses in the lens itself as shown in figure 3.29 are unchanged. This strongly supports the previous assumption that the stress relaxation mechanism in the contact lens is not required in an investigation into the initial fit of a contact lens.

The argument that the viscoelastic properties of the hydrogel lens does not claim, however, that the lens' viscoelastic nature will not affect the lens mechanics in the longer term. Blinks are about 5 to 15 seconds apart for the average human eye. At this point, some lens relaxation may occur. Still, it is most likely that the majority of the relaxation will be taken up by the tear film and that the relaxation of the lens will not significantly alter the general mechanics of the lens. This statement will become less true as longer and longer time intervals are investigated.

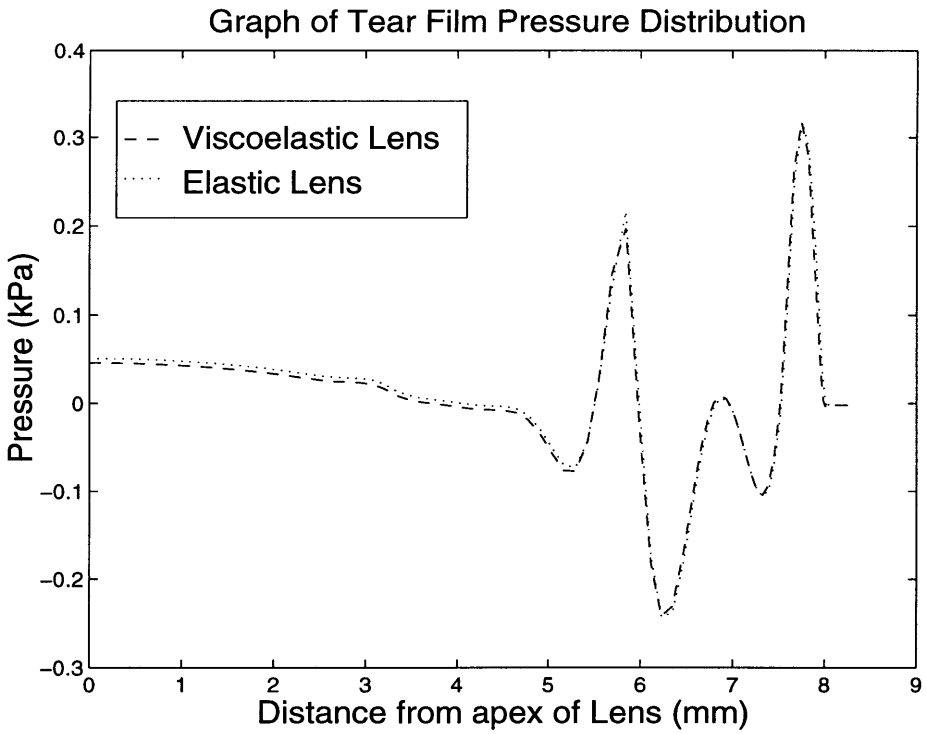

Figure 3.28: Effect of Viscoelastic Lens Properties on Tear Film Pressure Distribution.

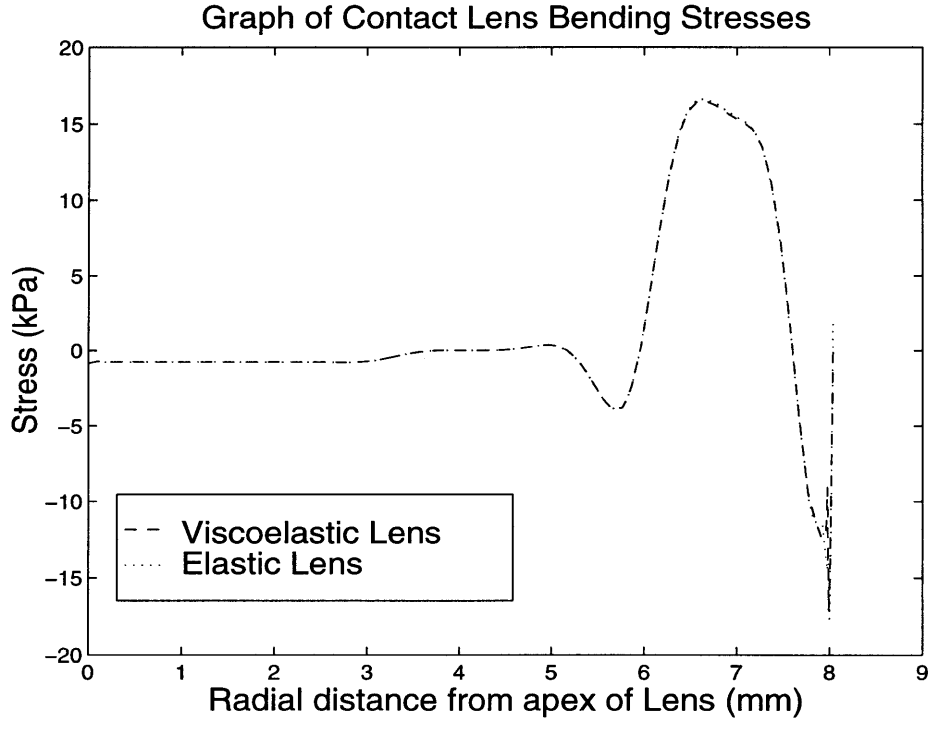

Figure 3.29: Effect of Viscoelastic Lens Properties on Lens Bending Stresses.

3.5 Summary

The discussion above and the presentation of results give a solid basis of verification for the numerical results based on both experimental results and on the parametric study of the effect of modeling assumptions and values. From a purely theoretical basis, the results are shown to be reasonable based on a Poiseuille's flow model. Correlation was shown between a model presented by Jenkins and Shimbo previous published in the literature. Further correlation was shown between the experimental results obtained by Martin and Holden and the numerical simulations. Finally, modeling assumptions were investigated to see how sensitive the modeling parameters are. Dealing with a somewhat ill conditioned system, it is acknowledged that the material and geometric properties of the tear film are critical to achieve realistic results. It has been shown, however that the results do have physical significance and the assumptions seem valid.

With the model fully developed, an investigation can now commence to look at the effect of the lens geometries on the mechanics of the system. This will be the major focus of the subsequent chapter.

Chapter 4

Parametric Study of Lens Parameters

4.1 Outline of Parameters of Interest

The long term goal of this work as stated earlier was to develop a design tool that could help quantify the design process. In an industry that is empirically based, the ability to optimize lens geometries would be a tremendous asset. Thus, to investigate the feasibility of using the FEA model as a design tool, simulations have been run for different lens geometries. The results of these simulations are then analyzed to determine if there are any general indicators that imply a superior fit for the geometries tested.

Based on some clinical research that has been published by Young, Holden and Cooke [8] and Martin *et al.* [26] there were some lens design parameters that have been identified as having a significant impact on clinical performance. The two main factors that were identified as significant by Young, Holden and Cooke were back optic zone radius (BOZR) and back surface design. This effectively translated to variations in sagittal height for the BOZR and investigations into various designs including mono-curve and bi-curve lenses for a fixed sagittal height. Martin *et al.* also investigated lens thickness as a significant factor.

To analyze the geometric design of the contact lens, the goal was to vary different parameters and investigate the mechanical impact. As described in chapter one, the lens has three regions of interest: the optical zone covering the cornea, the lenticular zone over the limbus, and the bevel zone that covers a portion of the sclera. One restriction in modifying the geometry of the lens is that optical properties must be maintained through the optical region for a given diopter lens. In this work, the lenses are all of -0.5 dp as stated earlier.

4.2 Parametric Study of Lens Design

In this investigation, six different lens parameters have been selected for the simulations. It is recognized that these are just a sample of all the potential geometry changes that could be considered. It is hoped, however, that these modifications will demonstrate the

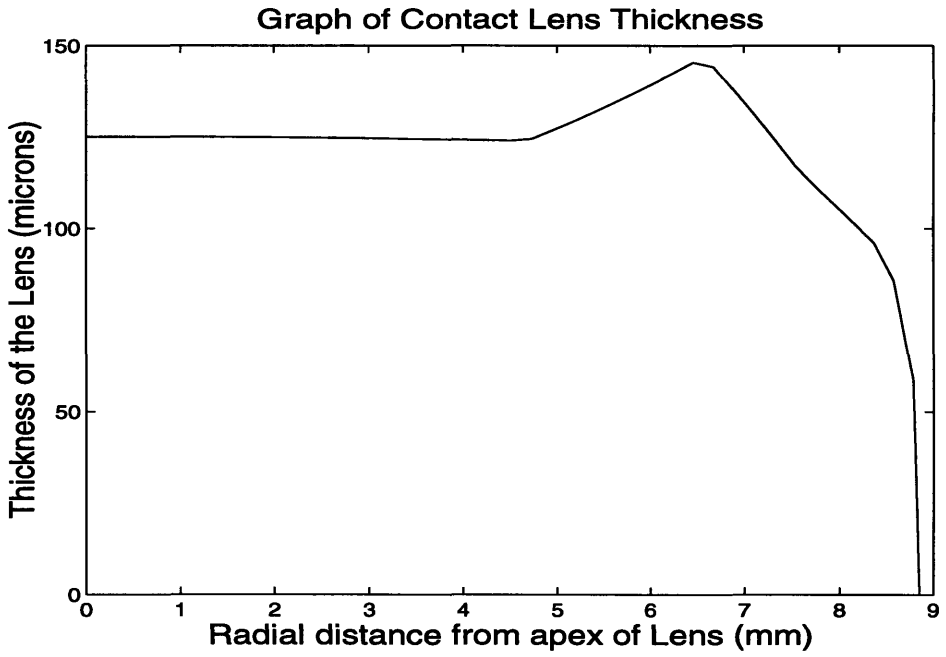

Figure 4.1: Base Geometry Contact Lens Thickness Profile.

parametric effect from fundamental changes in the lens design. The parameters chosen for analysis are:

1) Variations in the overall lens thickness

2) Variations in the thickness through the lenticular region

3) Variations in the optical zone thickness

4) Modifications of the bevel radius at the edge of the lens

5) Variations in Sagittal Height

6) Changes in the BOZR with a constant sagittal height

An attempt has been made to maintain all additional parameters identical to the initial trial run in chapter three. The lens from which all parametric changes are made is a -0.5 diopter lens with center thickness of 125 μm. The thickness through the lenticular zone reaches a maximum thickness of 160 μm measured parallel to the axis of symmetry which translates to a maximum thickness of just less than 150 μm measured normal to the surface as seen in figure 4.1. The edge thickness is 75 μm. The eye geometry used is very similar to that shown previously in figure 2.3. One main exception has been made. Based on the results presented in chapter three and additional information gained through a pub-

lication [16] the limbal radius being investigated will be 4 mm as opposed to the 8 mm used in the initial simulations. This limbus is still taken to be tangential to both the cornea and the sclera. This was done to reflect a more accurate representation of the standard human eye. It is also expected that this increase in bending required for the hydrogel lens to conform to the eye will increase the sensitivity of the analysis.

4.2.1 Variations in Lens Thickness

The first simulations involved the geometric modification of the lens thickness over the entire lens. The range investigated was from a center thickness of 100 - 177 μm which translates to an edge thickness of 49 - 126 μm. This range was chosen to reflect general thicknesses used in the industry. There appeared to be two major effects on the tear film pressure distribution as illustrated in figure 4.2. Primarily, the increase in lens thickness increased the magnitude of the pressure experienced through the tear layer. The pressure increase observed is much more significant over the regions of high pressure but there is an increase of almost 100% at the center of the lens as well. It is also interesting to note that the uniform reduction in thickness causes a more dramatic reduction in the tear film pressure near the edge of the lens. As the bending stiffness for the lens is proportional to the thickness cubed, reductions in thickness near the edge would have a greater impact. The decrease in center thickness from 177 μm to 100 μm reduces the center thickness by 44% but it reduces the edge thickness by over 60%. Also, as the stresses through this region are primarily membrane stresses which are proportional to the thickness of the lens, it is expected that the increase in stresses will be less. This will translate into greater reductions in edge stiffness than in central thickness with an overall uniform decrease in lens thickness.

The increase in pressure observed due to the increase in lens thickness will cause the pressure applied to the corneal surface to increase. Higher tear film pressures would also increase the flow rate of the tear layer away from the regions of positive pressure. This increase in flow leads to a thinner tear film layer. This tear film thinning is shown in figure 4.3. There is a 20% increase in tear film thickness through the limbus region with the thickest lens of 177 μm center thickness. As with the tear film pressure, the tear film thickness is reduced more near the edge of the lens where the lens is thinner.

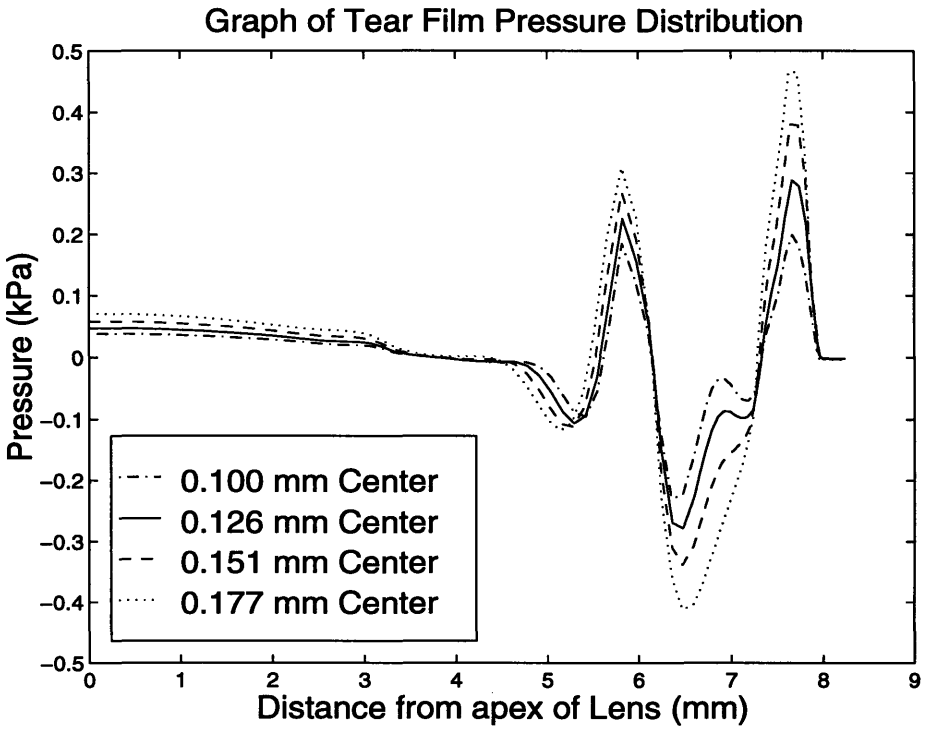

Figure 4.2: Effect of Lens Thickness on Tear Film Pressure Distribution.

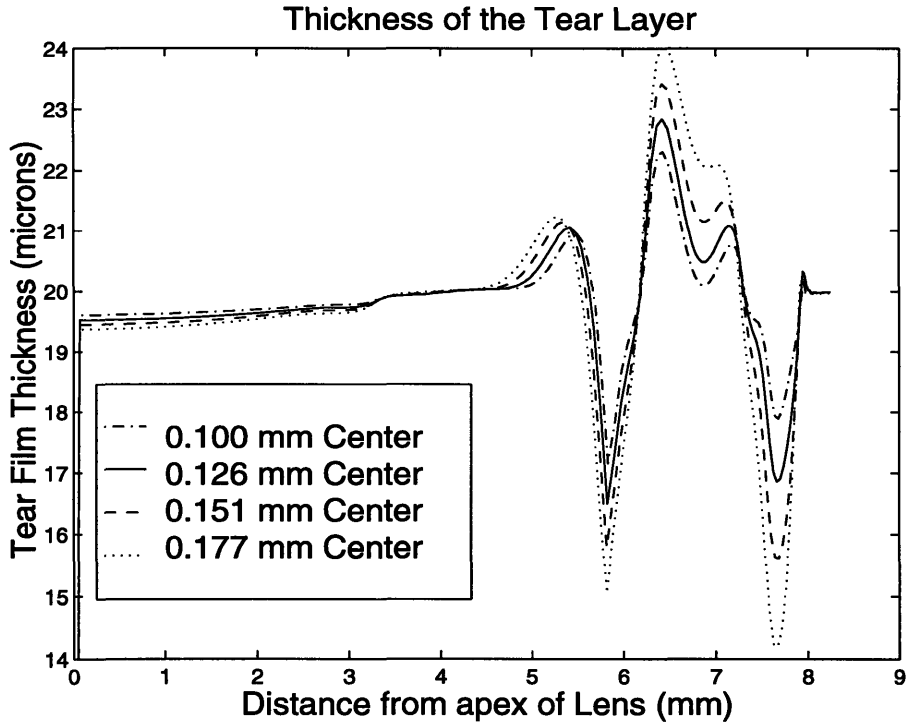

Figure 4.3: Effect of Lens Thickness on Tear Film Thickness.

Both the increase in contact pressure and the reduction of the tear film thickness could negatively affect lens comfort. With the aim of developing a lens that produced a more uniform tear film pressure distribution and maintained a thicker tear film layer, it would appear that thinner lenses would be the ideal geometry to manufacture. There are, however, some limitations and additional considerations that must be acknowledged. For handling purposes, lens thickness cannot be reduced too low or the lenses become too compliant and difficult to manage. There is an additional long term concern with thinner lenses. Due to the reduced thickness, lenses are able to dehydrate at a faster rate [27]. This dehydration sets up an osmotic gradient that encourages mass transport of the tear fluid through the hydrogel lens at an increased rate. This would tend to lead to a reduction in the tear film thickness as opposed to an increase and would result in an increased adherence of the lens to the eye [27]. Due to the relatively thin film of tear fluid present, this mass transport through the lens appears to present a significant effect that is not modeled with this simulation. Thus, a compromise must be found where the handling of the lens is acceptable, the mass flow rates through the lens are not overly significant relative to the volume of post lens tear fluid, and where the contact lens is thin enough to give reduced pressure gradients in the tear film.

4.2.2 Variations in Lenticular Thickness

The next geometric modification involved varying the thickness of the contact lens locally through the lenticular region. The values of thickness used for the investigation ranged from 120 μm to 240 μm measured parallel to the axis of symmetry. For these simulations, the optical and bevel regions were kept constant. The back surface design of the lens was also kept constant and the thickness was varied through changes in the front surface of the lens. This localized thickness variation was investigated because it lies over the region of the largest bending stresses. It was hypothesized that changes in thickness through this region would have a significant impact on the mechanics of the lens. It was also hoped that local changes in the geometry would yield local changes to the lens mechanics. With the ability to make localized modifications without impacting the global mechanical behavior, optimization could be done on specific areas of a given lens design and then an optimum total geometry could be assembled.

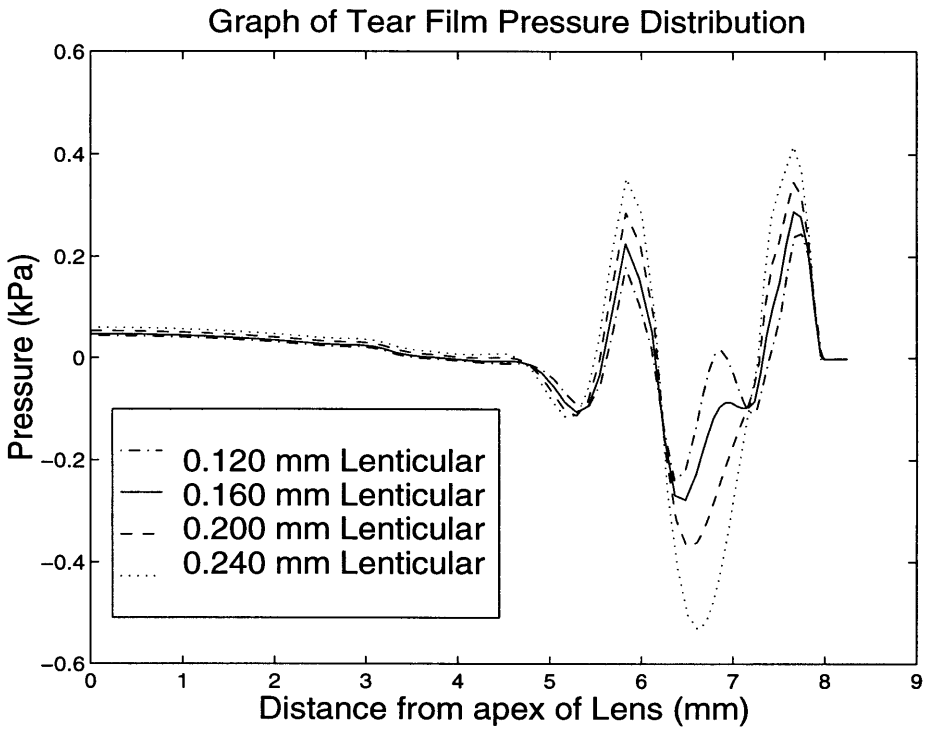

Figure 4.4: Effect of Lenticular Thickness on Tear Film Pressure Distribution.

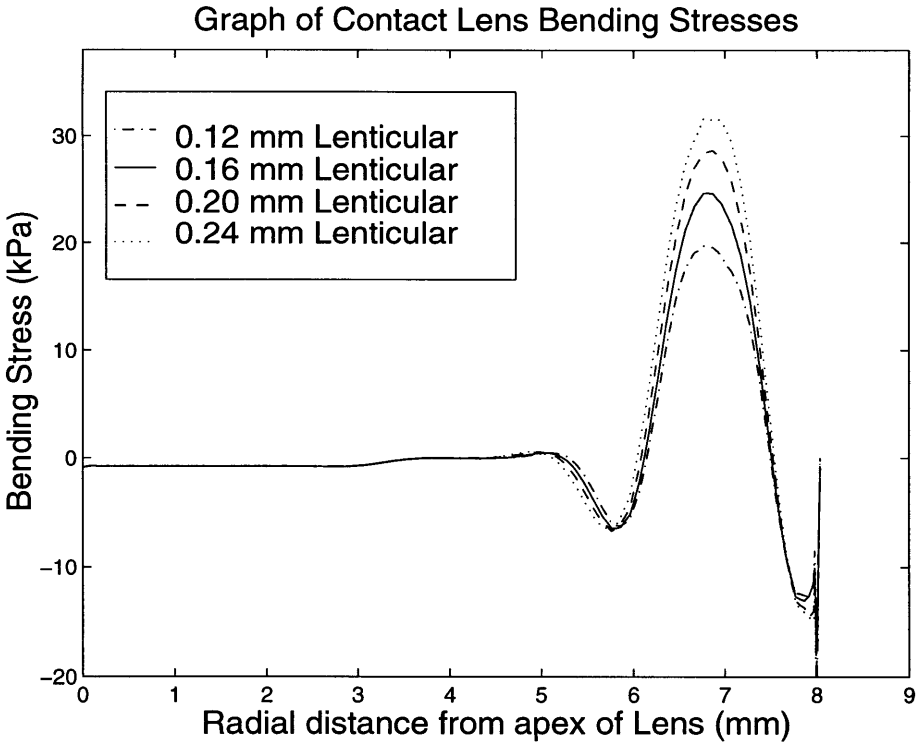

Figure 4.5: Effect of Lenticular Thickness on Lens Bending Stresses.

The results observed for the tear film pressure distribution reflect the results for the increase in total lens thickness and are shown in figure 4.4. As the thickness is increased through the lenticular zone, the pressure in the tear film increases but only through the lenticular region. The pressure distribution through the optical region was largely unaffected and there was a limited impact through the bevel region. This increase in pressure is mainly due to an increase in the bending stresses experienced in the lens. The increase in bending stress is shown in figure 4.5. Due to the increase in bending stiffness the bending stresses increase by more than 50% over the range of values used.

These results are very encouraging from a design standpoint. The localized effect of the increase in thickness implies that localized optimization can occur. Such localized changes in geometry have been the practice in industry through trial and error experiments. These results demonstrate that simulations can help determine the effectiveness of such changes prior to actually making the lenses. This will assist in developing a better lens as it will allow the design team to focus on a region of concern and investigate geometric modifications without impacting the performance of the lens through other regions.

4.2.3 Variations in Optical Thickness

For a final test in varying the thickness parameters of the lens, the thickness through the optical region was modified while keeping the later sections of the lenticular region and the bevel zone constant. The center thickness has been varied between 100 - 177 microns. To reiterate the results of the previous two sections, as the thickness of the optical zone increased, the tear film pressure increased in magnitude which is seen in figure 4.6. The tear film pressure was only affected through the optical region and through the optical/lenticular transition where there was still some thickness variations between the trials. The tear film thickness profile is shown below the pressure distribution in figure 4.7. As observed previously, the tear film thickness profile mirrors the pressure distribution.

As an interesting note, it can be seen that the minimum point on the tear film thickness profile is shifted from near the edge of the lens to the start of the lenticular zone closer to the apex of the lens. This could become a very useful design tool to balance the peak pressures, or the minimum thickness in the tear film. As the optical zone appears to be less sensitive to variations in geometry, the maximum pressure readings through the tear layer

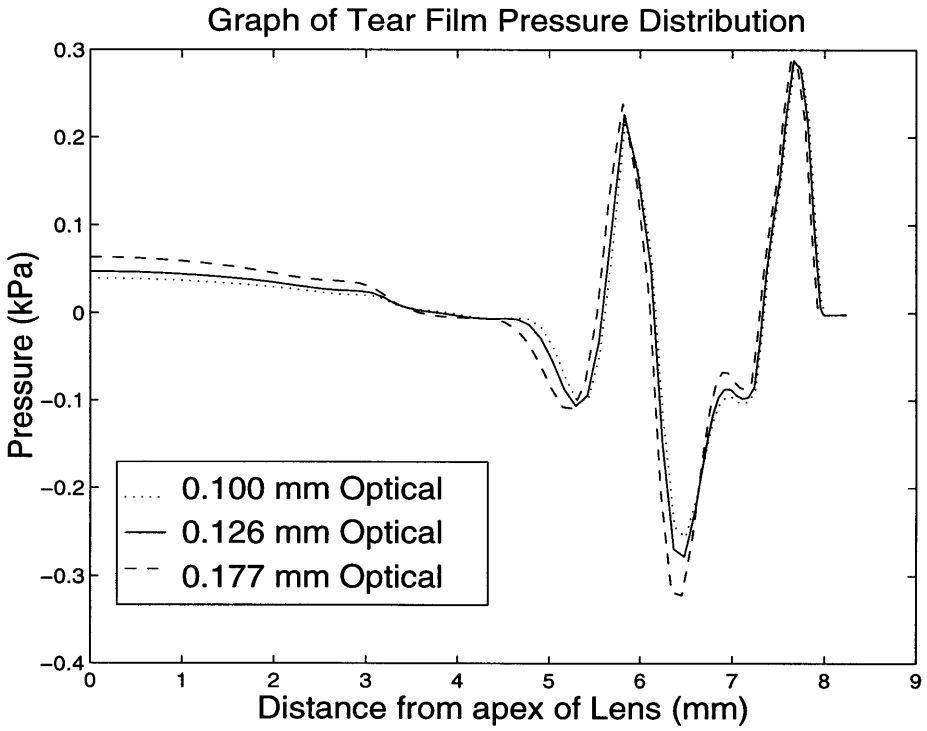

Figure 4.6: Effect of Optical Thickness on Tear Film Pressure Distribution.

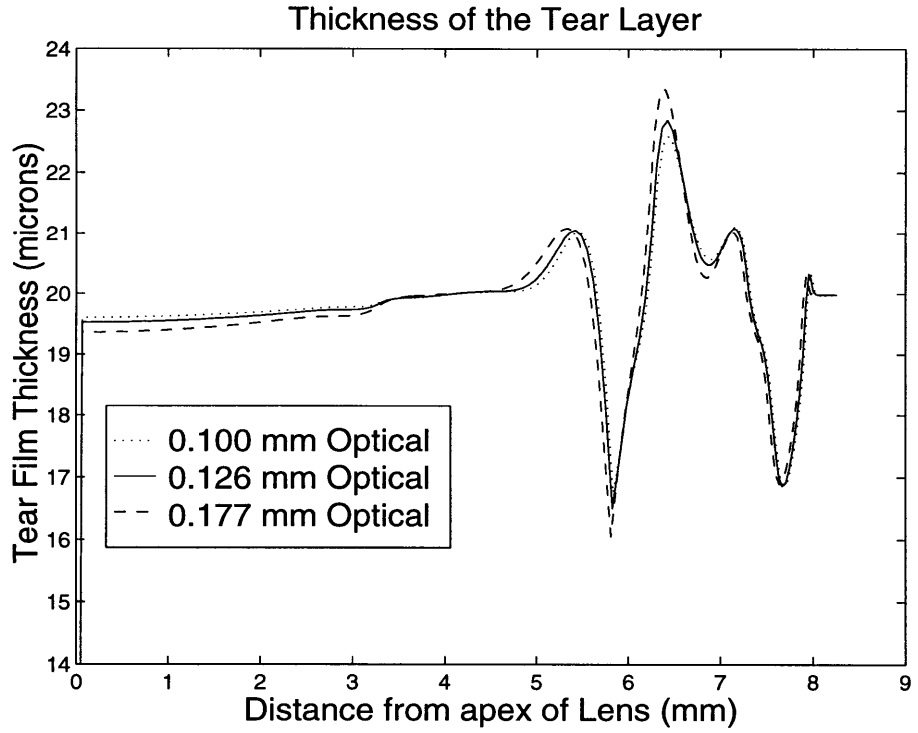

Figure 4.7: Effect of Optical Thickness on Tear Film Thickness.

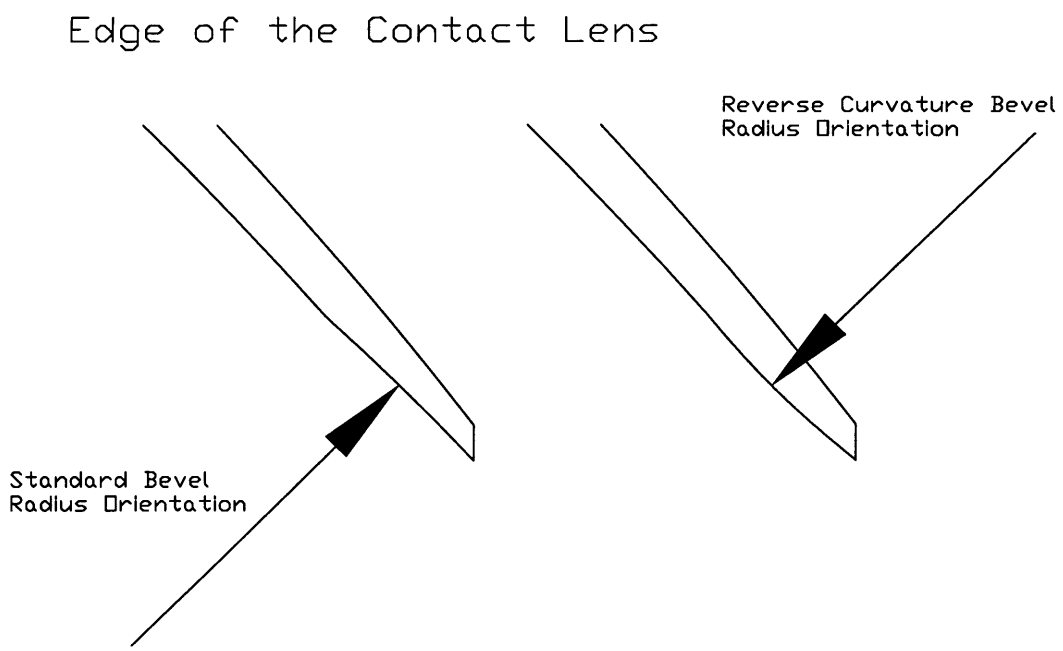

Figure 4.8: Illustration of modifications to the bevel radius.

could be balanced by increasing or decreasing the thickness through the optical region to the optical/lenticular transition region. This balancing of the maximum pressure readings would help to achieve a more uniform pressure distribution through the tear layer.

4.2.4 Modification of the Bevel Zone

The next investigation into the lens parameters was to look at the effect from modifications to the bevel zone. The bevel zone consists of a thin ring at the edge of the contact lens with relatively little cross sectional area. There has been a debate in the literature recently over whether or not geometric parameters through the bevel zone like edge finish and edge thickness might have an impact on the clinical performance of the lens [8,9]. To investigate the potential effect from slight variations in the bevel zone, the back surface radius was varied. The range of radii tested included both standard and reverse curvatures as illustrated in figure 4.8. The reverse curvatures tested were 2.0 mm and 4.0 mm. The standard curvatures on the back surface of the bevel zone were 5.0 mm and 9.0 mm.

The tear film pressure distribution is shown in figure 4.9. There is quite a surprising difference between the different lens geometries. As observed in previous simulations, the effect in modifying the bevel radius only has a localized effect. It is interesting to note that the lenses with the reverse curvature in the bevel region do not induce a suction pressure

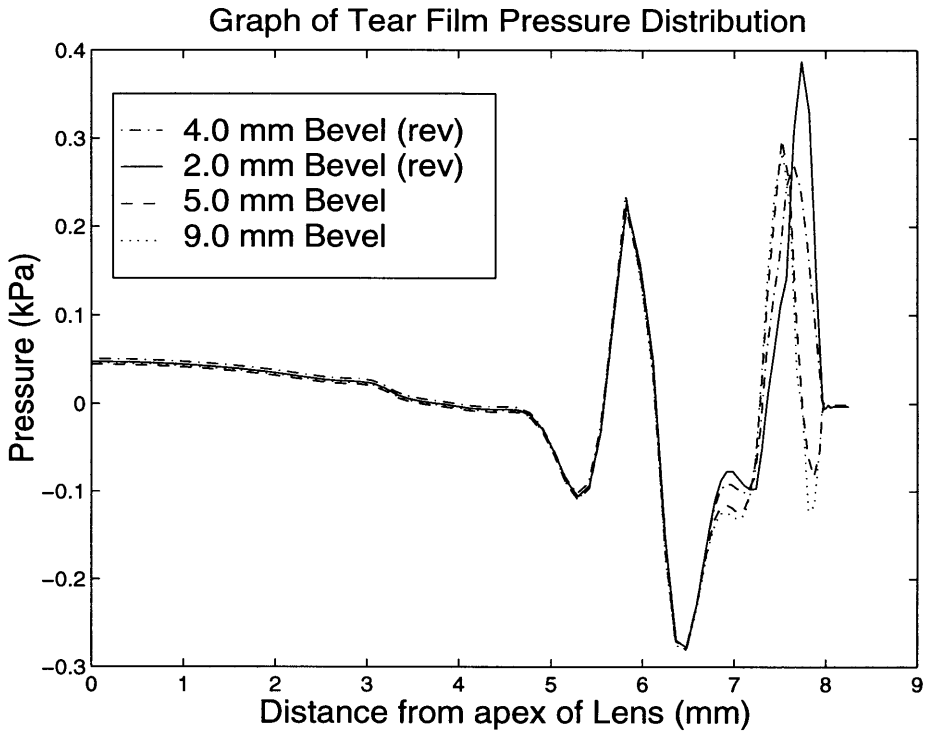

Figure 4.9: Effect of Bevel Radius on the Tear Film Pressure Distribution.

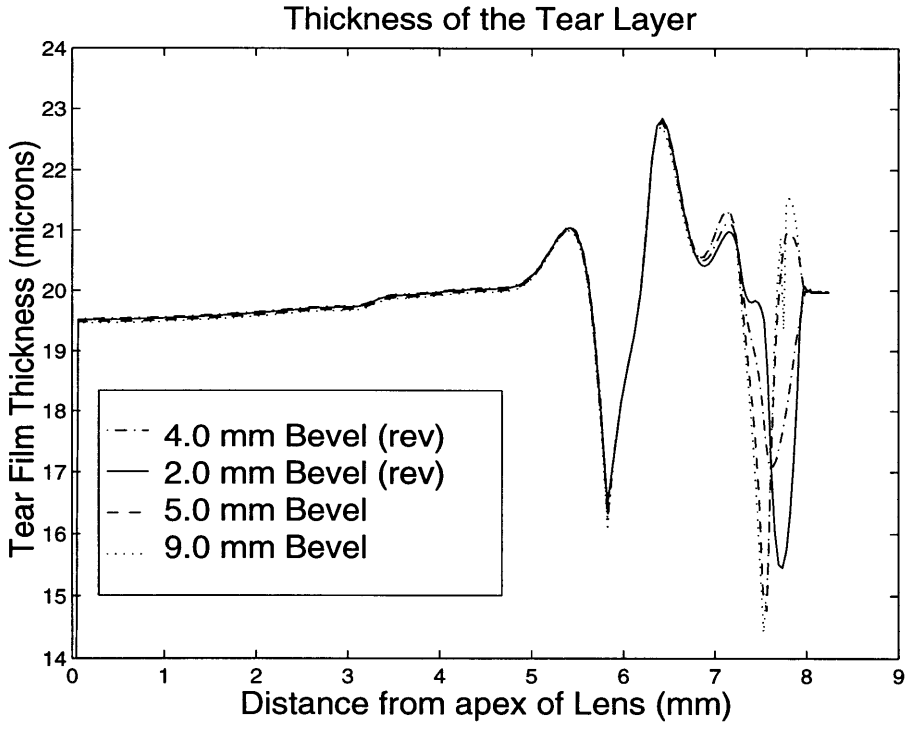

Figure 4.10: Effect of Bevel Radius on the Tear Film Thickness.

near the edge of the lens. This suction pressure, which is observed for the lenses with the standard bevel radius orientation, would imply that the lens is attempting to lift off of the eye slightly. The cause of the suction pressure at the lens' edge with the standard curvature is due in part to the implicit boundary condition at this location. The pressure of the tear fluid at the edge of the lens should be atmospheric and thus, the edge will not be applying a significant normal pressure to the tear surface. This means that the end of the lens should not penetrate into the tear film and the tear film thickness at the edge should be approximately 20 μm. With the regular bevel radius orientation, the curvature encourages the tear fluid up into the concave section thereby causing the suction pressure. In contrast, the convex shape of the reverse curvature bevel radius yields a compressive pressure to the tear film. Thus, the reverse curvature bevel radius should allow the lens to sit lower down on the tear film with less chance of lifting off the tear layer due to the positive applied pressure. It has been hypothesized that the lens lifting off of the eye at the edge of the lens might cause discomfort for the wearer as this would result in the eye lid rubbing against the edge of the lens. As this corresponds to the case of the standard bevel radius orientation, these lenses appear to be less clinically suitable for a comfortable fit.

How the tear film thickness is affected by the changes in the bevel radius is shown in figure 4.10. As expected, the tear film thickness increases just before the edge of the contact lens for the two standard curvature bevel zones. As discussed above, this could dramatically affect the comfort of the lens as there would be more propensity for abrasive contact with the eye lid. It would appear that the result for the reverse curvature radius of 4.0 mm would be ideal. There is a reduced pressure applied to the edge of the lens and therefore there is reduced disruption of the tear film.

4.2.5 Variation in Sagittal Height

Sagittal height is given by the distance parallel to the axis of symmetry from the edge of the lens to the apex of the lens. This measure is generally referred to as the steepness of fit for the contact lens. As the sagittal height increases, the lens is said to have a steeper fit. This parameter has been identified in clinical trials as having a significant impact on the fit and comfort of the lens [8].

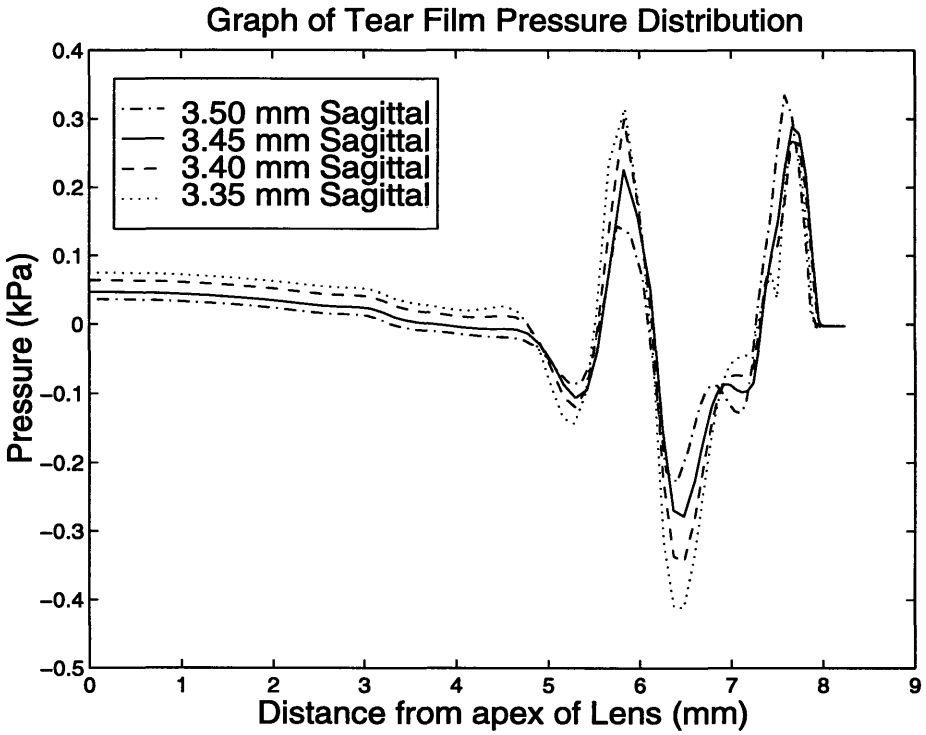

Figure 4.11: Effect of Lens Sagittal Height on Tear Film Pressure Distribution.

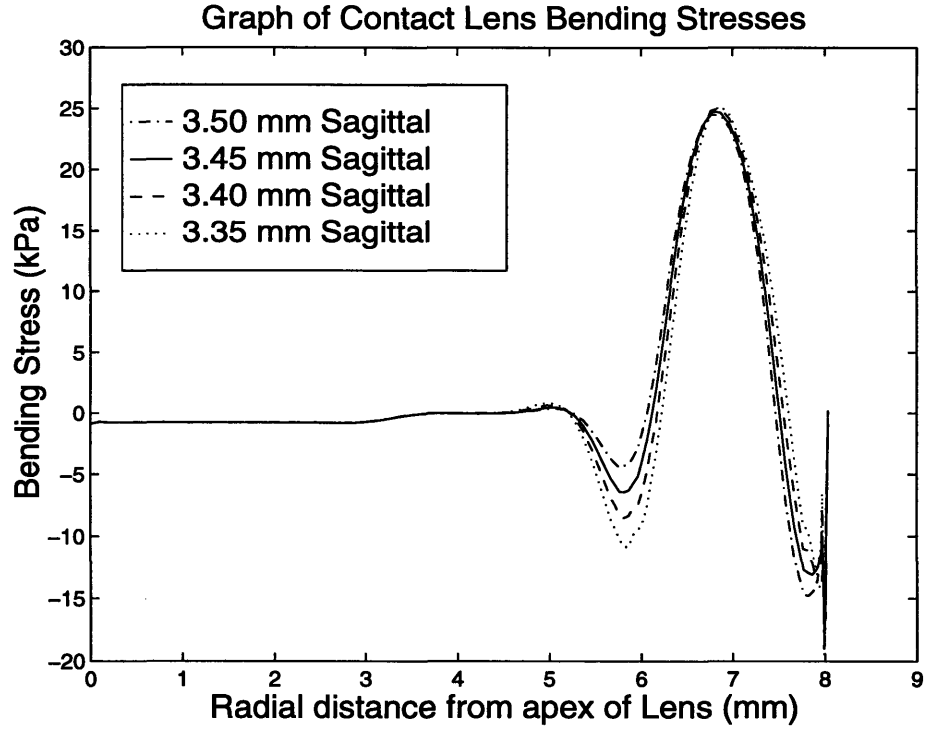

Figure 4.12: Effect of Lens Sagittal Height on Lens Bending Stresses.

To determine the mechanical impact of varying the sagittal height, a range of 3.35 mm to 3.5 mm was studied. This difference in sagittal height was achieved by varying the curvature of the lens through the lens' lenticular section. The pressure distribution shows an interesting trend (figure 4.11). As the lens fit becomes steeper, there is a shift of the maximum tear film pressure from the optical/lenticular transition to the lenticular/bevel transition. It is worthy to note that at the sagittal height of 3.45 mm, the two maximum pressure readings at the transition areas are nearly identical. Balancing these pressure readings has been suggested as a potential means to develop a better fit for the soft contact lenses as it would make the pressure distribution more uniform. It was also noted that the pressure at the center of the lens decreased in magnitude as the sagittal height was increased.

The bending stresses experienced in the contact lens itself are shown in figure 4.12. In support of the previous results, the steeper fitting lenses have reduced bending stresses except through the bevel region. This implies that the steeper fitting lenses are digging further into the tear layer. This could pose problems as the lens dehydrates and the tear film thickness depletes over time. If the lens applies too high of a contact force against the tear layer, physical contact could occur and this could lead to corneal ulceration and irritation. It would thus appear critical to limit the pressure applied at the edge of the lens to ensure no abrasive contact.

4.2.6 Variations in Back Optical Zone Radius

A final parameter that was investigated is variation in the back optical zone radius. As previous results have indicated that the back surface design has a dramatic impact on the mechanics of the system[8], variations were done on different BOZR while keeping the sagittal height constant. The BOZR was modified from 8.0 mm to 8.5 mm.

The pressure distribution through the tear layer is shown in figure 4.13. There is a dramatic reduction in pressure through the tear layer through the later section of the optical zone and the initial section of the lenticular zone as the BOZR increases to 8.5 mm. Over the range tested, the maximum pressure at the optical/lenticular transition region is reduced by 80%. Towards the bevel region, however, the maximum pressure increases slightly as the BOZR increases. One appealing feature of the pressure curve for the lens with a BOZR of 8.5 is that through the central lenticular region, the pressure is relatively

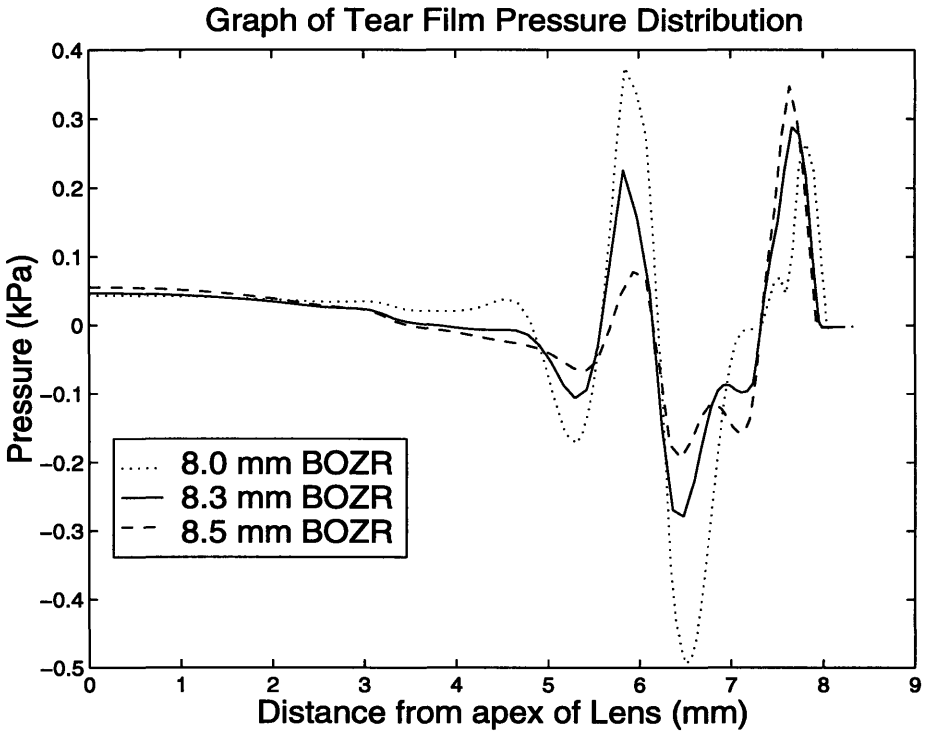

Figure 4.13: Effect of Back Optical Zone Radius on Tear Film Pressure Distribution.

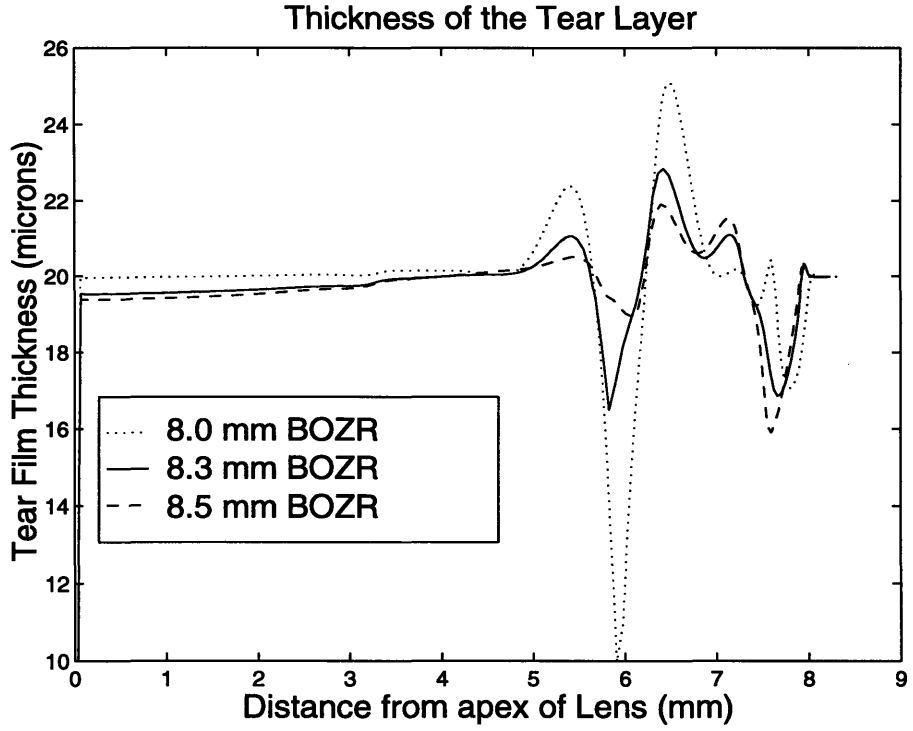

Figure 4.14: Effect of Back Optical Zone Radius on Tear Film Thickness.

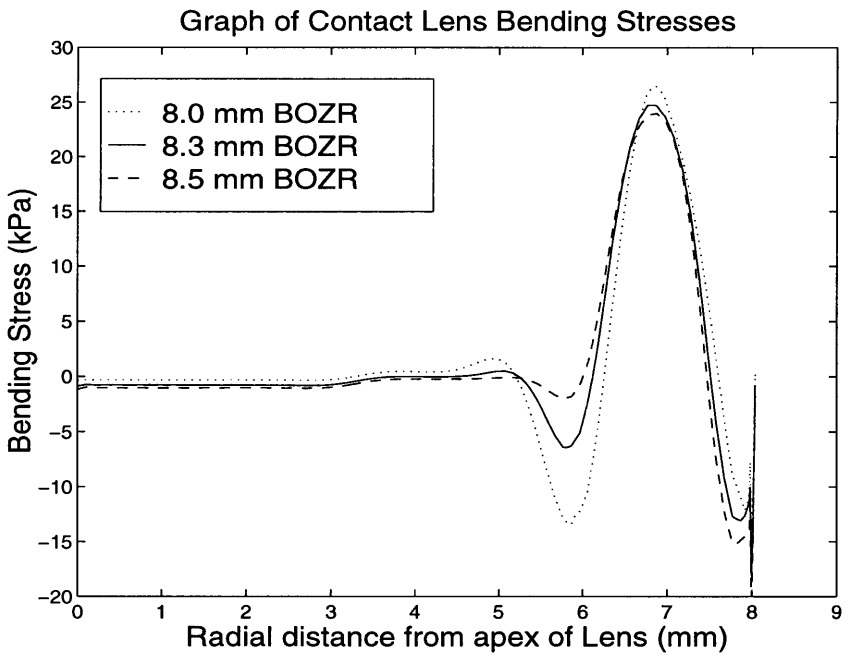

Figure 4.15: Effect of Back Optical Zone Radius on Lens Bending Stresses.

uniform. To maintain stability of the lens on the eye, some negative pressure is required or the lens would simply fall off the eye. To achieve this adherence and stability, however, it would be advantageous to maintain a lower magnitude pressure over a larger area so that the total applied force would be the same without the severe disruption in the tear film thickness that can result from the larger pressure readings.

The increase in pressure at the optical/lenticular transition region does result in a very large increase in the disruption of the tear film thickness. The tear film thickness is reduced to half the thickness for the BOZR of 8.0 mm (figure 4.14). This could have negative clinical results for the performance of the lens. A reduced tear film thickness will be more prone to trapping small particles of debris leading to corneal irritation. Furthermore, the chance of abrasive contact of the lens with the eye is increased as the lens gets closer to the eye. The cause for this large increase in pressure and the resulting decrease in tear film thickness is primarily a function of the bending stresses in the lens. As shown in figure 4.15, the bending stresses are much greater for the lens with the smaller BOZR. It is also interesting to note that the bending stresses are not that dissimilar for the maximum bending stress experienced through the lenticular region. As it would be these bending stresses causing the suction pressure through the central lenticular zone and therefore the

adherence of the lens to the eye, the flatter fitting lens could exhibit almost the same degree of stability if the bending stresses were maintained at a high enough magnitude.

4.3 Summary of the Parametric Lens Study

There were numerous valuable lessons to be gained from the parametric study performed on the lens geometry. Localized modifications are feasible and modifications in lens thickness can have a direct impact on the local mechanics of the system. As the lens becomes thicker, bending stresses increase in magnitude and the resulting pressure in the tear film is also amplified. This in turn results in an amplification to the tear film thickness deformations. The simulations indicated that a flatter reverse curvature at the bevel edge of the lens may reduce some of the deformations in the tear layer at the edge of the lens. Also, the reverse curvature kept the lens sitting lower on the tear layer may be clinically significant as it reduces the abrasion between the lens and the eye lid during blinking. Variations in sagittal height shifted the maximum tear film pressure towards the bevel region as the sagittal height increased. For a given general lens geometry, it should be possible to balance the two local pressure maximums by modifying the sagittal height. Finally, the BOZR dramatically reduced the pressure experience in the tear film at the optical/lenticular transition zone for a flatter lens. Although there was a slight increase in pressure applied to the tear film at the edge of the lens, this was not as significant as the reduction through the optical/lenticular transition region.

4.4 Example of Implementing the Results into a Design Setting

To illustrate how using a FEM model like the one presented here could be used to assist in the design process, a first iteration will be presented for a new lens geometry. Based on the results from the investigation into variations of BOZR, a BOZR of 8.5 mm was chosen as it yielded a reduced tear film pressure at the optical/lenticular transition. To reduce the corresponding pressures through the bevel zone, the bevel radius was taken as a reverse curvature of 4.0 mm and the sagittal height was taken as 3.40 mm. To try and give the lens adequate stability, the lenticular zone thickness was increased to a maximum value of 200 microns measured parallel to the axis of symmetry. The central thickness was taken as 125 microns as this yielded a general balance between the two maximum pressure

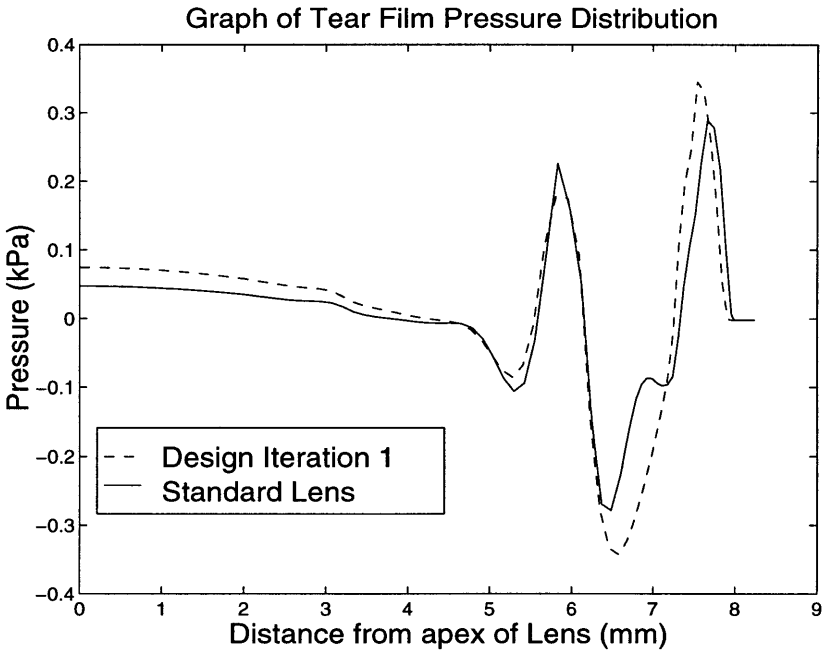

Figure 4.16: Tear Film Pressure Distribution for First Iteration of the New Lens Design.

readings in the tear layer.

The results of the design study are shown in comparison with the standard test lens that was used for the previous simulations. The results obtained were very encouraging as most design objectives were achieved. As illustrated in figure 4.16, the new lens has a lower tear film pressure reading at the optical/lenticular transition. The new lens also had a decreased pressure through the lenticular region (more negative) which will assist in making the lens more stable (a problem often encountered with flatter fitting lenses). Unfortunately, the tear film pressure reading in the bevel zone was not reduced past that of the previous test lens. This result does, however, indicate one of the main advantages of the FEA modeling. With this first iteration done, modifications can be made to the new lens geometry to attain the desired pressure distribution. The lens thickness could be decreased, the bevel radius could be flattened further while still maintaining the reverse curvature, the sagittal height could be further reduced, or the BOZR could be increased slightly. All of these modifications will shift the maximum pressure point away from the bevel region in an attempt to make the pressure distribution in the tear layer more uniform.

In attempt to further illustrate this proposed design strategy, a second iteration was attempted. To reduce the stress applied through the bevel region, the thickness through the

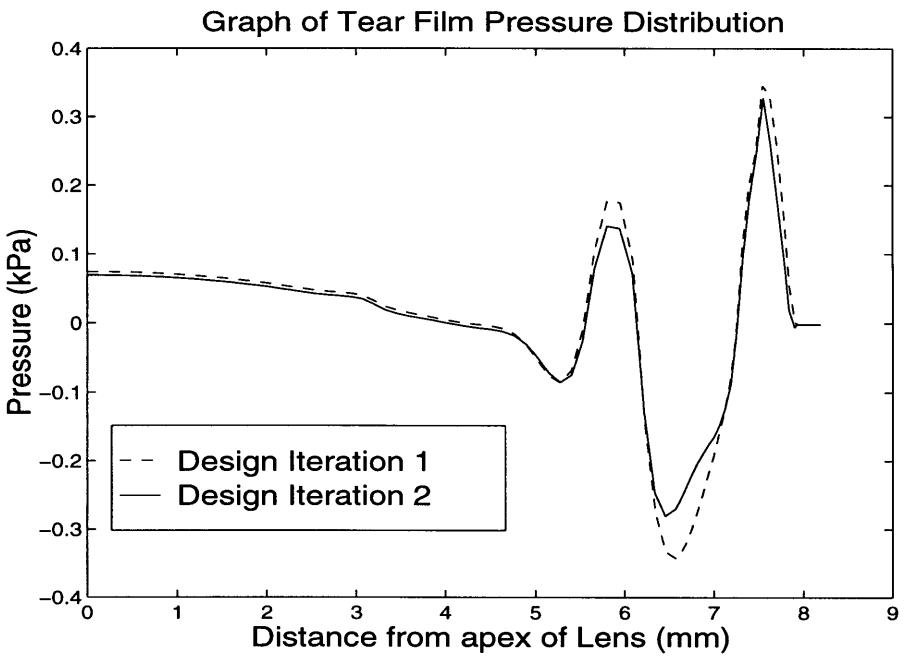

Figure 4.17: Comparison of First and Second iteration of the New Lens Designs.

lenticular region was reduced to 180 μm measured parallel to the axis of symmetry. In addition to this, the bevel radius was increased to 6.0 mm with the reverse curvature maintained. The comparison between the two iterations is shown in figure 4.17. Although the pressure in the tear film did decrease slightly through the bevel region, this decrease wasn't too significant. There was also a loss of pressure through the lenticular region that was hoped to increase the stability of the lens. This suggests that further iterations would be required to determine the lens geometry that would give the desired tear film pressure distribution. For the next iteration to achieve a further reduction in the pressure at the edge of the lens, the edge thickness might be reduced. Once the iterations yield a desired pressure distribution or characteristic stress field in the contact lens, physical experimentation and clinical studies can follow to determine the clinical performance of the lens.

Now that the two dimensional axisymmetric model has been developed, the system's mechanics have been analyzed, and the FEA model's capability to be used as a design tool has been explored, the focus of the research turned towards the development of a three dimensional model. With this model, additional issues concerning lens mobility and stability can be addressed and that is the focus of the following chapter.

Chapter 5

Development of the Three Dimensional Model

5.1 Motivation behind the Three Dimensional Model

In a recent study to determine the clinical performance of three different commercially available contact lenses, comfort, handling, and quality of vision were identified as the three most important factors[9]. As discussed earlier, lens mobility is a critical element of lens comfort. With inadequate motion, oxygen transport to the corneal surface can be reduced and particulate debris can become trapped more easily between the lens and the eye. Too much mobility, however, can start to interfere with the quality of vision. If a lens does not center on the eye well, the optical zone will not align with the cornea properly and quality of vision will suffer.

To investigate how to quantify mobility and stability of a lens, it became necessary to develop a three dimensional model. Although the geometry of the system is axisymmetric, the loading conditions are not. Mobility and stability of the lens must be driven by the differential or unsymmetrical bending as emphasized by Taylor and Wilson[5]. In this paper, Taylor and Wilson also suggest that looking at the differential strain energy would be an ideal means to determine the mobility of the lens. To make their calculation, however, Taylor and Wilson are required to make assumptions. One assumption was regarding the stress state of the edge of the lens. It was assumed that the lens could relax significantly enough so that stresses through the bevel region of the lens were considered to be negligible. They also assumed that all differential strain energy was based on changes in curvature through the lenticular region, and therefore only investigated bending stresses. Small displacement assumptions were also made. The calculations are also based on more simplified geometries of the eye and the lens. Although it appears that this is not required, calculations become much more involved for complex geometries.

For an initial investigation into mobility, it was proposed to look at a plane strain, two-dimensional model of a complete cross section of the contact lens as illustrated in figure 5.1. It was hoped that these simulations might yield a means of analyzing lens mobility due to differential strain energy from bending while avoiding the development of a three

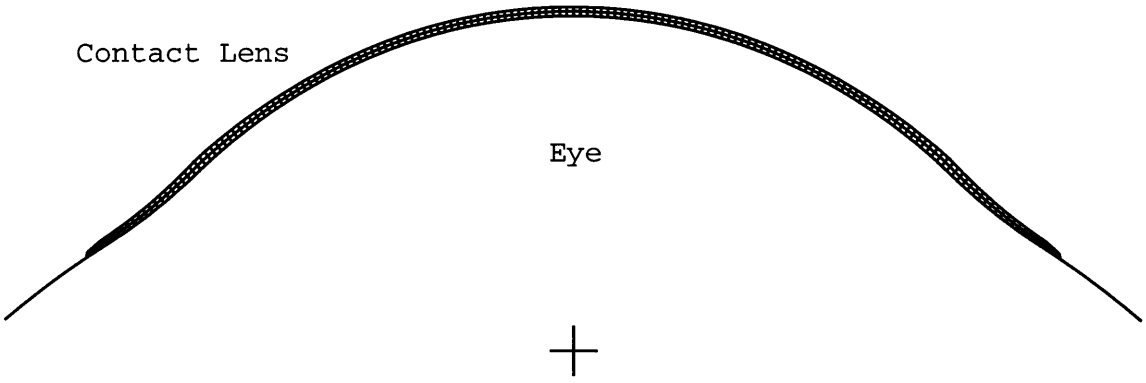

Figure 5.1: Plane Strain Model of the Contact Lens on the Eye with No Tear Layer.

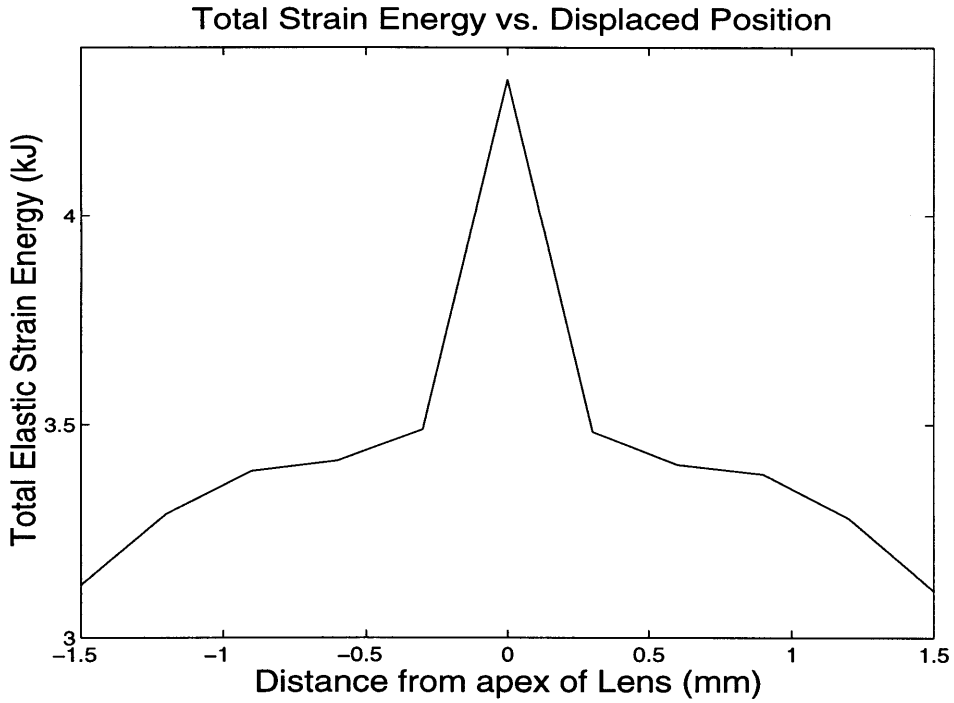

Figure 5.2: Total Strain Energy in the Contact Lens as a function of Displacement from the Centered Position.

dimensional model. Unfortunately, this did not prove to be possible. Without the additional constraint from the hoop stresses that would be present in the lens, the centered position was an unstable equilibrium point. The strain energy was maximized at the centered position (figure 5.2). This meant that convergence of the solution was quite difficult to achieve. Physically, the lens shifts so that only one portion of the lens is being bent through the lenticular region. This mode of displacement would not be energetically favorable if the axisymmetric hoop stresses were present. As returning to the centered position is critical for measuring stability and mobility this method of analysis was deemed to be unfeasible.

5.2 Development of the Three Dimensional Model

In developing the three dimensional model, one aspect of symmetry can be used to reduce the size of the model needed. Only one half of the lens must be modelled as displacements of the lens will not involve any rotation. To develop the three dimensional model, a few additional assumptions had to be made. The most significant initial assumption made was to remove the tear film from the model. This was done based on computational time constraints. Due to the nature of the problem, there is a large degree of contact involved in the modelling. To model the tear layer, contact would be doubled and the contact of two deformable bodies is much more computationally intensive to model than the contact of one deformable body and a rigid surface. Significant memory was required (approximately 750 Megabytes per simulation including 500 Megabytes of swap space) even for the reduced model.

In generating a three dimensional mesh of the contact lens, some care had to be taken. One of the main problems encountered was a numerical problem with mesh refinement. Normally when generating a mesh, especially if the mesh is being generated from an axisymmetric model, some refinement is done so that the aspect ratio both at the center of the object and at the edge of the object is not too large. An example of this is shown in figure 5.3. With this type of refinement, the mid-nodes of the smaller quadratic elements must be constrained to lie along the path defined by the side of the larger elements, a quadratic curve, to satisfy inter-element compatibility. The problem encountered is that the nodes are in full contact with a spherical rigid surface (thereby constraining the nodes to lie on

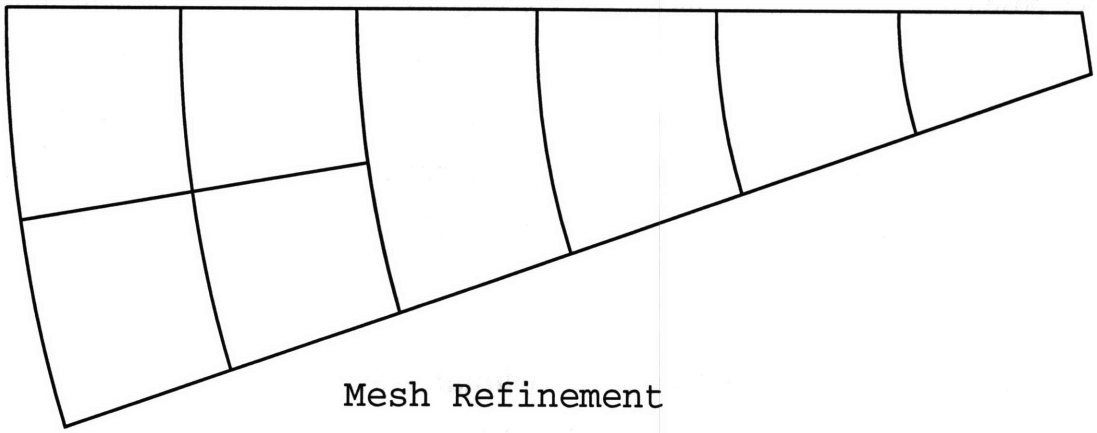

Figure 5.3: Illustration of Frequently used Mesh refinement.

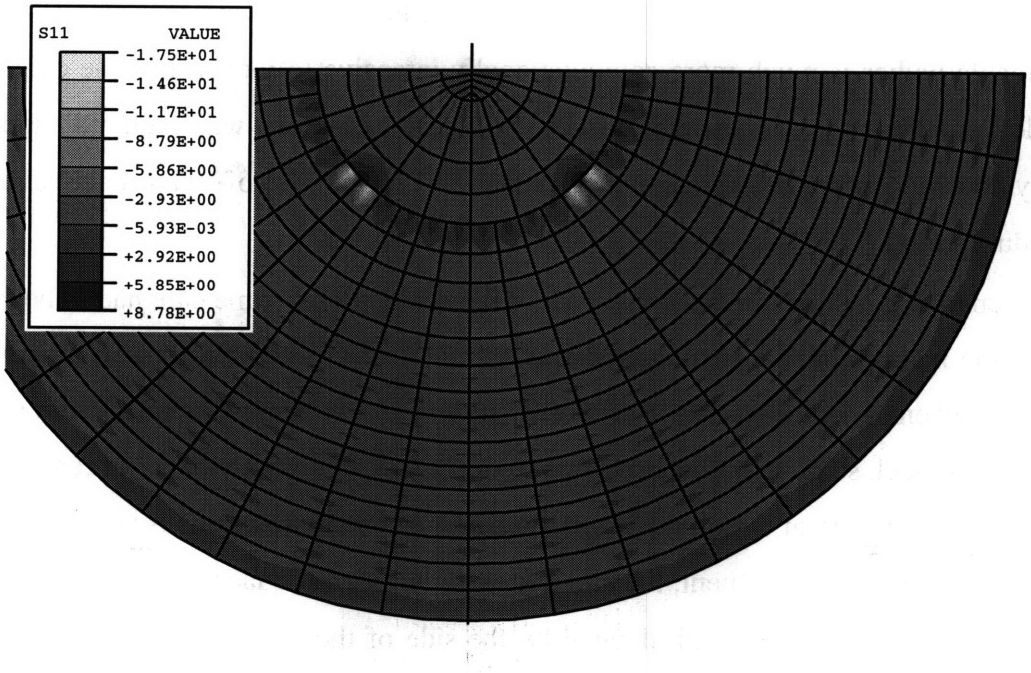

Figure 5.4: Contact Pressures for 3 Dimensional Model with MPC constraints.

the surface of the sphere or ellipsoid), and that surface cannot be defined by a quadratic equation. Thus, contact pressures at the point of refinement were very large due to the conflicting constraints. The contact pressures for such a model of the contact lens are shown in figure 5.4. It is noted that the contact stresses through the rest of the contact lens are an order of magnitude lower than those at the point of mesh refinement. Based on these results, it was determined that no mesh refinement of this nature could be implemented in the simulation.

To develop the model and generate the three dimensional mesh, a more involved procedure was required. As one of the steps taken to develop this new model, there was a shift of focus from using continuum elements to using shell elements. In the pre-processor for ABAQUS, one way to develop a three dimensional object was to define a geometric surface and then generate a mesh on that surface. This is ideal for generating shell elements as only the center plane has to be defined and then the thickness is defined independently. As the radii of the eye geometry is much larger than the thickness of the contact lens, shell elements present an appealing means of analysis.

To generate the geometric surface, the mid-plane of the contact lens was taken, and the surface was curve fit to the mid-plane. A β-spline curve of second order was used to fit the mid-plane using 41 points. As the assumption has been made that the shell elements can be used since the thickness is much smaller than the radii of the eye, the location of the mid-plane is not as sensitive an issue. With the spline curve fit there is some deviation from the true mid-plane but this is very minor and the analysis is not too sensitive to errors of this nature as the thickness profile is accurately defined.

The shell thickness distribution, which is calculated independently for all nodes, is calculated based on the distance of the node in question from the apex of the mid-plane. The shell thickness is a function of the linear distance from the apex of the mid-plane to any point on the mid-plane as the lens is axisymmetric and the curvatures are not too severe. Values of this linear distance vs. shell thickness were tabulated for each lens in question from the two dimensional, axisymmetric model. For each node of the three dimensional model, the linear distance from the apex to the node is calculated and then the shell thickness is determined from a linear interpolation of the previously tabulated values.

For the eye geometry, an axisymmetric rigid surface was still used. The dimensions for the eye were those used in the initial investigation into the two dimensional model as described in chapter two. The limbus radius of 8 mm was chosen to reflect a slightly more relaxed shape for the contact lens mid plane to conform to than would be present with the limbus radius of 4 mm used in chapter four. This was done to accommodate the no tear film assumption.

5.3 Loading Procedure

To achieve full contact of the lens with the rigid surface, a function available from ABAQUS was used called contact interference. The function allows the user to shrink fit one object to another. This brings the two surfaces directly into full contact. Once this is achieved, the system is given time to relax to a final equilibrium condition as the interference shrink fit is achieved through a displacement approach rather than through the minimization of the potential energy in the material.

Once equilibrium has been achieved, the lens is displaced 0.6 mm from the centered position. The total strain energy of the lens is monitored as the lens is moved from the centered position and displaced the 0.6 mm. The displacement of 0.6 mm was chosen based on an internal report provided by CIBA/Vision. In this report, lenses were reported to be tight fitting if motion was less than or equal to 0.2 mm after a blink. Motion in the range of 0.3 mm to 0.5 mm was indicated as an ideal range. Displacement of the lens in the simulation is achieved by prescribing a displacement to a single node located approximately 1 mm from the edge of the lens. This node is displaced away from the apex of the eye. After the lens has been moved across the eye, the prescribed displacements are removed and the lens is once again allowed to reach a state of equilibrium.

5.4 General Results from the Model

The generated mesh is shown in figure 5.5. With the given model, no additional mesh refinement constraints are required so there are no mathematical constraint problems. In the analysis of mobility, one of the key factors that will be considered is the strain energy density in the lens. This strain energy density for the contact lens is shown in figure 5.6. The view is taken from above the lens, looking down on the front surface. The section

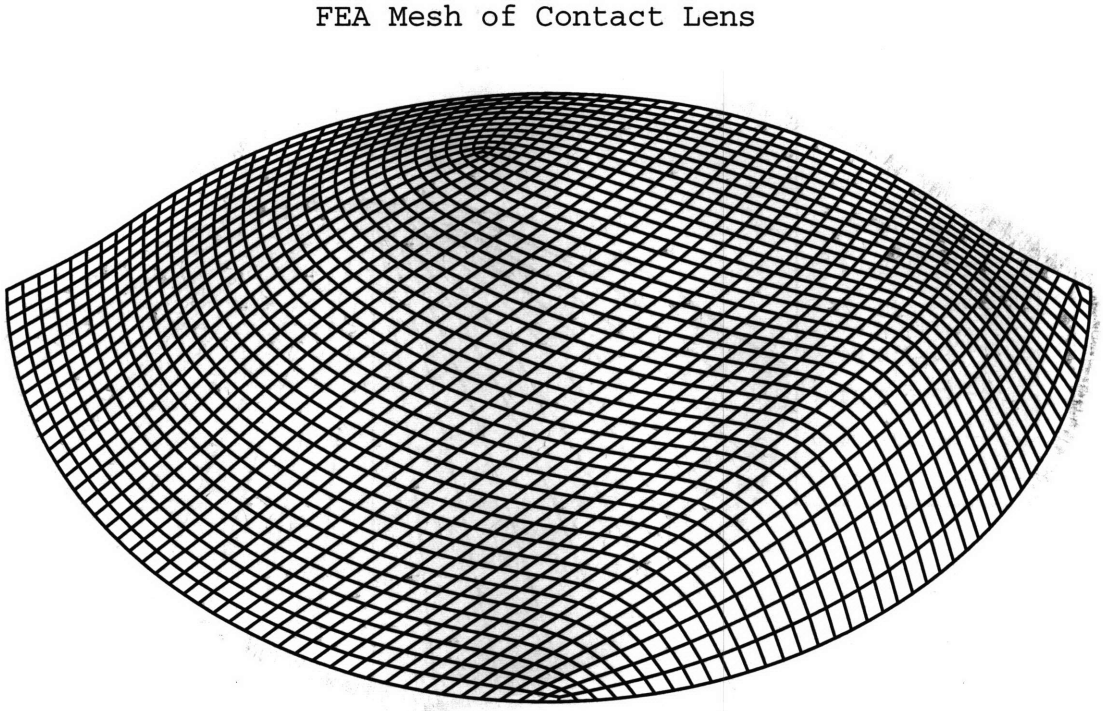

Figure 5.5: Three Dimensional Mesh of the Contact Lens.

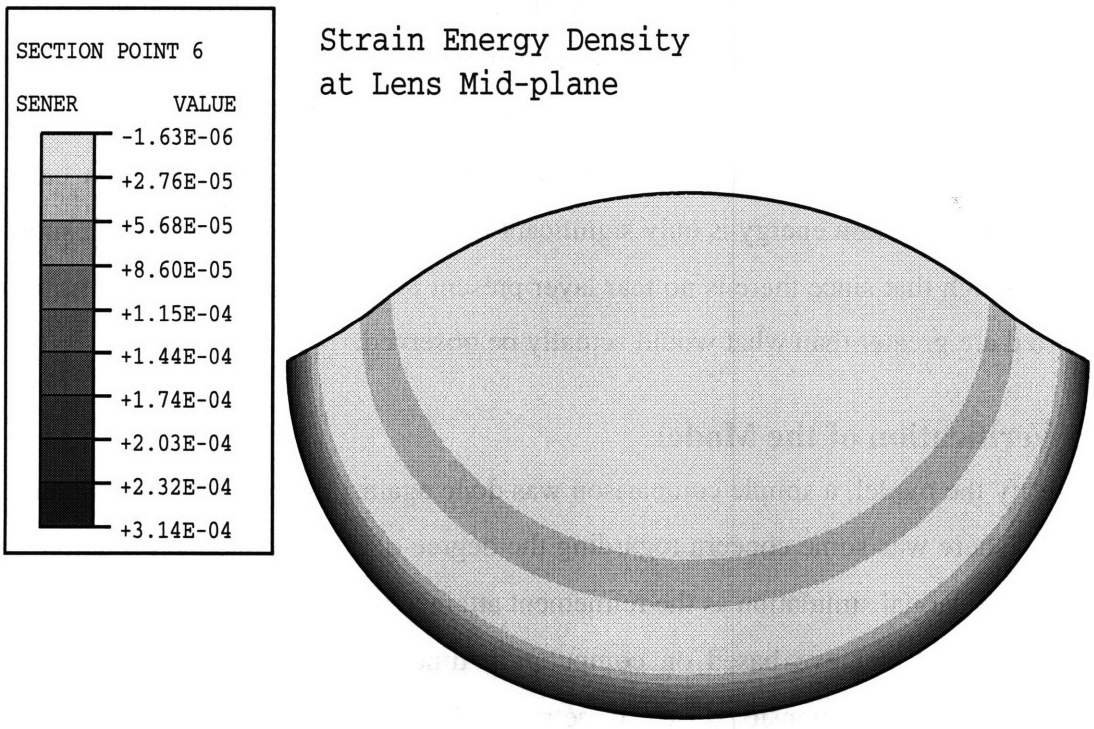

Figure 5.6: Strain Energy Density for the Three Dimensional Model of the Contact Lens at the Mid-plane of the Lens.

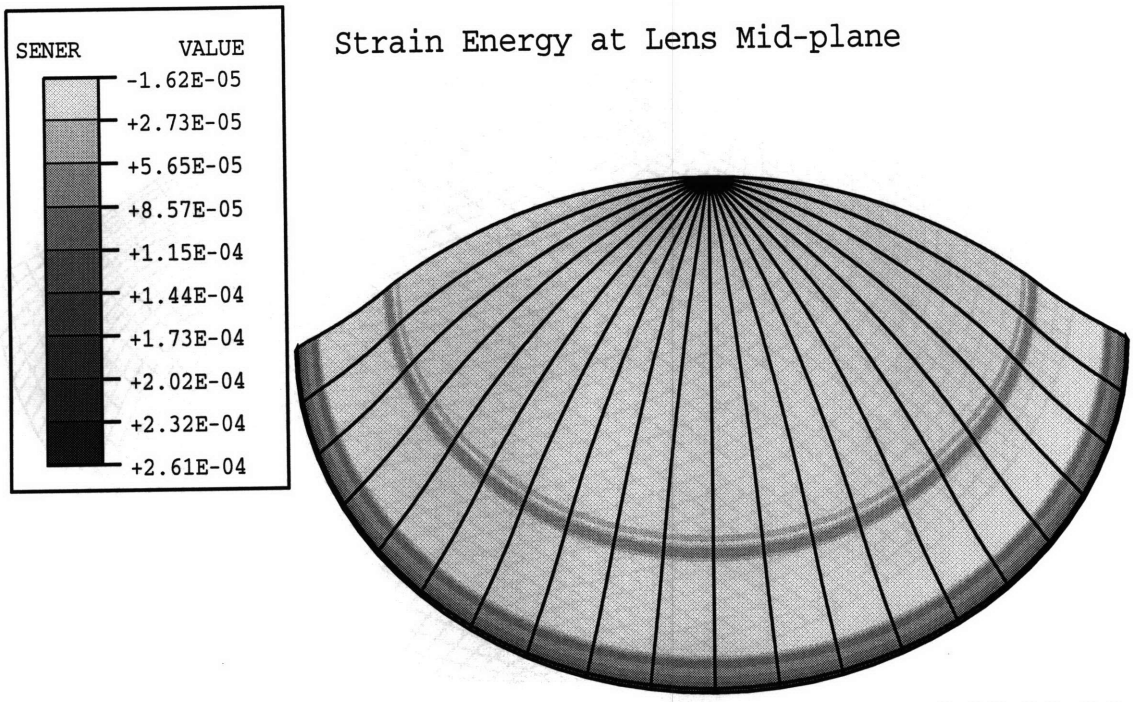

Figure 5.7: Strain Energy Density for the Two Dimensional Axisymmetric Model of the Contact Lens at the Mid-plane of the Lens.

point is taken to be the mid-plane of the shell elements. This plot illustrates what was observed in the previous studies for the two dimensional case. The key areas with the highest strain energy density in the lens are located at the end of the lens and through the limbal region of the eye. This is an important observation as the assumption has often been made that strain energy is only significant through the lenticular region. It should be noted though that since there is no tear layer present in this model, the actual magnitudes reported are greater than what would actually be observed.

5.5 Verification of the Model

To verify the model, a simple comparison was done against the previous two dimensional model. There was some concern regarding the degree of mesh refinement required in the three dimensional simulation as the refinement attained in the two dimensional model was not possible to achieve based on computation time and space limitations. The strain energy for the two dimensional axisymmetric model with no tear layer is shown in figure 5.7 and can be compared to figure 5.6. A comparison of the two contour plots illustrates

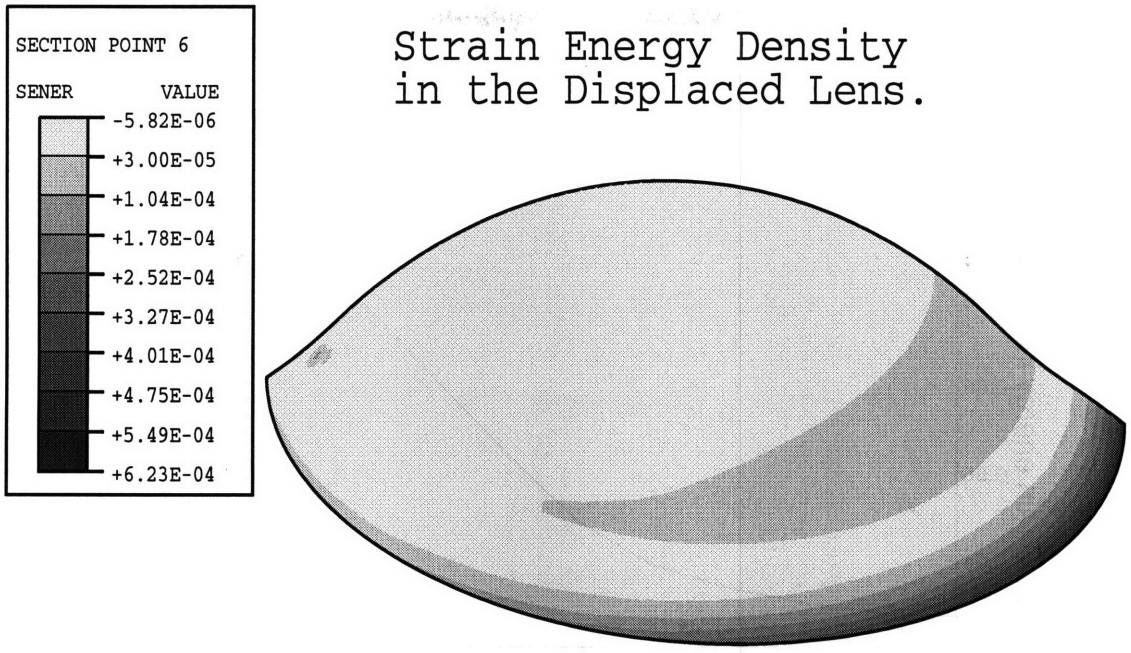

Figure 5.8: Strain Energy Density for the Contact Lens Displaced from the Centered position on the Eye.

that the results from the new three dimensional model are in fact, very similar to the two dimensional results. As a comprehensive verification was done for the previous model, no further verification was deemed necessary. With this model, it now becomes possible to analyze the mobility of the lens.

5.6 A Measure of Mobility

To measure lens mobility, a difference in strain energy in the lens must be measured. To do this, variations in the strain energy are observed as the lens moves across the surface of the eye. To gain a better appreciation for how the strain energy changes as the lens moves, the strain energy for the lens is shown for the displaced configuration in figure 5.8. It is interesting to note the dramatic changes in the strain energy density occur both at the edge of the lens and through the lenticular region. It certainly appears that strain energy from both the lenticular region and the edge of the lens is a significant factor in determining the contact lens mechanics.

The total strain energy of the standard trial lens described in chapter four as a function of position on the eye is given in figure 5.9. The general increase in lens strain energy as it

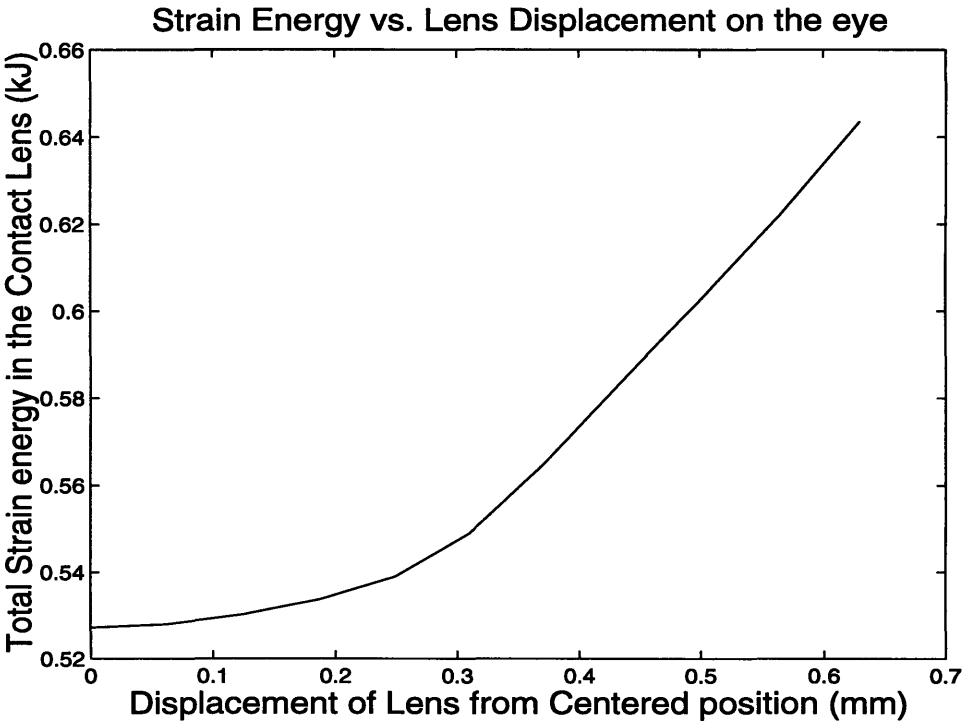

Figure 5.9: Strain Energy as a function of Lens position on the Eye for the standard Test Lens.

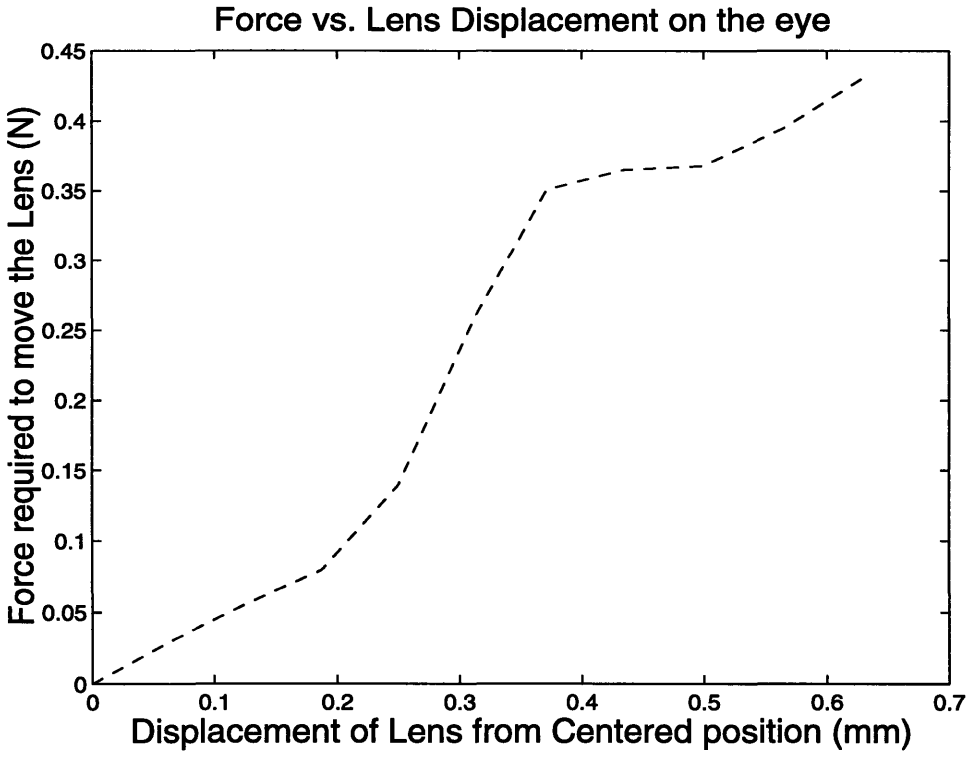

Figure 5.10: Force Required to Move the Lens across the Eye as a function of Lens Position on the Eye.

is moved across the eye occurs because there is an increase in bending and membrane stresses as the lens is forced to conform off-center to the eye geometry. Initially, there is only a slight difference between the off-centered and centered configurations. As the lens is displaced further from the centered position, however, the differences become greater and the strain energy increases at a faster rate. From this graph, some appealing features are observed. As some mobility is required for optimum clinical performance, it is good to have a very small strain energy gradient near the lens' centered position. As too much motion (in excess of 0.5 mm) negatively affects quality of vision through lens instability, a much steeper gradient would be ideal to resist excessive motion. The increase in strain energy gradient should make the lens move more quickly towards the lower energy state.

This point is further emphasized if the force required to move the lens at the given node is monitored. This force vs. displacement graph is shown in figure 5.10. As expected, the force required to move the lens is quite low near the centered position. As the lens is moved further away from the centered position, however, the force required to move the lens increases. Beyond the 0.2 mm point, there is a dramatic increase in the force required to move the lens. This corresponds to where there is an increase in the strain energy gradient shown previously. With the ability to determine both the changes in total strain energy and the force required to move the lens, this provides a valuable method of quantifying stability and mobility of the lens on the eye.

5.7 Parametric Study of Lens Features on Mobility.

To get a better feel of how good of a measure the strain energy provides, a parametric study was undertaken to investigate how lens mobility is affected by the variations in lens geometry similar to those performed in chapter four. Only two different features were investigated and these were the lens thickness and the BOZR. These two features were chosen as they highlight the major factors of thickness variations and back surface design of the lens.

5.7.1 Lens Thickness

Simulations were performed on four different lenses with a center thicknesses ranging from 100 μm to 177 μm. The strain energy as a function of displacement on the eye is shown for the four lenses in figure 5.11. There are three significant observations. First, as

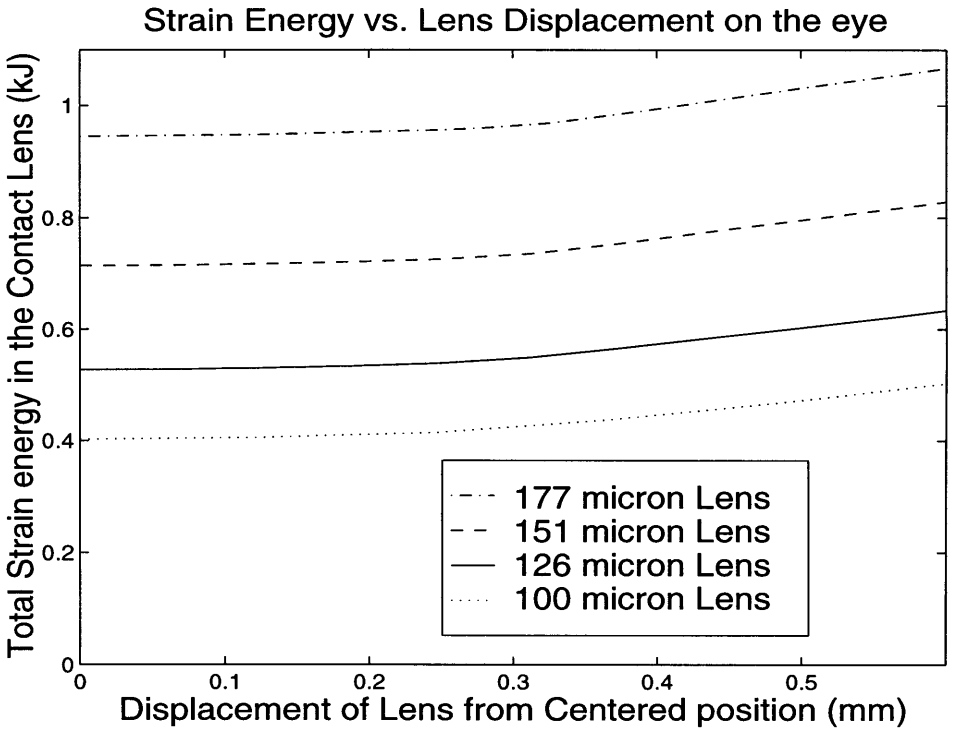

Figure 5.11: Effect of Lens Thickness on the Strain Energy as a function of Lens position on the Eye.

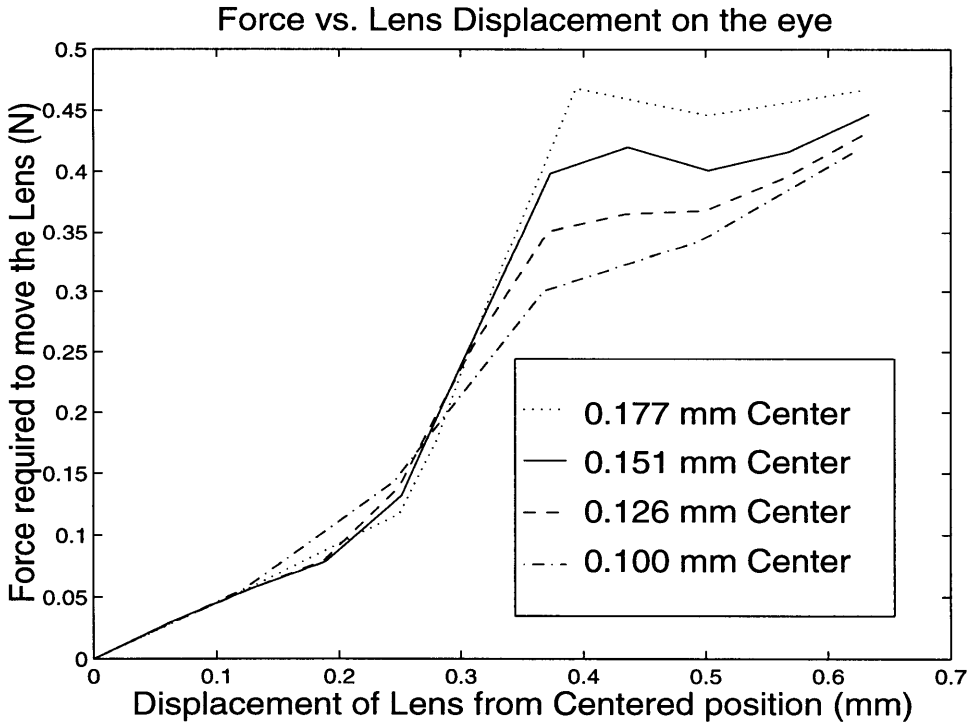

Figure 5.12: Effect of Lens Thickness on the Force required to move the Lens as a function of Lens position on the Eye.

the lens gets thicker, the total strain energy in the lens increases. This was expected and is a function of the increased stiffness and volume of material. The second observation is that the strain energy gradient near the centered position is roughly the same for all four of the lenses. In fact, the gradient is steepest for the thinnest lens. The thinnest lens experiences an increase of 12.0 J over the first 0.24 mm displacement where the thickest lens experiences an increase of only 11.1 J. This implies that the mobility of the lenses over a region of 0.1 to 0.25 mm centered over the apex of the lens is not affected by the increase in thickness. As the lenses are displaced up to 0.6 mm from the centered position, the strain energy gradient for the thicker lenses becomes slightly larger than for the thinner lenses. Between the displacements of 0.24 mm and 0.6 mm, the strain energy in the thickest lens increases by 120 J while the strain energy in the thinnest lens increases by 94.5 J. This implies, therefore, that the thicker lenses would be more adherent to the eye as the lens is displaced beyond the 0.25 mm range.

In support of the above discussion, the graph demonstrating the force required to move the lens across the eye is shown in figure 5.12. It is interesting to note that though the initial displacement of 0.25 mm, the thicker lens moves with less force. This agrees with the smaller gradient observed previously. As the lens is displaced beyond the 2.5 mm range, the thicker lens requires more force to move the lens across the eye.

5.7.2 Back Optical Zone Radius

One of the clinical observations that have been made is that flatter fitting lenses, or lenses with a larger BOZR, tend to move more on the eye than the tighter fitting, steeper lenses [8]. In an attempt to quantify this clinical observation, simulations were run for the three different lens geometries with BOZR ranging from 8.0 mm to 8.5 mm. The strain energies determined from the simulations are shown in figure 5.13. As with the previous simulations, the gradient at the centered position is similar for all lens geometries. With a BOZR of 8.0 mm, the strain energy increases by 8.8 J and with a BOZR of 8.5 mm, the strain energy increases by 12.2 J. Beyond 0.25 mm from the centered position, the steeper fitting lenses has a steeper gradient. Strain energy in the lens with a BOZR of 8.5 mm only increases by 99.8 J where the 8.0 mm BOZR lens increases by 115 J. This would imply, complimentary to what clinical results have reported, that the lenses with a larger BOZR would tend to exhibit more motion after an initial displacement of 0.25 mm.

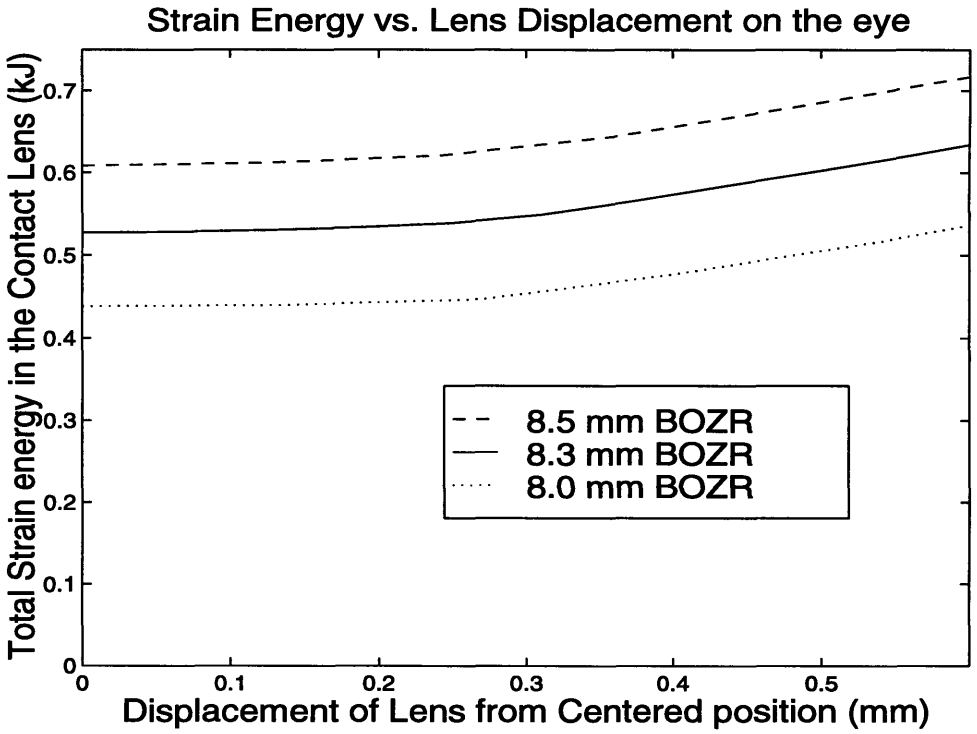

Figure 5.13: Effect of BOZR on the Strain Energy as a function of Lens position on the Eye.

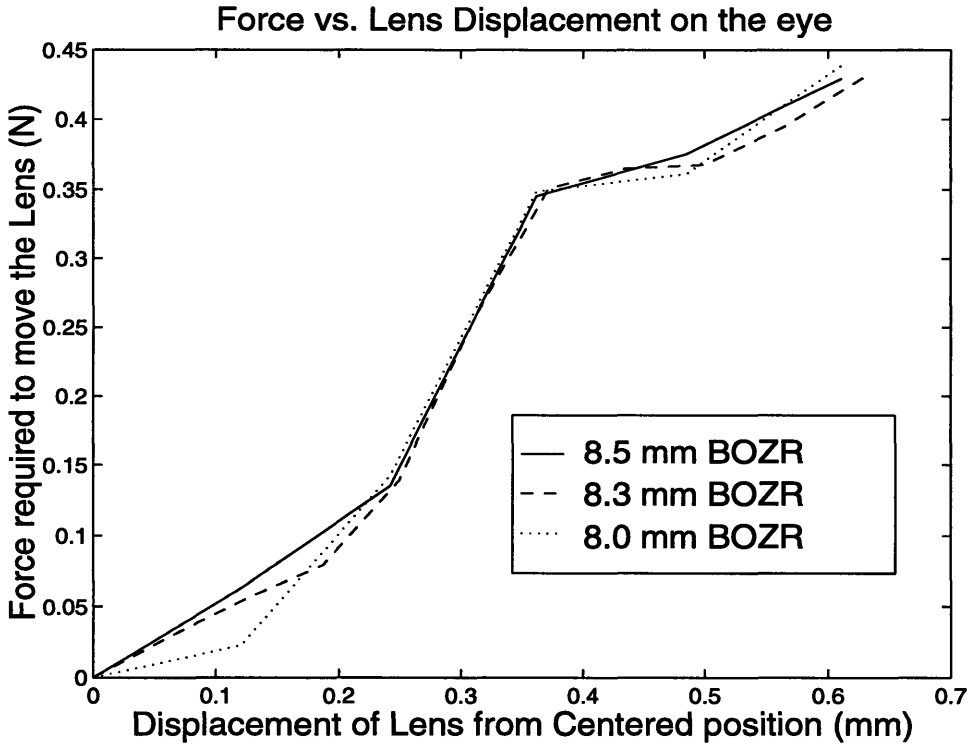

Figure 5.14: Effect of BOZR on the Force required to move the Lens as a function of Lens position.

The force required to move the three lenses is shown in figure 5.14. Over the initial 0.25 mm range of motion, the expected result is observed. The steeper lens that had the lower strain energy gradient requires less force to move it. Beyond this point, however, the results are not as dramatic. The three lenses exhibited very similar force requirements to initiate movement. It would appear that the magnitude of the strain energy may effect the clinical performance of the lens as well as the gradient. Although the flatter fitting lens had a flatter strain energy gradient, the total strain energy in the lens was higher. This may cause the required force to move the lens to be higher than expected based on the magnitude of the strain energy gradient. As the strain energy gradients of the three lenses were not very different, the secondary factor of total strain energy might become significant.

5.7.3 New Design Lens

To further investigate the proposed first iteration of the new lens design, the strain energy vs. position graph was compared to the standard lens. Before the results are discussed, however, a quick summary will be given of the design goals that were considered when the lens geometry was made. The geometry was chosen to try and balance the pressure distribution in the tear layer, reduce the maximum pressure experienced through the tear layer, and yet, achieve a stable fit by increasing the lens thickness through the lenticular region. The BOZR was increased to 8.5 mm, the sagittal height was decreased to 3.4 mm and the bevel radius was modified to try and reduce the pressure in the tear layer near the edge of the lens.

With this in mind, the results comparing the strain energy as a function of position of this simulation are shown in figure 5.15. From an initial glance, the lens does appear to be less stable than the previous lens. In fact, the difference in strain energy gradients is more dramatic than any of the previous simulations. The total strain energy only increases by 85.8 J over the range of 0.25 mm to 0.6 mm compared to 104 J for the standard lens. It would appear that the difference may be from the decrease in sagittal height as this had a significant impact on the pressure distribution in the tear layer as discussed in chapter four and this parameter was not modified in the previous simulations.

To investigate the effect of a dramatic difference in strain energy gradients, the required force to move the lens is considered in figure 5.16. These results support the

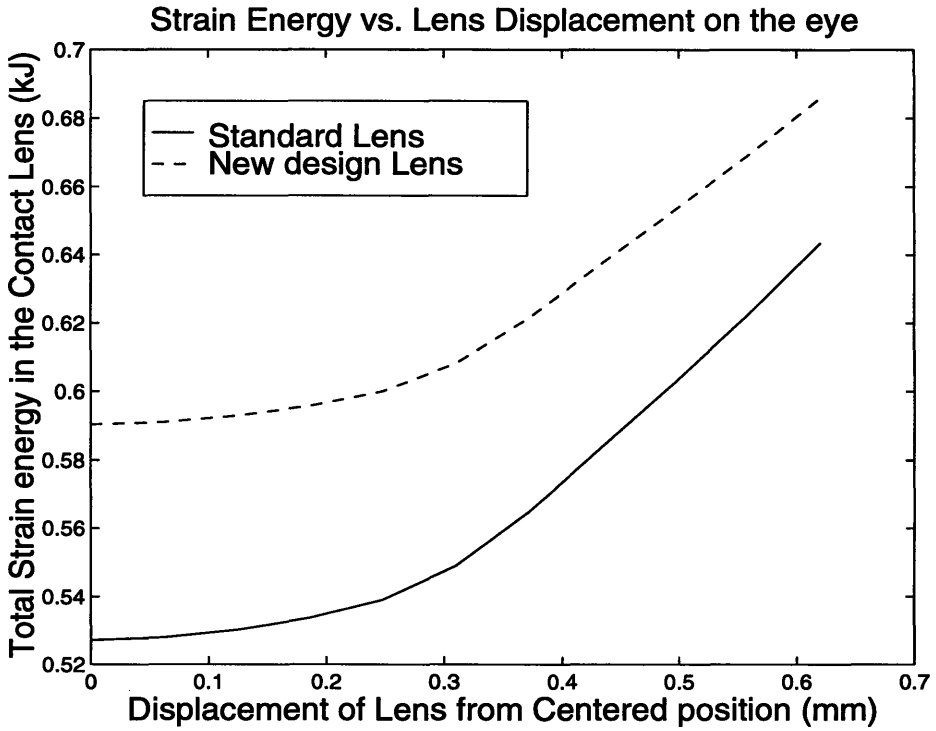

Figure 5.15: Effect of New Lens Design on the Strain Energy as a function of Lens position on the Eye.

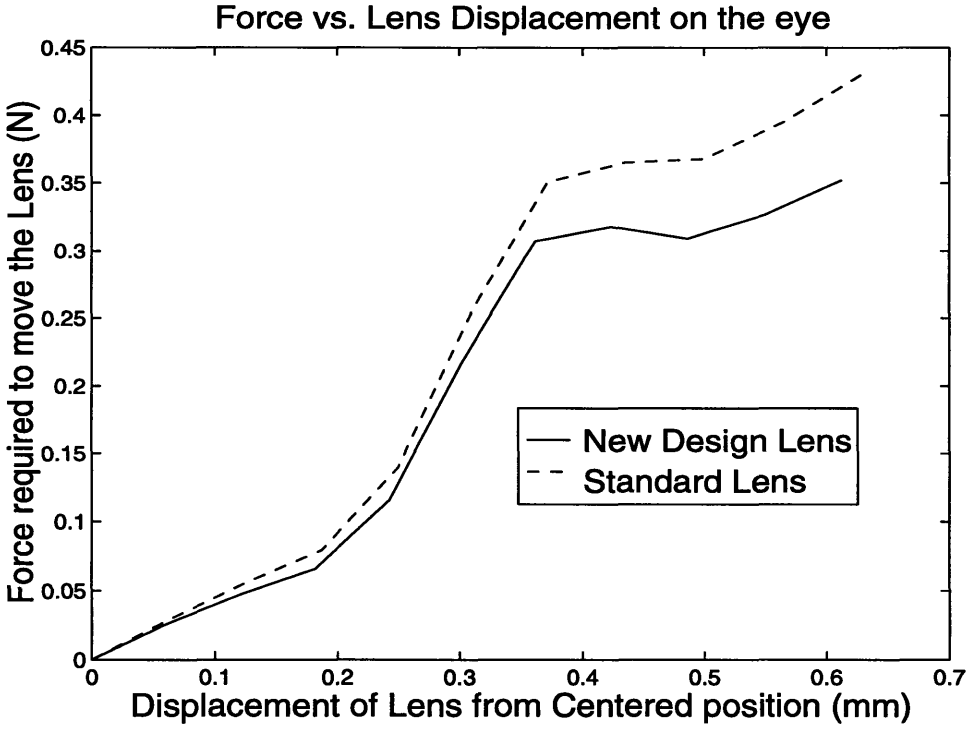

Figure 5.16: Effect of New Lens Design on the Force Required to move the Lens as a Function of Lens Position.

notion that the strain energy gradient is the key factor when considering the potential mobility of the lens. The force to move the new design lens is much less than that required to move the standard lens. Thus, the new design lens would be more prone to moving on the eye after a blink. This would cause poorer quality of vision as the contact lens would not center of the eye as well and thus, render the lens less clinically acceptable. If the standard lens was reported to be too tight, however, the increased motion of the new lens would be desired as it could increase comfort by reducing irritation and potential damage to the corneal surface. It is very encouraging to note that the strain energy gradient can be dramatically altered based on modifications to the lens geometry. With using the FEA model as a design tool, lens geometries could be developed and refined to yield the desired mobility characteristics.

5.8 Discussion of Results

It is worth while noting what the results from the present chapter represent. The actual magnitudes of the strain energy and the force required to move the lens on the eye are likely quite representative of the true *in vivo* values even without the tear layer. This is primarily due to the increased limbus radius that reduces the bending stresses in the lens. To further illustrate this, a comparison can be done between two of the axisymmetric simulations. In figure 5.17, the strain energy density for the standard lens with a limbus radius of 4 mm and a tear layer is shown. Immediate below in figure 5.18, the strain energy density for the lens with no tear layer but a limbus radius of 8 mm is shown. Comparing these two contour plots, it can be seen that the two results are quite comparable. Thus, the strain energy densities should reflect the strain energy density of a lens on an eye with a limbus radius of 4 mm. Thus, the results provide is a useful tool to measure mobility of lens geometries before they are manufactured.

There is some concern with using the shell elements in the analysis. The problem arises from sensitivity of the simulations to geometry and how the lens geometry can affect the contact between the lens and the eye. To model a shell using FEA, the mid-plane must be defined. The analysis then determines a thickness for the shell (which may vary along the length of the shell) which affects the shell's stiffness. Consider, however, the impact this will have at the end of the lens. Due to a dramatic decrease in lens thickness,

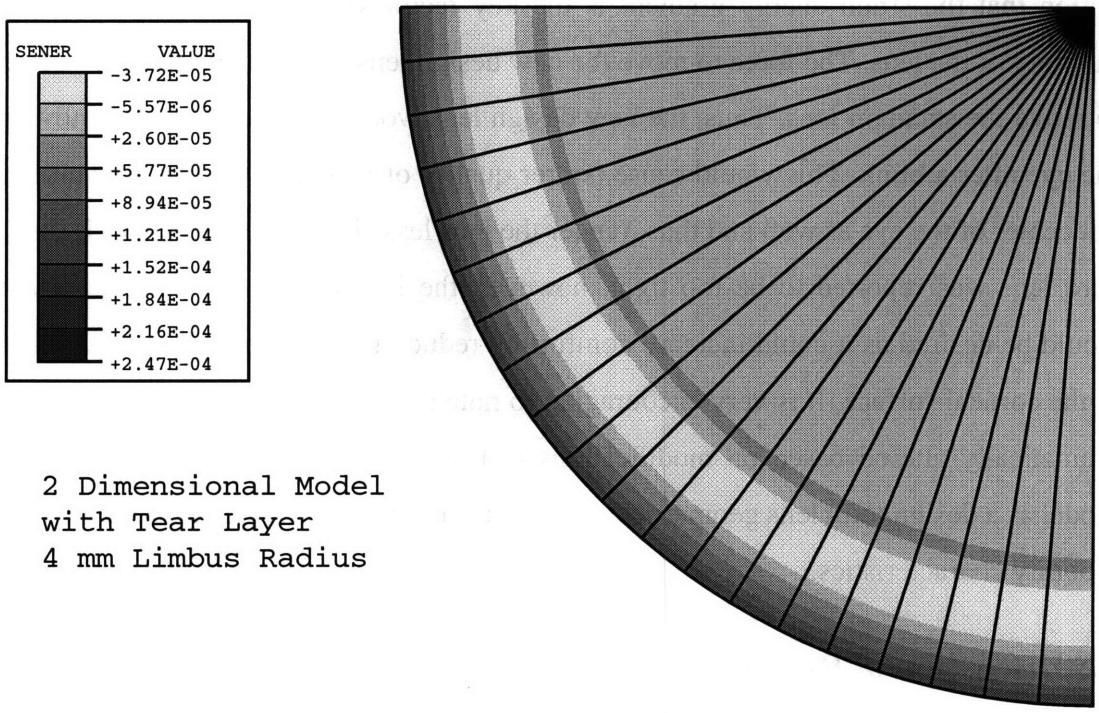

Figure 5.17: Strain Energy Density for Lens with Tear Layer and 4.0 mm Limbus Radius.

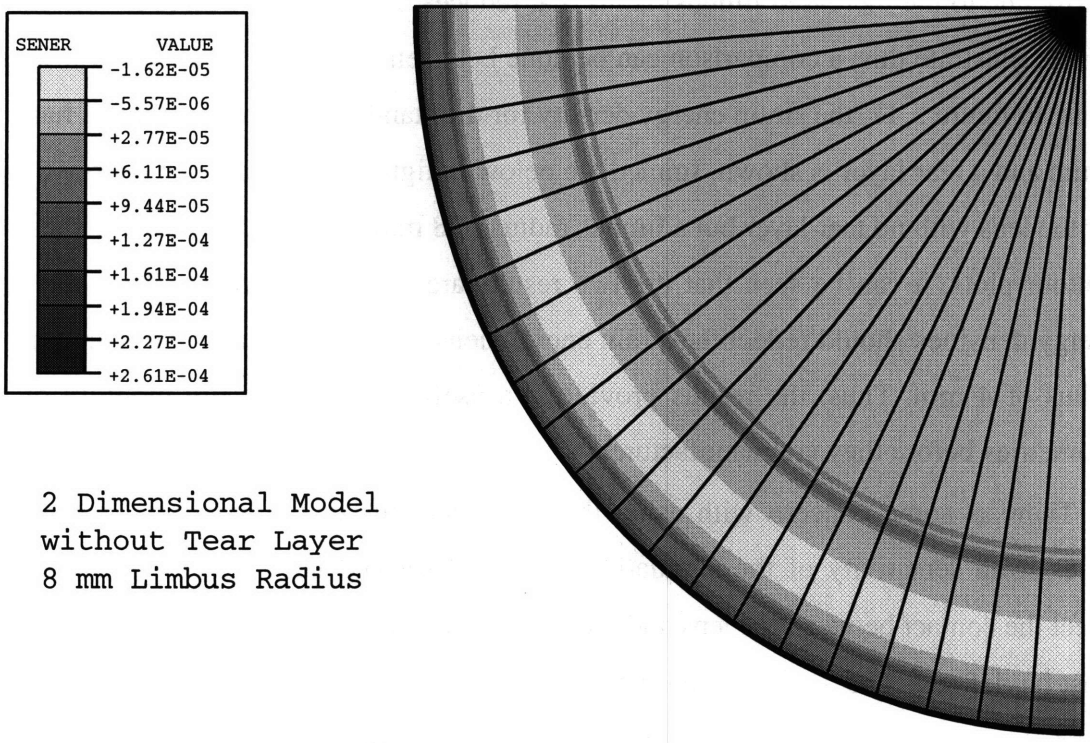

Figure 5.18: Strain Energy Density for Lens with no Tear Layer and 8.0 mm Limbus Radius.

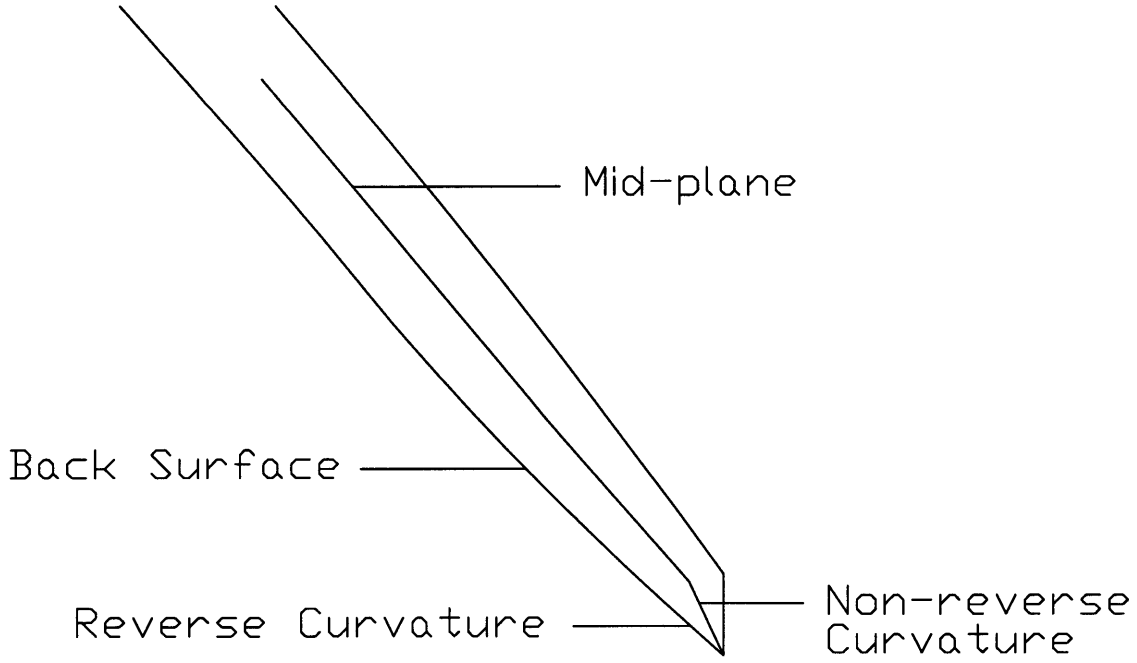

Figure 5.19: Illustration of Mid-plane not Reflecting the True Contact Lens Geometry

the general geometry of the lens at the edge is not properly represented by the mid-plane as shown in figure 5.19. Even though the back surface design incorporates a reverse curvature which contacts with the surface of the eye, the mid-plane of the lens has a standard, non-reversed curvature. Thus, for an investigation into bevel design, shell elements would not be appropriate and solid continuum elements must be used. This problem with the mid-plane not reflecting the true geometry of the lens may cause the stresses through the bevel region to be larger in magnitude than solid continuum elements would predict.

5.9 Summary

It has been observed that the strain energy density and the strain energy gradient can be used as gauges to investigate the mobility and stability of the lens as it moves across the eye. Steeper strain energy gradients will tend to make the lens return to a centered position faster and with greater force. These results were further supported by looking at the force required to move the lens across the surface of the eye. The steeper strain energy gradients corresponded to a larger required force to move the lens. Using these results, it has been demonstrated that new lens geometries can be developed that can have an increased, or decreased range of mobility to improve the clinical performance of the contact lenses.

The three dimensional simulations are still based on the assumptions of an initial fit. Mass flow of the tear fluid through the lens is not considered. As discussed previously, the mass flow of fluid through the lens can have a significant impact on the long term clinical performance of the lens as it can act to reduced the tear film thickness. To achieve a more sensitive analysis of lens motion, these longer term considerations must be accounted for.

Chapter 6

Future Directions and General Summary of the Results Presented

6.1 Future Directions

In the research conducted, investigating the initial fit of the contact lens was the primary goal. It would be interesting to further investigate the significant effects of time over the period of minutes and hours. There are a few factors that would come into play that were neglected in this model. These include mass transport of the tear fluid through the contact lens, changes in the material properties of the contact lens both as a function of time and as a function of the position in the through-thickness direction, and the long term viscoelastic behavior of the contact lens itself.

Of primary interest is the mass transport of fluid through the lens and the potential resulting lens dehydration. The main concern with this work is that for thinner lenses, there could be a greater transport of the tear fluid through the lens. This result is expected due to the decrease in lens thickness leading to an increase in the osmotic gradient. This would lead to thinner tear films under thinner lens and would thus, have a significant effect on the contact lens mechanics. Also, as the contact lens is thinner, there is less total fluid present in the lens. Since lens dehydration would be a function of surface area exposed, the thinner lenses would tend to dehydrate at the rate as the thicker lenses. This would mean the thinner lenses would lose a greater percentage of their water content and thus, create an even greater osmotic gradient from the increased total dehydration.

Lens dehydration would also affect the long term material properties of the lens. As water content decreases, the lens tends to contract. The decrease in lens volume from the contraction would not be uniform through the thickness of the lens. The front surface would dehydrate at a much faster rate because this surface is exposed to the atmosphere whereas the back surface is exposed to the fluid tear layer. To determine the possible impact of dehydration, a simulation could be run which models the gradient in volume change through the thickness of the lens. The gradient in volume change would tend to bend the lens away from the eye making the fit of the lens more flat. The flatter fit of the

contact lens would thus increase the interference pressure needed at the edge of the lens to maintain conformity with the eye. In a study of the lens' long term clinical performance, contact lens dehydration could easily be included in the model.

Although the viscoelastic nature of the contact lens is neglected in the model proposed in this thesis, this is done based on an initial fit assumption that the lens will not relax significantly over the time period under investigation. If this time period is increased, then the viscoelastic effects of the lens become increasingly important. Again, if the analysis were to focus on the long term mechanics of the soft contact lens resting on the eye then the viscoelastic nature of the hydrogel should be accounted for.

All of these factors would have to be considered in future models that focused on the long term clinical performance of the contact lens. This once again illustrates the powerful usefulness of developing a FEA model. As more and more factors are identified as clinically significant, these can be added onto the current model. With the closed form solutions and analytic models, these modifications require significant alterations to the model. As these modifications tend to be straight forward to incorporate into a FEA model, new iterations of the model can be developed faster, thereby decreasing the required research time involved in developing new generations of contact lenses.

6.2 Implementation into a Design Setting

It has been shown that various contact lens geometries can be analyzed and compared. Therein lies the most critical, and the most practical aspect of the work presented. FEA simulations can be used to compare and modify current geometries. Although the actual magnitudes of pressure readings and pressure gradients in the tear film might be high, this does not impact the sensitivity of the analysis. From a design perspective, the critical feature is being able to compare and critically modify the mechanics of the given system. If clinical trials are performed in conjunction with the numerical analysis, strong correlations should be determined between the lens' mechanics and its clinical performance. As the correlations are developed, optimization of the lens geometry will become increasingly accurate.

The use of FEA will thus allow the design process to become more analytic in nature. Although some initial clinical trials would be required determine and identify which

lenses perform better, analysis will be possible once this has occurred. This will alleviate the current reliance on empirical data and move the industry towards a more fundamental understanding of the contact lens mechanics.

6.3 Summary

In this thesis, a FEA model of a contact lens resting on the human eye with a lubricating tear layer has been developed. The results have been verified against analytical and experimental results that have been published in the literature. Results were obtained from a two dimensional axisymmetric model for various lens geometries in the form of tear film pressure distribution, tear film thickness, and bending and membrane stresses in the lens. The central tear film pressure reading varied from 0.05 kPa to 0.1 kPa. Maximum pressure readings were observed up to 0.3 kPa through the lenticular and edge region of the lens. Tear film thickness was decreased from the initial 20 μm thickness to 10 μm for some lens geometries. Lens thickness, sagittal height, back surface design, and bevel design were all shown to have significant impact on the contact lens mechanics.

In the development of the three dimensional model of the contact lens, strain energy density and strain energy gradients were analyzed to determine an appropriate gauge for an investigation of lens mobility and stability. The lens was displaced up to 0.6 mm from the centered position on the eye to observe variations in the strain energy. In support of this work, the force required to displace the lens from its centered position was investigated. Supported by clinical observations, justification was given to show that steeper strain energy gradients would yield lenses more apt to center on the eye faster and with greater force. Strain energy gradients of up to 340 kJ/m were observed from the simulations performed with forces being estimated at up to 0.5 N.

Appendix A

User Subroutine to control Positioning of the End of the Lens.

A.1 Program Listing

```
C     This subroutine Determines where the Lens' end node lies on in relation to the tear layer
C     nodes.
C
      SUBROUTINE SPLINT(XA,YA,N,X,Y,KHI,KLO)
      REAL*8 XA,YA,X,Y
      INTEGER KLO,KHI,N
      DIMENSION XA(N),YA(N)
      KLO=1
      KHI=N
 1    IF (KHI-KLO.GT.1) THEN
        K=(KHI+KLO)/2
        IF (XA(K).GT.X) THEN
          KHI=K
        ELSE
          KLO=K
        ENDIF
        GOTO 1
      ENDIF
      RETURN
      END
C
C     This subroutine determines the location of the nodes on the tear layer.
C
      SUBROUTINE UEL(RHS,AMATRX,SVARS,ENERGY,NDOFEL,NRHS,NSVARS,
     1   PROPS,NPROPS,COORDS,MCRD,NNODE,U,DU,V,A,JTYPE,TIME,DTIME,
     2   KSTEP,KINC,JELEM,PARAMS,NDLOAD,JDLTYP,ADLMAG,PREDEF,NPREDF,
     3   LFLAGS,MLVARX,DDLMAG,MDLOAD,PNEWDT,JPROPS,NJPROP,PERIOD)
C
      INCLUDE 'ABA_PARAM.INC'
      DIMENSION RHS(MLVARX,*),AMATRX(NDOFEL,NDOFEL),PROPS(*),
     1   SVARS(*),ENERGY(8),COORDS(MCRD,NNODE),U(NDOFEL),
     2   DU(MLVARX,*),V(NDOFEL),A(NDOFEL),TIME(2),PARAMS(*),
     3   JDLTYP(MDLOAD,*),ADLMAG(MDLOAD,*),DDLMAG(MDLOAD,*),
     4  PREDEF(2,NPREDF,NNODE),LFLAGS(*),JPROPS(*)
      INTEGER MAXSIZ
      PARAMETER (MAXSIZ = 100)
      COMMON KX(MAXSIZ),KY(MAXSIZ),KN,KKX,KKY,KKY2,KKYC
```

```
      REAL*8 KX,KY,KKX,KKY,KKY2,KKYC
      INTEGER KN
C
      DO 20 I=1,NNODE
        KX(I)=COORDS(1,I)+U(2*I - 1)
        KY(I)=COORDS(2,I)+U(2*I)
 20   CONTINUE
C
      KN=NNODE
      RETURN
      END
C
C     This subroutine constrains the end node of the lens to lie on the piecewise continuous
C     quadratic path defined by the top layer of the tear film. The main section of this procedure
C     is only performed after the first 9 steps are performed to position the system correctly. The
C     subroutine also determines the location of the end point of the lens.
C
      SUBROUTINE MPC(UE,A,JDOF,MDOF,N,JTYPE,X,U,UINIT,MAXDOF,LMPC,
     1    KSTEP,KINC,TIME,NT,NF,TEMP,FIELD)
C
      INCLUDE 'ABA_PARAM.INC'
      DIMENSION A(N), JDOF(N), X(6,N), U(MAXDOF,N), UINIT(MAXDOF,N),
     2    TIME(2), TEMP(NT,N), FIELD(NF,NT,N)
      PARAMETER (PRECIS = 1.D-15)
      INTEGER TOP,BOT,FIR,SEC,TRD
      REAL*8 XX,YY,TEMP1,TEMP2,TEMP3
      INTEGER MAXSIZ
      PARAMETER (MAXSIZ = 100)
      COMMON KX(MAXSIZ),KY(MAXSIZ),KN,KKX,KKY,KKY2,KKYC
      REAL*8 KX, KY, KKX, KKY, KKY2, KKYC
      INTEGER KN
C
      IF (KN .NE. 15) THEN
        LMPC = 0
      ELSE IF (JTYPE .EQ. 1 .AND. KSTEP .GT. 9) THEN
        JDOF(1) = 2
        JDOF(2) = 1
        XX = X(1,1) + U(1,1)
        CALL SPLINT (KX,KY,KN,XX,YY,TOP,BOT)
        IF (MOD(BOT,2) .EQ. 0) THEN
          FIR = BOT
          SEC = TOP
          TRD = TOP + 1
        ELSE
          FIR = BOT - 1
          SEC = BOT
          TRD = TOP
        END IF
        YY=((XX-KX(SEC))*(XX-KX(TRD))*KY(FIR))/((KX(FIR)-KX(SEC))*
     *       (KX(FIR)-KX(TRD))) + ((XX-KX(FIR))*(XX-KX(TRD))*KY(SEC))
```

```
*         /((KX(SEC)-KX(FIR))*(KX(SEC)-KX(TRD))) + ((XX-KX(FIR))*
*         (XX-KX(SEC))*KY(TRD))/((KX(TRD)-KX(FIR))*(KX(TRD)-
*         KX(SEC)))
          A(1) = -1.
          A(2) = ((2*XX-KX(SEC)-KX(TRD))*KY(FIR))/((KX(FIR)-KX(SEC))*
*         (KX(FIR)-KX(TRD))) + ((2*XX-KX(FIR)-KX(TRD))*KY(SEC))
*         /((KX(SEC)-KX(FIR))*(KX(SEC)-KX(TRD))) + ((2*XX
*         -KX(FIR)-KX(SEC))*KY(TRD))/((KX(TRD)-KX(FIR))
*         *(KX(TRD)-KX(SEC)))

          UE = YY - X(2,1)
        ELSE
          LMPC=0
          XX = X(1,1) + U(1,1)
          CALL SPLINT (KX,KY,KN,XX,YY,TOP,BOT)
          IF (MOD(BOT,2) .EQ. 0) THEN
            FIR = BOT
            SEC = TOP
            TRD = TOP + 1
          ELSE
            FIR = BOT - 1
            SEC = BOT
            TRD = TOP
          END IF
          YY=((XX-KX(SEC))*(XX-KX(TRD))*KY(FIR))/((KX(FIR)-KX(SEC))*
*         (KX(FIR)-KX(TRD))) + ((XX-KX(FIR))*(XX-KX(TRD))*KY(SEC))
*         /((KX(SEC)-KX(FIR))*(KX(SEC)-KX(TRD))) + ((XX-KX(FIR))*
*         (XX-KX(SEC))*KY(TRD))/((KX(TRD)-KX(FIR))*(KX(TRD)-
*         KX(SEC)))
        ENDIF
        IF ((KSTEP .LT. 10) .AND. (KX(1) .NE. 0)) THEN
          TEMP1 = KKX - U(1,1)
          TEMP2 = KKY2 - U(2,1)
          TEMP3 = KKY - (YY - X(2,1))
          IF (((ABS(TEMP1) .LT. 1E-3) .AND. (ABS(TEMP2) .LT. 1E-3)
*           .AND. (ABS(TEMP3) .LT. 1E-3)) .OR. (KKX .EQ. 0)) THEN
            KKX = U(1,1)
            KKY2= U(2,1)
            KKY = YY - X(2,1)
          END IF
        END IF
        RETURN
        END
C
C     This subroutine is required by ABAQUS and ensures that the user element used to
C     monitor the top of the tear film surface has no stiffness or effective material properties.
C
        SUBROUTINE UMAT(STRESS,STATEV,DDSDDE,SSE,SPD,SCD,
*       RPL,DDSDDT,DRPLDE,DRPLDT,
*       STRAN,DSTRAN,TIME,DTIME,TEMP,DTEMP,PREDEF,DPRED,CMNAME,
```

```
     *    NDI,NSHR,NTENS,NSTATV,PROPS,NPROPS,COORDS,DROT,PNEWDT,
     *    CELENT,DFGRD0,DFGRD1,NOEL,NPT,LAYER,KSPT,KSTEP,KINC)
C
      INCLUDE 'ABA_PARAM.INC'
      CHARACTER*8 CMNAME
      DIMENSION STRESS(NTENS),STATEV(NSTATV),
     *    DDSDDE(NTENS,NTENS),DDSDDT(NTENS),DRPLDE(NTENS),
     *    STRAN(NTENS),DSTRAN(NTENS),TIME(2),PREDEF(1),DPRED(1),
     *    PROPS(NPROPS),COORDS(3),DROT(3,3),DFGRD0(3,3),DFGRD1(3,3)
C
      DDSDDE=0
      STRESS=0
      STATEV=0
      SSE=0
      SPD=0
      SCD=0
      RETURN
      END
C
C     This subroutine imposes a displacement on the end on the node just prior to the application
C     of the MPC subroutine. The lens is displaced to lie on the tear layer surface so that the
C     MPC constraint will function easier.
C
      SUBROUTINE DISP (U,KSTEP,KINC,TIME,NODE,JDOF)
C
      INCLUDE 'ABA_PARAM.INC'
      DIMENSION U(3),TIME(2)
      INTEGER MAXSIZ
      PARAMETER (MAXSIZ = 100)
      COMMON KX(MAXSIZ),KY(MAXSIZ),KN,KKX,KKY,KKY2,KKYC
      REAL*8 KX, KY, KYY, KKX, KKY, KKY2, KKYC
      INTEGER KN
C
      IF ((KINC .EQ. 1) .AND. (KSTEP .EQ. 9)) THEN
        KKYC = KKY2
      END IF
      IF (JDOF .EQ. 1) THEN
        U(1) = KKX
      ELSE
        U(1) = KKYC+TIME(1)/100*(KKY-KKYC)
      ENDIF
      RETURN
      END
```

Appendix B

Calculation of Poiseuille's Flow for an Axisymmetric Disk

B.1 Calculations

$V_\theta = V_z = 0$

$V_r = V_r(z, r)$

The General Naiver Stokes Equation for quasi-steady state:

$$0 = -\frac{1}{\rho}\frac{\partial p}{\partial r} + \upsilon\left[\frac{\partial^2}{\partial r^2}V_r + \frac{1}{r}\left(\frac{\partial}{\partial r}V_r\right) + \frac{1}{r^2}\left(\frac{\partial^2}{\partial \theta^2}V_r\right) + \frac{\partial^2}{\partial z^2}V_r - \frac{V_r}{r^2} - \frac{2}{r^2}\left(\frac{\partial}{\partial \theta}V_\theta\right)\right]$$

$$\frac{\partial^2}{\partial r^2}V_r = 0 \qquad \frac{\partial}{\partial r}V_r = 0 \qquad \frac{\partial^2}{\partial \theta^2}V_r = 0 \qquad \frac{\partial}{\partial \theta}V_\theta = 0$$

Considering two terms given above that are a function of V_r

$$\frac{\partial^2}{\partial z^2}V_r \sim \frac{V_r}{h^2} \qquad \frac{\frac{\partial^2}{\partial z^2}V_r}{\frac{V_r}{r^2}} \sim \frac{R^2}{h^2} \gg 1$$

$$\frac{V_r}{r^2} \sim \frac{V_r}{R^2}$$

Note that the other terms are then also negligible as

$$\frac{\partial^2}{\partial r^2}V_r \sim \frac{V_r}{R^2}$$

$$\frac{1}{r}\left(\frac{\partial}{\partial r}V_r\right) \sim \frac{V_r}{R^2}$$

Where R is the radius of the Disk and h is the depth of the region of flow. Therefore, the V_r / r^2 term is negligible. This yields the further simplified relationship:

$$0 = -\frac{1}{\rho}\frac{\partial p}{\partial r} + \upsilon\frac{\partial^2}{\partial z^2}V_r$$

$$\mu V_r = \left(\frac{\partial p}{\partial r}\right)\frac{z^2}{2} + C_1 z + C_2$$

@ z=0, $V_r = 0 : C_2 = 0$

@ z=h, $Vr = 0 : \left(\frac{\partial p}{\partial r}\right)\frac{h^2}{2} + C_1 h = 0$

$$C_1 = -\left(\frac{\partial p}{\partial r}\right)\frac{h}{2}$$

This gives the equation for V_r as:

$$V_r = \frac{1}{2\mu}\left(\frac{\partial p}{\partial r}\right)[z^2 - hz]$$

The equation for the flow rate is as follows:

$$Q = \int_0^{2\pi}\int_0^h V_r\, dz r d\theta$$

$$Q = 2\pi r \int_0^h \frac{1}{2\mu}\left(\frac{\partial p}{\partial r}\right)[z^2 - hz]\, dz$$

$$Q = \frac{\pi r}{\mu}\left(\frac{\partial p}{\partial r}\right)\frac{h^3}{6}$$

Assuming that the height is approximately constant, this yields:

$$-\left(\frac{\partial p}{\partial r}\right) = \frac{6\mu Q}{\pi r h^3}$$

$$\int_P^{P_o} -dp = \frac{6\mu Q}{\pi}\int_R^{R_o}\frac{1}{rh^3}dr$$

$$P - P_o = \frac{6\mu Q}{\pi h^3}\ln\left(\frac{R_o}{R}\right)$$

This leads to the final equation for the flow rate which is:

$$Q = \frac{\pi h^3 (P - P_o)}{6\mu \ln\left(\frac{R_o}{R}\right)}$$

The average flow velocity is given by:

$$\bar{V} = \frac{Q}{2\pi R h}$$

The shear stress at the wall is given by the equation:

$$\tau_w = \mu \left.\frac{\partial u}{\partial z}\right|_{z=0}$$

$$\tau_w = \frac{1}{2}\left(\frac{\partial p}{\partial r}\right)(2z - h)\,|_{z=0}$$

This leads to the final shear stress relation:

$$\tau_w = \frac{-h}{2}\left(\frac{\partial p}{\partial r}\right)$$

Note: This derivation is a dramatic simplification and should only be considered as an order of magnitude estimation at a specific given time. For a more complete analysis, time rate of change effects must be considered.

References

[1] Tsubota, K. et.al. Extended wear soft contact lenses induce corneal epithelial changes. Br J Opthamol 1994;78:907-911.

[2] Jenkins, J.T. and M. Shimbo. The Distribution of Pressure Behind a Soft Contact Lens. J. Biomech Engin 1984;106:62-65.

[3] Hayashi, Tommy T. and Irving Fatt. Forces Retaining a Contact Lens on the Eye between Blinks. Am J. Optom. & Physiol. Opt. 1980;57:485-507.

[4] Conway, H.D. and M. Richman. Effects of Contact Lens Deformation on Tear Film Pressures Induced during Blinking. Am J. Optom. & Physiol. Opt. 1982;59:13-20.

[5] Taylor, A.J. and S.D.R. Wilson. Centration Mechanism of Soft Contact Lenses. Optom Vis Sci 1996;73:215-221.

[6] Martin, D.K. and B.A. Holden. Forces developed beneath hydrogel contact lenses due to squeeze pressure. Phys. Med. Biol. 1986;30:635-649.

[7] Martin, D.K. Empirical analysis of the motion of soft contact lenses across the human eye. Aust. Phys & Engin Sci Med. 1987;10:214-220.

[8] Young, G., B. Holden and G. Cooke. Influence of Soft Contact Lens Design on Clinical Performance. Optom Vis Sci 1993;70:394-403.

[9] Pesudovs, K. and A. J. Phillips. A clinical comparison of the Johnson & Johnson Acuvue, the Barnes-Hind Calendar and the Bausch & Lomb Medalist disposable contact lenses. Clin Exp Optom 1994; 77: 264-271.

[10] Hibbit, Karlsson & Sorensen, Inc., ABAQUS/Standard Version 5.5, Pawtucket, RI, 1995.

[11] Conway, H.D. and M.W. Richman. The Effects of Contact Lens Deformation on Tear Film Pressure and Thickness During Motion of the Lens Towards the Eye. J. Biomech Engin 1983;105:47-50.

[12] Meier, Daniel. Das Corneo-Skleral-Profil - ein Kriterium individueller Kontaktlinsenanpassung. die Kontaktlinse 1992;10:6-11.

[13] Hamano, Hikaru and Herbert E. Kaufman. The Physiology of the Cornea and Contact Lens Applications. Churchhill Livingstone NY, 1987.

[14] Knoll, H.A. and H.D. Conway. Analysis of Blink-Induced Vertical Motion of Contact Lenses. Am J. Optom. & Physiol. Opt. 1987;64:153-155.

[15] Prydal, J.I. and P.N. Dilly. In Vivo Confocal Microscopy of the Cornea and Tear Film. Scanning 1995;17:133-135.

[16] Funkenbusch, GuoMing T. and Richard C. Benson. The Conformity of a Soft Contact Lens on the Eye. J. Biomech Engin 1996;118:341-348.

[17] Gere & Timoshenko. Mechanics of Materials. 3rd ed. PWS-KENT Boston, 1990.

[18] Kikkawa, Yoshizo. Kinetics of Soft Contact Lens Fitting. Contacto 1979;23(4):10-17

[19] Orsborn, Gary N., Steve G. Zantos. Corneal Desiccation Staining With Thin High Water Content Contact Lenses. Contact Lenses 1988;14(2):81-85.

[20] Holden, Brien A., Deborah F. Sweeney, Ronald G. Seger. Epithelial Erosions Caused by Thin High Water Content Lenses. Clin Exp Optom 1986; 69(3):103-107.

[21] Battaglioli, J.L. and R.D. Kamm. Measurements of the Compressive Properties of Scleral Tissue. Invest Ophthalmol Vis Sci 1984; 25:59-65.

[22] Kragha, IK. Causes of Blindness in northern Nigeria. Am J Optom Physiol Opt 1987; 64(9):708-710.

[23] Mark, BiKales, Overberger, Uluges eds. Encyclopedia of Ploymer Science and Engineering, 2nd Edition. Volume 4, 1986.

[24] Kikkawa, Yoshizo. Elastic Properties of the Soft Contact Lens. Contacto 1980; 24(3):8-15.

[25] Tiffany, John M. The Viscosity of Human Tears. Internat Ophthalmol 1991; 15: 371-376.

[26] Martin, D. K., *et al.* A unifying Parameter to Describe the Clinical Mechanics of Hydrogel Contact Lenses. Optom Vis Sci 1989; 66(2): 87-91.

[27] Little, S. A. and A. S. Bruce. Hydrogel (Acuvue) Lens Movement is Influenced by the Postlens Tear Film. Optom Vis Sci 1994; 71(6): 364-370.

[28] The New Encyclopaedia Britannica, 15th ed., Chicago, 1990

[29] U.S. Bureau of the Census, Statistical Abstract of the United States: 1995, 115th ed., Washington DC, 1995.

[30] Holt, V., M.C. Boyce, D. Hart. Laser Induced Fluorescence Measurement of the Tear Film Thickness under a Contact Lens, M.I.T. press, 1997.

[31] Strang, G., Introduction to Applied Mathematics, Wellesley-Cambridge Press, Wellesley MA, 1986